Probing the Morphology of Bulk Heterojunctions with Phthalocyanine and Naphthalocyanine Small Molecules: A Microwave and Solar Cell Device Study

by

Adam David Brunell

B.S., University of California Los Angeles, 2012

A thesis submitted to the

Faculty of the Graduate School of the

University of Colorado in partial fulfillment

of the requirement for the degree of

Master of Science

Department of Chemistry and Biochemistry

2014

This thesis entitled:

Probing the Morphology of Bulk Heterojunctions with Phthalocyanine and Naphthalocyanine Small Molecules: A Microwave and Solar Cell Device Study

written by Adam David Brunell

has been approved for the Department of Chemistry and Biochemistry

_____

(Garry Rumbles)

_____

(David M. Walba)

Date:_____

The final copy of this thesis has been examined by the signatories, and we Find that both the content and the form meet acceptable presentation standards Of scholarly work in the above mentioned discipline.

Brunell, Adam David (M.S., Chemistry, Department of Chemistry and Biochemistry)

Probing the Morphology of Bulk Heterojunctions with Phthalocyanine and Naphthalocyanine Small Molecules: A Microwave and Solar Cell Device Study

Thesis directed by Professor Garry Rumbles

Organic photovoltaics (OPVs) have the potential to provide clean, renewable energy. In this thesis work, solar devices were constructed by using an inverted architecture. Silicon naphthalocyanine (SiNc) and one of three phthalocyanine molecules (Pc1, Pc2, or Pc3) were separately added to the active layer of OPV solar cells in order to determine their impact on the performance and spectral response. Also, time-resolved microwave conductivity (TRMC) measurements were performed on thin films of P3HT:$PC_{60}BM$ with SiNc or one of three phthalocyanine molecules, neat P3HT with one of the small molecules, and neat $PC_{60}BM$ with a small molecule. The results from the TRMC experiments demonstrate that ternary blends showed characteristics of a three-phase morphology and it was possible to provide insight into the location of the molecules in the bulk heterojunction by analysis of the data. Therefore, TRMC has the potential to probe the morphology of different systems used for solar devices.

Contents

Tables

Figures

Chapter I: Introduction

Humans use over 10^{16} watt-hours (Wh) of electricity every year. The source for the vast majority of electricity comes from coal and oil, also known as fossil fuels.[1] In order to reduce the carbon footprint from these processes and minimize the negative effects on the environment, renewable energy, such as solar, wind, and water energy, needs to replace fossil fuels as the major electricity producer. Solar energy generation, involving the use of organic and inorganic semiconductors, represents a clean, renewable source of continuous energy that has the possibility of handling the high energy needs of the world.[2] The most promising sources of renewable energy are solar, nuclear, and wind.[3] However, each source of energy has its advantages and disadvantages. For example, nuclear energy has the potential to create vast amounts of energy without production of any green house gases, but there are concerns about nuclear waste and accidents.[2] Solar energy, on the other hand, is environmentally friendly and is completely scalable. The major problem with solar energy, at the moment, is the cost. The materials used for solar devices and the manufacturing process is too expensive in money and energy requirements at the moment. Biomass and biofuels have also entered into the renewable energy conversation, however, as currently envisioned these approaches do not possess the capability of handling the required large energy demands.[4]

Figure 1-1 illustrates the record efficiencies for all types of solar cell devices.[5] Research in these different photovoltaics approaches focuses on optimization, stability, cost, and efficiency. In order to increase the efficiency of these devices, the manufacturing procedure must first be optimized. Fabrication of organic photovoltaics depends on many different parameters including: annealing temperature, ambient moisture, light, water, and oxygen. In several cases, exposure of solar cell devices to air will severely degrade the active layer. This is due to the fact

that the components of the bulk heterojunction, required for efficient solar cell design, react photochemically with water and oxygen in the air.[6,7,8,9] The most promising photovoltaic devices are perovskite cells,[10,11,12] organic tandem cells,[13,14] and quantum dot cells.[15,16,17] Three-junction solar cells hold the record for efficiency, 44.4%. Even though this efficiency is acceptably high, these devices are extremely expensive and are primarily used for satellites and space craft.[18] Since these devices cannot be used commercially, there is a need for less expensive solar-based energy devices. Organic photovoltaics, the orange data points in the figure below, use cheaper and more easily manufactured and recycled materials in order to decrease the price of production.[19,20,21]

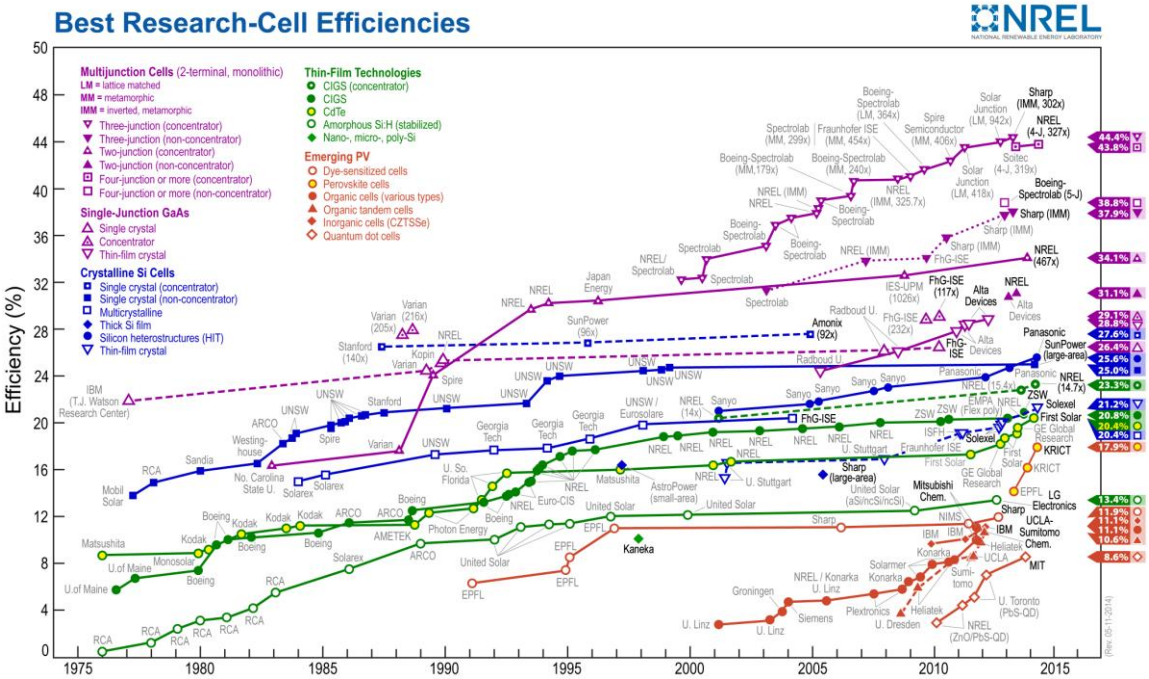

Figure 1-1. Record solar cell efficiencies from 1976 - 2014. The data presented is determined by the National Renewable Energy Lab (NREL).[5]

Organic photovoltaics (OPV) are one of the most researched solar energy sources in the world. Organic solar cell devices have the potential to decrease the cost of manufacturing

through the use of cheaper, abundant materials. Companies and research groups are continuing to break efficiency records for organic photovoltaics. For example, the Mitsubishi Chemical Corp. currently holds the record for organic solar cell device efficiency, 11.1%. The popularity of these devices is due to the use of easily-processed, since they do not require a large amount of energy during the manufacturing process, which is not true for inorganic materials such as silicon. The materials used in these devices can also be deposited onto flexible substrates, which is another attraction for studying this area of research.[22,23] Organic photovoltaics are completely scalable, which is a key aspect in replacing fossil fuels as the world's major energy source. The major problems facing organic photovoltaics at the moment includes cost, efficiency, and stability. Even though the materials used in these devices are scalable, they are yet to be cost-effective. Also, the efficiency of organic photovoltaics have not matched the efficiencies of inorganic solar cell devices. The stability of the organic materials is an issue because they are unstable when in contact with water and oxygen.

In order to generate current in an organic solar cell device, multiple processes must occur, including: absorption of light, exciton photogeneration, exciton diffusion, exciton dissociation, dissociation of bound charges, transport, and removal of charges at the electrodes. The organic materials used in these devices have small dielectric constants, so when the acceptor molecules absorb light, Frenkel excitons are generated. Frenkel excitons are strongly bound, singlet charge pairs which do not freely dissociate into separate charges.[24] Optimization of these devices proves difficult due to the fact that an increase in one area usually results in a decrease in a different area. For example, the thickness of the active layer needs to be at least 100 nm thick in order to absorb most of the solar spectrum, however, the diffusion length of excitons is only 10 to 15 nm.[25,26,27,28,29,30] This phenomenon is known as the excitonic bottleneck. The motivation

for using bulk heterojunctions (BHJ) in organic photovoltaics is to solve this problem. Bulk heterojunction organic solar devices mix the acceptor and donor molecules on a nanometer length scale.[31,32] Bulk heterojunction solar cells solve the excitonic bottleneck by creating a matrix of connecting materials, but it unfortunately creates another problem. The distance between the donor and acceptor molecules is now less than the exciton diffusion length, but the pathways for charge extraction become complicated. This problem causes the recombination of free charges to increase.[33,34] However, bulk heterojunction solar devices have the shown the most potential for creating an efficient organic solar device.

In bulk heterojunction solar cells containing P3HT:$PC_{60}BM$, three phases are present: P3HT crystallites, $PC_{60}BM$ crystallites, and an amorphous mixture of P3HT and $PC_{60}BM$.[35,36,37,43] In the past, mixed phases in a bulk heterojunction photovoltaic device were thought to decrease the performance of the device, since isolated molecules could act as traps to free charges.[44] As P3HT molecules crystallize, any $PC_{60}BM$ molecules that are present will be extruded into the mixed phase.[39] Therefore, a P3HT-rich phase, a $PC_{60}BM$-rich phase, and a mixed phase exist in the bulk heterojunction. However, in the P3HT-rich region, there can exist both pure P3HT crystals and pure P3HT amorphous chains. If SiNc molecules were mixed into the bulk heterojunction of P3HT:$PC_{60}BM$, there are three locations where these molecules could be positioned: the amorphous chains in the pure P3HT region, the $PC_{60}BM$-rich phase, or the mixed phase. Figure 1-2 shows a representation of the three phase morphology in bulk heterojunctions. This illustration is adapted from Yin and Dadmun 2011. The straight, yellow lines in the figure represent pure P3HT crystal chains while the curved lines represent amorphous P3HT chains. The black circles represent $PC_{60}BM$ molecules and the red diamonds represent possible locations of SiNc molecules. Ideally, SiNc molecules would be located in the

amorphous region in order to facilitate in the transport of charges between P3HT chains and $PC_{60}BM$ molecules. Organic solar cell devices can only be optimized when the morphology of the active layer is completely understood.[38,41] In bulk heterojunctions of P3HT:$PC_{60}BM$, the initial crystallization of P3HT chains is interrupted by the presence of $PC_{60}BM$ molecules. This interference results in the formation of the amorphous phase.[40] The diffusion and aggregation of $PC_{60}BM$ molecules are determined by the chain motion of P3HT because the activation energy of P3HT crystallization, 37.5 kcal/mol, is significantly larger than the activation energy of $PC_{60}BM$ aggregation.[42]

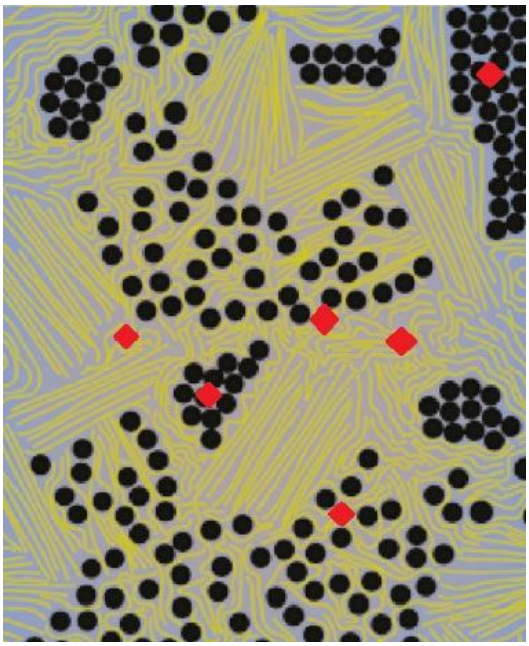

Figure 1-2. An adaptation, from Yin and Dadmun 2011, that illustrates the three phase morphology of bulk heterojunctions in organic photovoltaic devices. The yellow lines represent P3HT chains, the black circles represent $PC_{60}BM$ molecules, and the red diamonds represent SiNc molecules.

The method for the transport of free charges in conjugated polymers, such as P3HT, is complex because extrinsic and intrinsic factors are present. Some of these factors include

morphology, interface, inter-chain interactions, spatial disorder, conjugation length, and intra-chain interactions.[46] Transport of charges in P3HT occurs through hopping between chains, due to inter-chain interactions, and conduction along the backbone of the polymer chains.[45,46,47] Interestingly, the molecular weight of P3HT strongly influences the measured hole mobility.[48] The hopping process that is the most difficult is the limiting factor for the transport of charges on chains of P3HT.[50] Therefore, the morphology of the bulk heterojunction, including all three phases of molecules, is the key to increasing the transport of charges, since it plays such a crucial role in this process.[49,50]

The goal of this dissertation is to provide evidence that flash-photolysis time-resolved microwave conductivity (TRMC) measurements have the possibility of probing the morphological structure of bulk heterojunctions. Utilizing this technique may lead to a better understanding of optimizing the morphology of organic solar cell devices. Chapter II of this thesis discusses the results of adding small molecules to the active layer of organic photovoltaic devices. The bulk heterojunction of the organic solar cell devices contains poly(3-hexylthiophene) (P3HT) and [6,6]-phenyl C_{61}-butyric acid methyl ester ($PC_{60}BM$). Small molecules were subsequently added to the bulk heterojunction in varying concentrations. These small molecules included: tert-butyl functionalized silicon 2,3-naphthalocyanine bis(trihexylsilyoxide) (SiNc), dihydroxy-1,4,8,11,15,18,22,25-octabutoxyphthalocyaninatosilicon(IV) (Pc1), triethylsilyhydroxy-1,4,8,11,15,18,22,25-octabutoxyphthalocyaninatosilicon(IV) (Pc2), and 1,4,8,11,15,18,22,25-octabutoxy-25H,31H-phthalocyanine (Pc3).[51,52] Chapter III goes into the details of the flash-photolysis TRMC experiments and the analysis of the data.

Chapter II: Solar Cell Devices

2.1 Introduction

Tert-butyl functionalized silicon 2,3-naphthalocyanine bis(trihexylsilyoxide) (SiNc) was used as a sensitizer in ternary blends of P3HT:$PC_{60}BM$. The ternary blend of P3HT:$PC_{60}BM$ with SiNc was mixed to make a bulk heterojunction in an organic solar cell device, with an inverted structure. SiNc, as shown below in Figure 2-1, is a metallo-napthalocyanine with silicon at the core of the naphthalocyanine. The important addition to this small molecule is the four tert-butyl groups that are situated at the edges of the naphthalocyanine core. The addition of the tert-butyl groups, synthesized by Alan Sellinger's group at the Colorado School of Mines, provides the naphthalocyanine molecule with a smaller chance of aggregation, which is a major problem for small molecules due to intermolecular interactions between the cores of these molecules.[51] The four tert-butyl groups on the naphthalocyanine core also provide an increase in the solubility of the molecule in organic solvents. These new properties of the metallo-naphthalocyanine are very important to the success of organic solar cell devices because the spin coating process of manufacturing solar cell devices is sensitive to aggregates as well as molecules that are not completely dissolved.

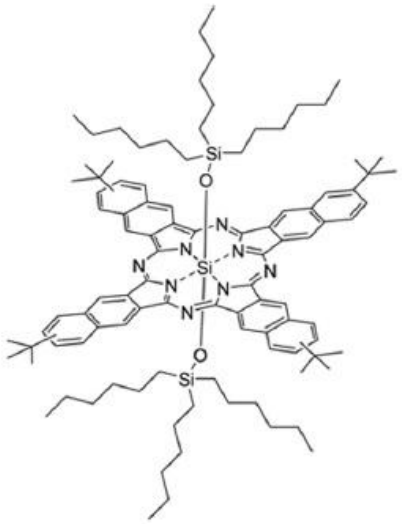

Figure 2-1. Structure of tert-butyl functionalized silicon 2,3-naphthalocyanine bis(trihexylsilyoxide) (SiNc).

The reason for adding small molecules into the bulk heterojunction of solar cells is to expand the amount of the solar spectrum that can be absorbed by the active layer. If more of the solar spectrum is absorbed by the active layer of the solar cell device, then the device can output more energy, as well as increase the efficiency and open-circuit voltage. Increasing the efficiency, open-circuit voltage, and short-circuit current density are the main foci of researchers working on organic solar cell devices. The goal is to improve the properties of organic devices beyond those of inorganic devices, in order to replace inorganic materials in commercial and industrial applications. SiNc provides an enhancement to the absorption of the active layer. As seen in Figure 2-2 below, the addition of SiNc to a blend of P3HT:$PC_{60}BM$ introduces a significant Q-band peak at 800 nm, as compared to P3HT:$PC_{60}BM$ control's absorptance spectrum. The absorptance spectra shown in Figure 2-2 were obtained on samples spin-coated onto quartz substrates and measured using a Shimadzu spectrophotometer with an integrating sphere attachment, as described in the experimental section. Notice that there is only one Q-band

peak at 800 nm, whereas there are two peaks in this region in the external quantum efficiency (EQE) of these devices, which will be discussed later.

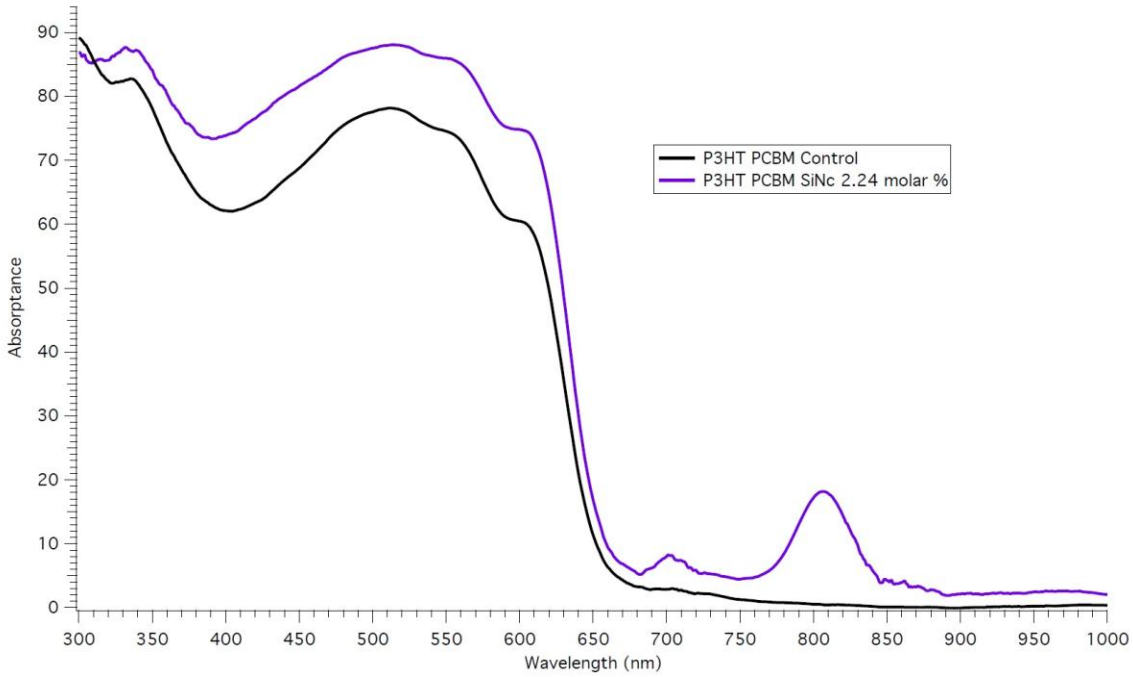

Figure 2-2. The absorptance spectra of P3HT:$PC_{60}BM$ and P3HT:$PC_{60}BM$ with SiNc (2.24 molar percent) on quartz substrates. The P3HT:$PC_{60}BM$ with SiNc sample has a strong Q-band peak at 800 nm.

The absorptance spectra for blends of neat P3HT with SiNc and neat $PC_{60}BM$ with SiNc were also obtained, as shown in Figure 2-3. There is a strong Q-band peak around 800 nm in the neat P3HT with SiNc sample and the neat $PC_{60}BM$ with SiNc sample. The Q-band peak is shifted to the blue for the neat P3HT with SiNc thin film, while it is shifted to the red for the neat $PC_{60}BM$ with SiNc thin film. This is due to the different thin film microstructures of P3HT and $PC_{60}BM$. The naphthalocyanine molecules interact differently with light when in contact with neat P3HT, as compared to neat $PC_{60}BM$. The absorptance spectra for the control thin films of neat P3HT and neat $PC_{60}BM$ are shown in Figure 2-3 as well. The absorptance spectrum of neat

P3HT is very similar to the spectrum of neat P3HT with SiNc, except for the Q-band peak around 800 nm, and the same is true for neat $PC_{60}BM$ and neat $PC_{60}BM$ with SiNc.

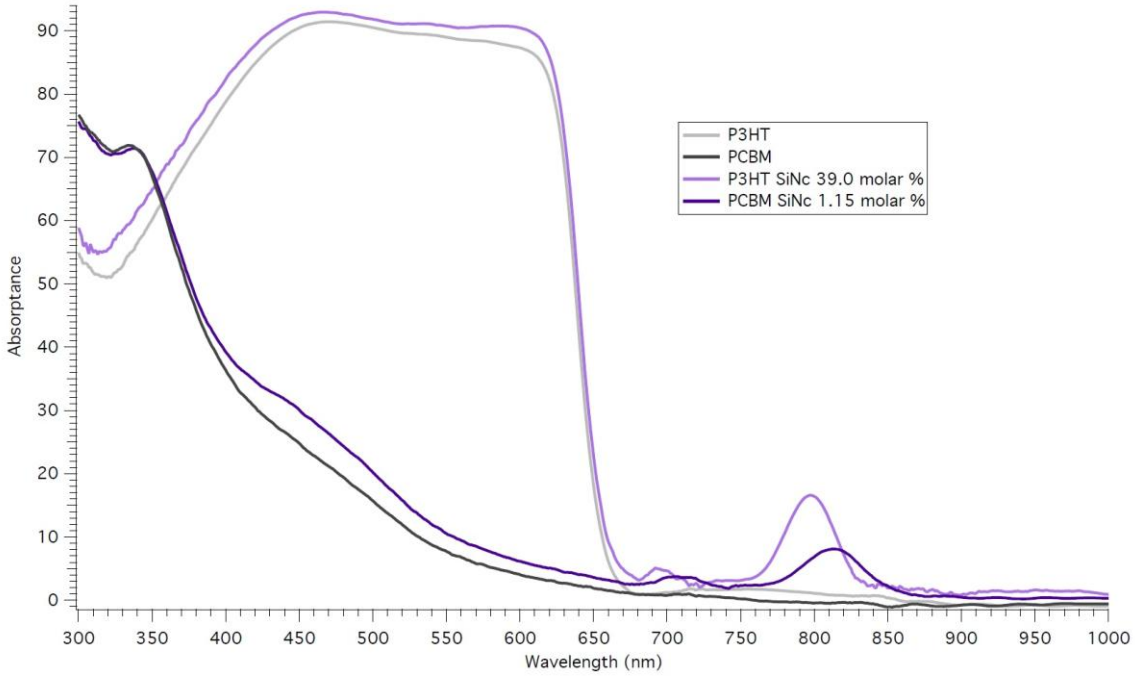

Figure 2-3. The absorptance spectra of neat P3HT, neat $PC_{60}BM$, neat P3HT with SiNc (39.0 molar percent), and neat $PC_{60}BM$ containing SiNc (1.15 molar percent). The strong Q-band peak around 800 nm is present in the samples with SiNc.

In addition to SiNc, three phthalocyanines were also used in ternary blends of P3HT:$PC_{60}BM$. The reason for incorporating these small molecules into bulk heterojunctions was to confirm that the addition of these molecules did not cause the device to fail and to demonstrate if a small molecule had appropriate energy levels that coincided with the donor and acceptor molecule's energy levels, then the device should be functional. The effect of energy levels on devices will be discussed in Chapter III. The three phthalocyanines introduced into the active layers of devices were: dihydroxy-1,4,8,11,15,18,22,25-octabutoxyphthalocyaninatosilicon(IV) (Pc1), as seen in Figure 2-4, triethylsilyhydroxy-

1,4,8,11,15,18,22,25-octabutoxyphthalocyaninatosilicon(IV) (Pc2), illustrated in Figure 2-5, and 1,4,8,11,15,18,22,25-octabutoxy-25H,31H-phthalocyanine (Pc3), shown in Figure 2-6 below.[52] These small molecules were obtained from Devens Gust at Arizona State University. It is important to note that Pc1 and Pc2 are metallo-phthalocyanines. Silicon sits at the core of Pc1 and Pc2, similar to the structure of SiNc. The only difference between Pc1 and Pc2 is the coordinated silicon that replaces one of the hydrogen atoms on the hydroxyl group. While Pc1 and Pc2 are nearly identical, Pc3 is the free base form of Pc1 and Pc2. Notice that Pc3 should have two Q-band peaks in its absorption spectrum due to the different transition energies from NH to NH and H to H in the core of the molecule. The method for obtaining the absorptance spectra, as seen in Figure 2-7, was not sensitive enough to detect the second Q-band peak for Pc3. However, the absorption spectrum of Pc3 was obtained in solution, which provided the sensitivity to show the second Q-band peak, as seen in Figure 3-15.

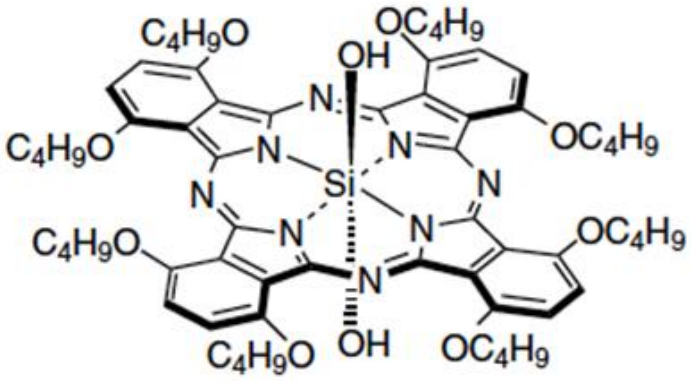

Figure 2-4. Structure of dihydroxy-1,4,8,11,15,18,22,25-octabutoxyphthalocyaninato-silicon(IV) (Pc1).[52]

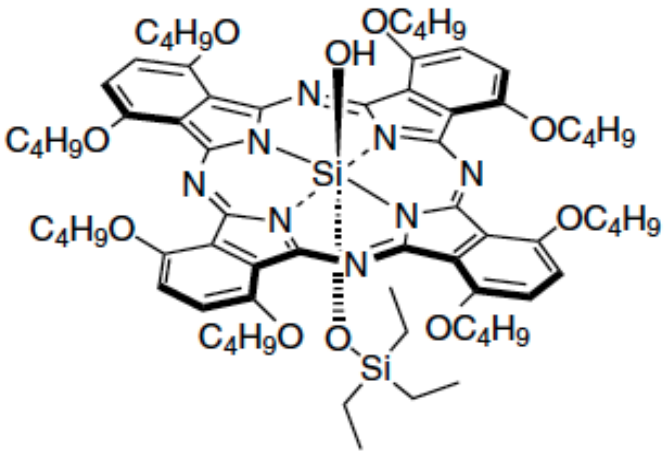

Figure 2-5. Structure of triethylsilyhydroxy-1,4,8,11,15,18,22,25-octabutoxyphthalo-cyaninatosilicon(IV) (Pc2).[52]

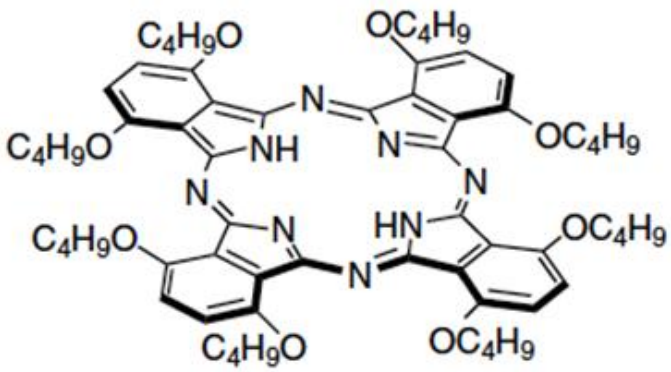

Figure 2-6. Structure of 1,4,8,11,15,18,22,25-octabutoxy-25H,31H-phthalocyanine (Pc3).[52]

The incorporation of Pc1, Pc2, and Pc3 into the active layer increases the amount of the solar spectrum that is absorbed by the solar cell devices, similar to the devices containing SiNc. The absorptance spectra of thin films containing Pc1, Pc2, and Pc3 are shown in Figure 2-7. When these phthalocyanines are introduced into a blend of P3HT:$PC_{60}BM$, a Q-band peak appears around 800 nm. The Q-band peak of Pc1 is broad and centers at 800 nm, while the peak of Pc2 and Pc3 are shifted to the blue. The peak of Pc2 is centered at 785 nm and the peak of Pc3 is centered at 788 nm. It is important to note that the Q-band peaks for Pc2 and Pc3 are more

defined than the peak for Pc1. These phthalocyanines only exhibit one Q-band peak in the red region of the spectrum, which is consistent with the EQE data for these devices.

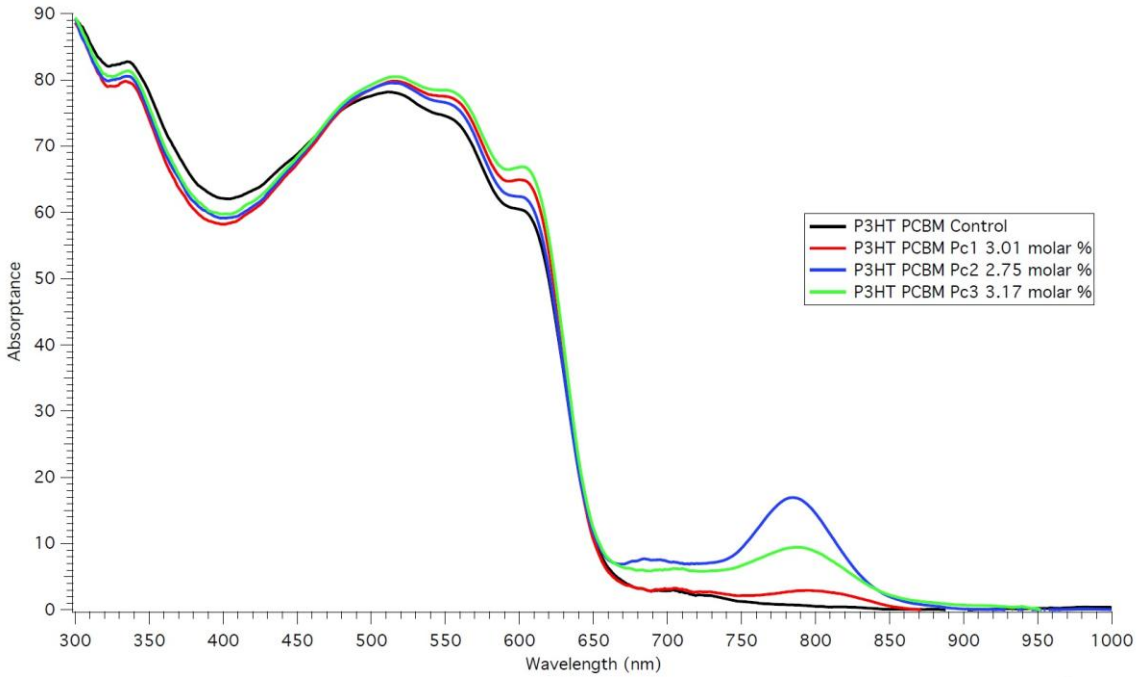

Figure 2-7. The absorptance spectra of P3HT:PC_{60}BM, P3HT:PC_{60}BM with Pc1 (3.01 molar percent), P3HT:PC_{60}BM with Pc2 (2.75 molar percent), and P3HT:PC_{60}BM with Pc3 (3.17 molar percent) on quartz substrates. Notice the Q-band peak in each sample containing a phthalocyanine.

Figure 2-8 illustrates the absorptance spectra for blends of neat P3HT with Pc1, Pc2, and Pc3 as well as blends of neat PC_{60}BM with Pc1, Pc2, and Pc3. The Q-band peak for samples containing neat P3HT and a phthalocyanine is shifted to the blue, but the peak for samples with neat PC_{60}BM and a phthalocyanine is shifted to the red. This observation is consistent with the data for neat P3HT with SiNc and neat PC_{60}BM with SiNc, as seen in Figure 2-3. The Q-band peak is shifted for samples containing phthalocyanines, due to the different morphologies of the neat films. Control absorptance spectra of neat P3HT and neat PC_{60}BM are shown in Figure 2-8

as well. There is only a single Q-band peak for the samples containing a phthalocyanine, which agrees with the EQE data.

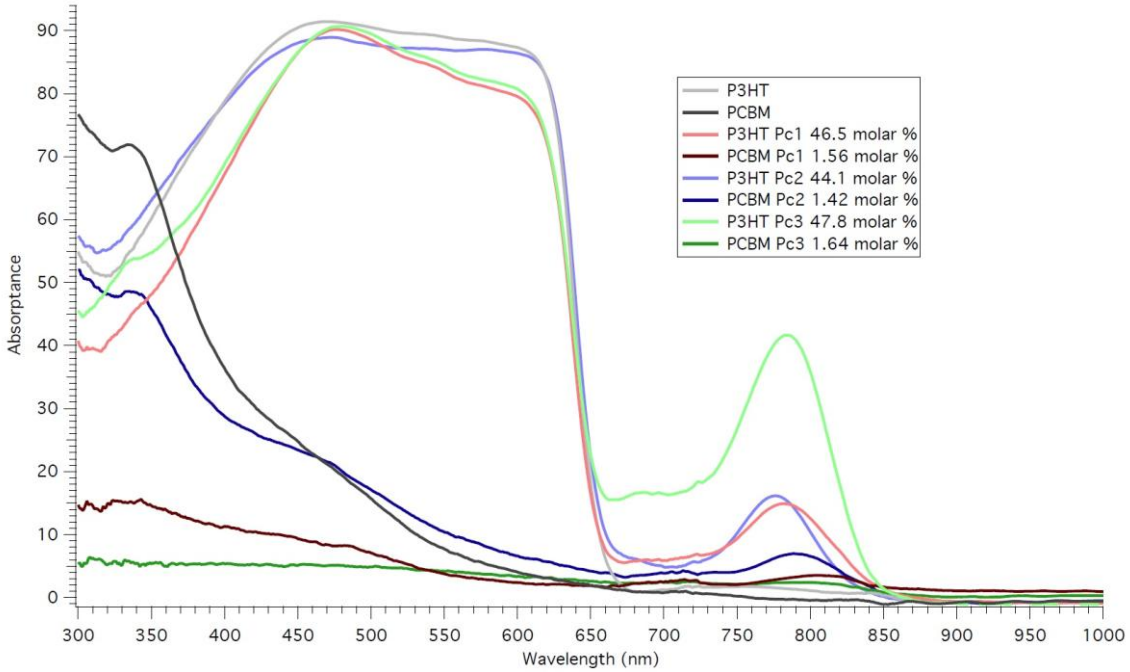

Figure 2-8. The absorptance spectra of neat P3HT, neat $PC_{60}BM$, neat P3HT with one of the phthalocyanines, and neat $PC_{60}BM$ containing one of the phthalocyanines on quartz substrates. There is a significant Q-band peak in the samples containing a phthalocyanine.

2.2 Current Density - Voltage Curves

Current density - voltage (JV) curves show the different combinations of current density and voltage that can be produced from a photovoltaic device. The current density is the current passed through the photovoltaic device per square centimeter. The voltage is the potential difference that is applied across the device. The power output of the photovoltaic device can be calculated by the product of the current density and voltage at a given point on the plot.

Inverted, organic solar cell devices were constructed in order to understand the impact of adding SiNc to the active layer. The structure of the inverted solar cell devices is as follows:

glass, indium tin oxide (ITO), zinc oxide (ZnO), ternary blend of P3HT, $PC_{60}BM$, and SiNc, molybdenum oxide (MoOx), and silver (Ag). The thickness of the ITO was approximately 150 nm, the ZnO layer was 30 nm, the active layer was roughly 250 nm (measured on a Dektak 8 Profilometer), the MoOx layer was 10 nm, and the Ag layer was 150 nm. The details of the construction of the solar cell devices will be discussed in the experimental section.

The JV curves were taken using a solar simulator under nitrogen atmosphere. JV curves for a P3HT:$PC_{60}BM$ solar cell device, a P3HT:$PC_{60}BM$ with SiNc (2.24 molar percent) solar cell device, and a P3HT:$PC_{60}BM$ containing SiNc (10.3 molar percent) solar cell device are present in Figure 2-9. Notice that the control device has a more ideal JV curve than the devices containing SiNc. An ideal JV curve is represented by two straight lines intersecting at the maximum power (P_{max}). The current density of an ideal organic solar cell device would be greater than 10 mA/cm^2 and the voltage would be in excess of 0.6 V. The control devices demonstrated average values of 0.600 V and 10.4 mA/cm^2, while the devices containing 2.24 molar percent of SiNc had average values of 0.574 V and 8.28 mA/cm^2 and the devices with 10.3 molar percent of SiNc had average values of 0.556 V and 8.40 mA/cm^2. Even though the current density and voltage decreased with increasing SiNc concentration, the fill factor and efficiency increased from the devices containing 2.24 molar percent of SiNc to the devices containing 10.3 molar percent of SiNc. This illustrates that not only are the devices functioning upon the addition of SiNc, but the efficiencies approach the values of the control devices and the fill factor values surpassed those of the control devices. The mismatch factor, as seen in Table 2-1, is the ratio between the experimental JV curve and the KG2-filtered Hamamatsu photodiode. The closer the mismatch factor is to one, the more similar the experimental data is to the calibration photodiode. The performance of the solar cell devices are summarized in Table 2-1.

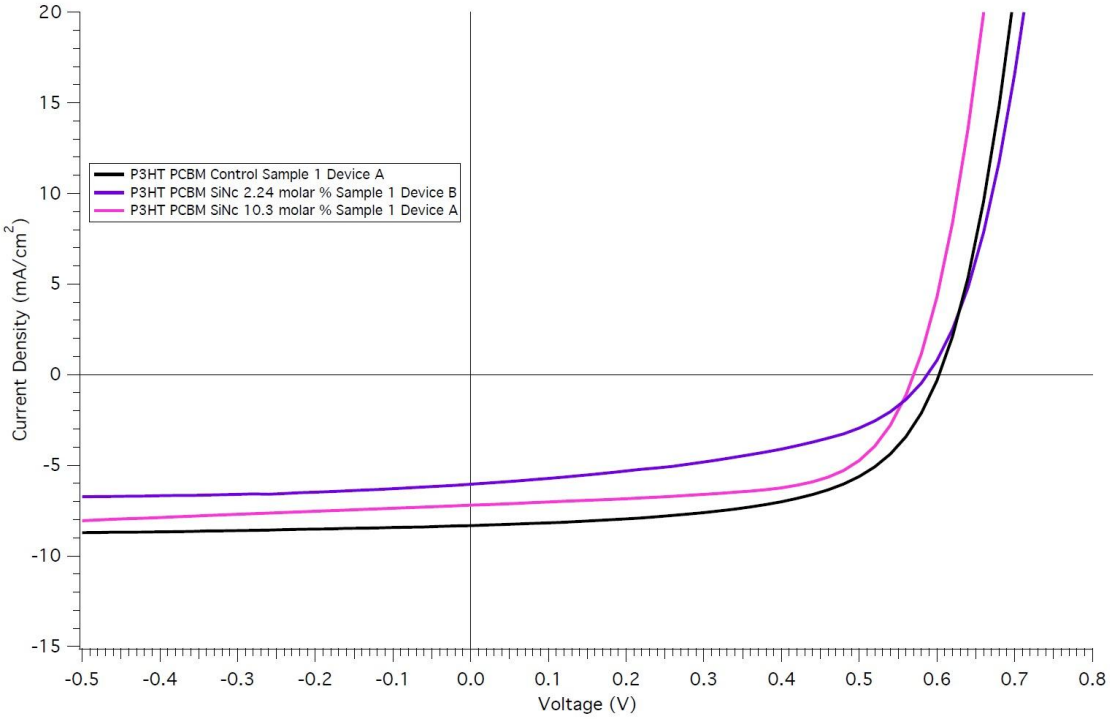

Figure 2-9. Current density - voltage (JV) curves of P3HT:PC_{60}BM, P3HT:PC_{60}BM with SiNc (2.24 SiNc molar percent), and P3HT:PC_{60}BM with SiNc (10.3 SiNc molar percent) devices. The full set of JV curves can be found in Figure A-1 in Appendix A.

SiNc Molar Conc. (%)	V_{OC} (V)	J_{SC} (mA/cm^2)	Fill Factor (%)	Efficiency (%)	Mismatch Factor
0	0.60026	10.421	57.498	2.8600	1.0435
2.24	0.57406	8.2803	43.270	1.4566	1.0167
10.3	0.55618	8.3984	60.444	2.4315	1.0113

Table 2-1. Average values for the current density - voltage (JV) curve data of P3HT:PC_{60}BM, P3HT:PC_{60}BM with SiNc (2.24 SiNc molar percent), and P3HT:PC_{60}BM with SiNc (10.3 SiNc molar percent) devices. The full set of data is in Table A-1 in Appendix A.

The JV curves for the photovoltaic devices of P3HT:PC_{60}BM, P3HT:PC_{60}BM with SiNc (2.24 molar percent), and P3HT:PC_{60}BM with SiNc (10.3 molar percent) were fitted using a procedure first developed by Zhang et al.[53] The procedure takes advantage of the Lambert W function, as well as some simplifications, in order to obtain values for the short-circuit current, open-circuit voltage, n factor, shunt resistance, and series resistance. The n factor, also known as

the ideality factor, is the ratio between the experimental JV curve and the ideal JV curve. If the experimental JV curve was perfectly ideal, then the n factor would equal one. Another fitting parameter, the shunt resistance, must be as large as possible, in order to avoid a different, less resistive path for current to flow. On the other hand, the series resistance needs to be as low as possible so that the fill factor, as well as the current, does not decrease significantly. The details of the fitting procedure can be found in the experimental section. Figure 2-10 demonstrates an example of the fitting procedure for experimental JV curves. In the figure, the data points are illustrated by black squares, while the fit is represented by the red line. The fit clearly does not properly match the curvature of the JV curve, however, it successfully fits the rest of the data points. It is difficult to match both the curvature and the extremes of the JV curve using this fitting procedure because the fit assumes an ideal diode. Since an experimental JV curve will never be ideal, the fitting procedure will not effectively fit all of the data points.

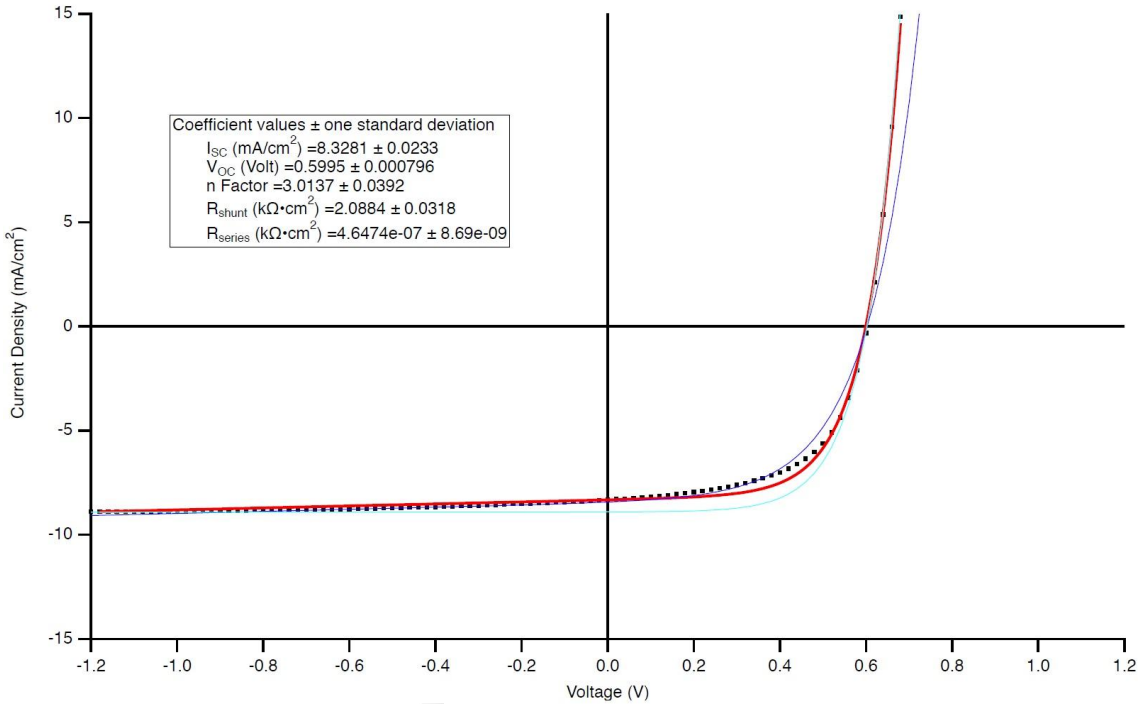

Figure 2-10. The fit of the current density - voltage (JV) curve of P3HT:PC_{60}BM solar cell device. The black squares represent the data points and the red line represents the fit.

Table 2-2 summarizes the average values for the n factor, shunt resistance, and series resistance of the solar cell devices. There are two clear trends occurring in the data seen below. The average n factor increases from the P3HT:PC_{60}BM control devices to the P3HT:PC_{60}BM with SiNc (2.24 molar percent) devices. However the average n factor value decreases, indicating a more ideal JV curve, for the P3HT:PC_{60}BM with SiNc (10.3 molar percent) devices. The average n factor of the 10.3 molar percent SiNc devices is even smaller than the n factor for the control devices. Second, the shunt resistance starts at a very high value for the control devices, but quickly decreases for the 2.24 molar percent SiNc devices, which shows that the addition of SiNc to the active layer created a lower performing solar cell device. The same idea is shown in the performance data of the devices, summarized in Table 2-1. The average shunt resistance does increase for the 10.3 molar percent SiNc devices, but does not reach, or exceed, the shunt resistance values of the control devices. Notice that a clear trend does not exist for the series resistance. The trends in the fitting parameters demonstrate that adding SiNc to the active layer creates a functioning solar cell device that under-performs the control devices. However, adding SiNc to solar cell devices does not destroy them completely, meaning that the SiNc molecules are ideally positioned in the active layer to absorb light and create charges.

SiNc Molar Conc. (%)	n Factor	R_{shunt} ($k\Omega \cdot cm^2$)	R_{series} ($k\Omega \cdot cm^2$)
0	2.9999	1.6046	2.1201e-6
2.24	4.0350	0.68476	5.0053e-6
10.3	2.5334	0.89770	2.7048e-6

Table 2-2. Average values for the fitting of the current density - voltage (JV) curves for P3HT:PC_{60}BM, P3HT:PC_{60}BM with SiNc (2.24 SiNc molar percent), and P3HT:PC_{60}BM with SiNc (10.3 SiNc molar percent) devices. The full set of data is in Table A-2 in Appendix A.

Active layers of solar cell devices were also created with Plexcore PV 1000 photoactive ink solution. Varying concentrations of SiNc were added to the PV 1000 ink solution in order to determine the effects of SiNc on an idealized system. Figure 2-11 illustrates four JV curves of solar cell devices containing the PV 1000 ink. The devices containing 2.24 molar percent and 10.3 molar percent of SiNc produce more ideal JV curves, as compared to the control device. However, once the molar percent of SiNc was increased to 31.4, the curvature of the JV curve was negatively affected. This is most likely due to unfavorable aggregation of SiNc molecules that disrupts the interaction of light with the photoactive ink or that inhibits the transport of charges to the electrodes. Table 2-3 summarizes the average values for the performance of these devices. The control devices had an average of 0.571 V and 8.53 mA/cm^2, while the addition of 2.24 molar percent of SiNc increased both the voltage and current density to 0.584 V and 9.82 mA/cm^2, respectively. The performance of the devices containing 10.3 molar percent of SiNc improved to 0.613 V and 9.544 mA/cm^2, which is a significant enhancement compared to the control devices. However, if the molar percent of SiNc is increased to 31.4, then the performance of the devices significantly decreases to 0.595 V and 8.89 mA/cm^2. The trend in the efficiencies of these photovoltaic devices follows an identical trend, since the most efficient device contains 10.3 molar percent of SiNc. The fill factor values are nearly identical for the control devices, the 2.24 molar percent SiNc devices, and the 10.3 molar percent SiNc devices. The fill factor decreases slightly for the 31.4 molar percent SiNc devices.

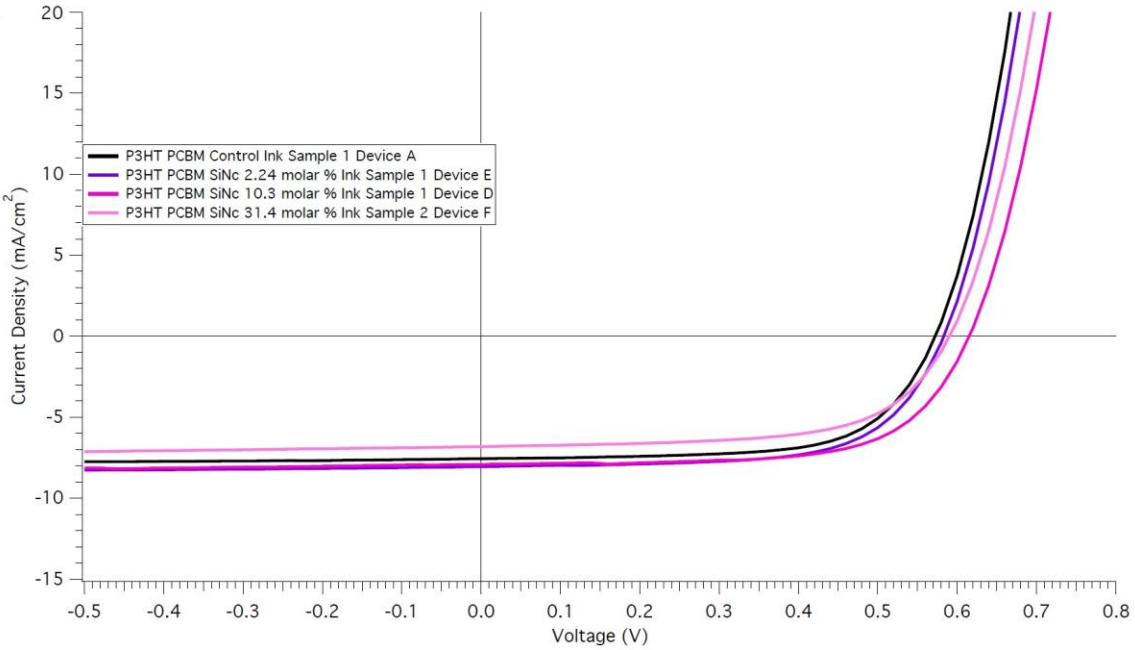

Figure 2-11. Current density - voltage (JV) curves of P3HT:PC_{60}BM PV 1000 ink, P3HT:PC_{60}BM PV 1000 ink with SiNc (2.24 molar percent), P3HT:PC_{60}BM PV 1000 ink with SiNc (10.3 molar percent), and P3HT:PC_{60}BM PV 1000 ink with SiNc (31.4 molar percent) devices. The full set of JV curves can be found in Figure A-2 in Appendix A.

SiNc Molar Conc. (%)	V_{OC} (V)	J_{SC} (mA/cm^2)	Fill Factor (%)	Efficiency (%)	Mismatch Factor
0	0.57118	8.5300	65.838	2.8459	1.0436
2.24	0.58430	9.8188	65.096	3.0454	1.0122
10.3	0.61310	9.5439	65.215	3.1400	0.97784
31.4	0.59538	8.8920	62.698	2.5419	0.98384

Table 2-3. Average values for the current density - voltage (JV) curve data of P3HT:PC_{60}BM PV 1000 ink, P3HT:PC_{60}BM PV 1000 ink with SiNc (2.24 molar percent), P3HT:PC_{60}BM PV 1000 ink with SiNc (10.3 molar percent), and P3HT:PC_{60}BM PV 1000 ink with SiNc (31.4 molar percent) devices. The full set of data is in Table A-3 in Appendix A.

The JV curves of devices containing PV 1000 ink in the active layer were fitted in order to determine the n factor, shunt resistance, and series resistance. The average values for these parameters are summarized in Table 2-4. The n factor for the devices containing SiNc are slightly larger than the control devices, but only by 0.21 to 0.25, which is not a significant margin. The average values for the shunt resistance of these devices decreased with increasing

the concentration of SiNc, which is interesting because the device with 10.3 molar percent of SiNc was the best performing device. However, there is a noticeable trend for the series resistance. As the SiNc concentration is increased, the series resistance decreased, indicating a better performing device.

SiNc Molar Conc. (%)	n Factor	R_{shunt} ($k\Omega \cdot cm^2$)	R_{series} ($k\Omega \cdot cm^2$)
0	2.5906	3.0077	2.2425e-5
2.24	2.8493	2.9183	1.0258e-5
10.3	2.8207	2.2024	1.2622e-5
31.4	2.8037	1.6018	1.3384e-6

Table 2-4. Average values for the fitting of the current density - voltage (JV) curves for P3HT:PC_{60}BM PV 1000 ink, P3HT:PC_{60}BM PV 1000 ink with SiNc (2.24 molar percent), P3HT:PC_{60}BM PV 1000 ink with SiNc (10.3 molar percent), and P3HT:PC_{60}BM PV 1000 ink with SiNc (31.4 molar percent) devices. The full set of data is in Table A-4 in Appendix A.

Solar cell devices were also constructed using a ternary blend of P3HT:PC_{60}BM containing either Pc1, Pc2, or Pc3. The JV curves for these devices, as well as a control device, are shown in Figure 2-12. The JV curves for devices containing a phthalocyanine are not as ideal as the curve for the control device, signifying that adding a phthalocyanine to the active layer of these photovoltaic devices decreases their performance. The average values for the performance of these devices are summarized in Table 2-5. The control devices have an average voltage of 0.600 V, while the voltage of devices containing a phthalocyanine is significantly lower, ranging from 0.529 to 0.541 V. Current density in devices with Pc1, Pc2, or Pc3 is also lower compared to the control device. Even though the fill factor and efficiency of devices with phthalocyanines are lower than the control, the devices are still functioning after adding these small molecules to the active layer. This supports the idea that adding small molecules, with the appropriate energy levels, to solar cell devices will still produce functioning products.

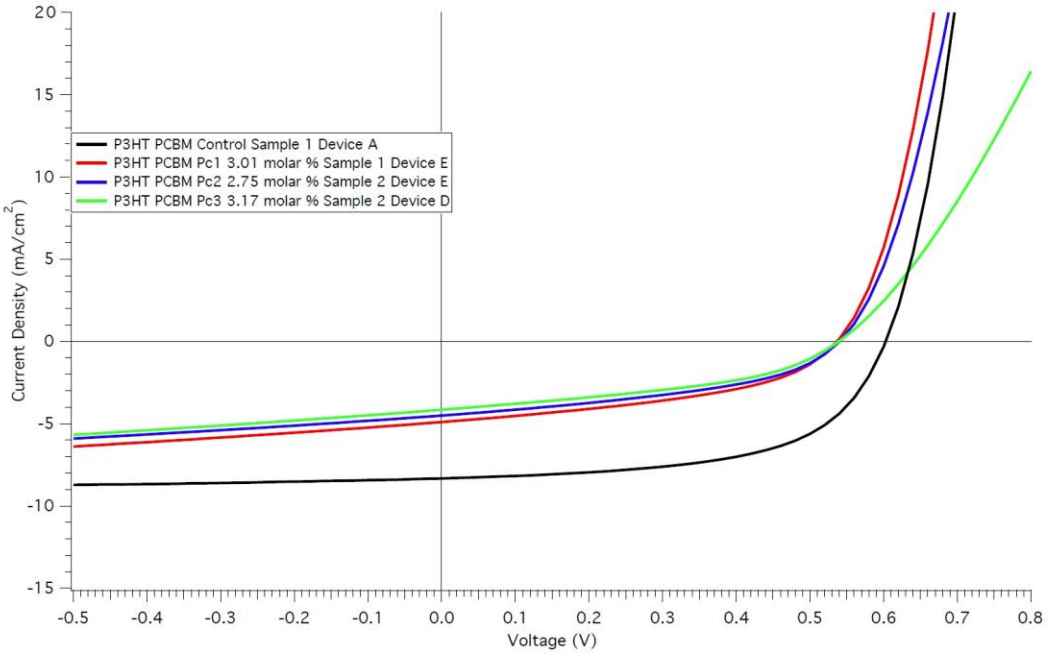

Figure 2-12. Current density - voltage (JV) curves of P3HT:$PC_{60}BM$, P3HT:$PC_{60}BM$ with Pc1 (3.01 molar percent), P3HT:$PC_{60}BM$ with Pc2 (2.75 molar percent), and P3HT:$PC_{60}BM$ with Pc3 (3.17 molar percent) devices. The full set of JV curves can be found in Figure A-3 in Appendix A.

Phthalocyanine Molar Conc.	V_{OC} (V)	J_{SC} (mA/cm^2)	Fill Factor (%)	Efficiency (%)	Mismatch Factor
Control (0 %)	0.60026	10.421	57.498	2.8600	1.0435
Pc1 (3.01 %)	0.52933	7.9915	42.029	1.0827	1.0434
Pc2 (2.75 %)	0.54090	8.0851	43.031	1.0473	1.0311
Pc3 (3.17 %)	0.53854	7.2832	42.135	0.93317	1.0212

Table 2-5. Average values for the current density - voltage (JV) curve data of P3HT:$PC_{60}BM$, P3HT:$PC_{60}BM$ with Pc1 (3.01 molar percent), P3HT:$PC_{60}BM$ with Pc2 (2.75 molar percent), and P3HT:$PC_{60}BM$ with Pc3 (3.17 molar percent) devices. The full set of data is in Table A-5 in Appendix A.

The same fitting procedure was used on the JV curves of devices containing either Pc1, Pc2, or Pc3, in order to quantify the parameters of the curve. The average values from the fitting procedure are in Table 2-6. The trend for the n factor is interesting because it improves for devices with Pc1 and Pc2, while it is significantly worse for devices with Pc3. The n factor is very poor for devices containing Pc3 due to the non-ideality of the JV curve, as seen in Figure 2-

12. While the shunt resistance of devices containing a phthalocyanine is lower than the control device, the series resistance does not show a discernible trend. The results of the fitting procedure are in agreement with the data from the performance of the solar cell devices, since the devices with a phthalocyanine under-perform the control devices. However, the proof of concept is still valid since adding one of the three phthalocyanines produced a functioning solar cell device.

Phthalocyanine Molar Conc.	n Factor	R_{shunt} ($k\Omega \cdot cm^2$)	R_{series} ($k\Omega \cdot cm^2$)
Control (0 %)	2.9999	1.6046	2.1201e-6
Pc1 (3.01 %)	2.5866	0.30551	5.8165e-7
Pc2 (2.75 %)	2.8203	0.36452	2.7751e-6
Pc3 (3.17 %)	5.7009	0.39618	6.2216e-7

Table 2-6. Average values for the fitting of the current density - voltage (JV) curves for P3HT:PC_{60}BM, P3HT:PC_{60}BM with Pc1 (3.01 molar percent), P3HT:PC_{60}BM with Pc2 (2.75 molar percent), and P3HT:PC_{60}BM with Pc3 (3.17 molar percent) devices. The full set of data is in Table A-6 in Appendix A.

2.3 External Quantum Efficiency

External quantum efficiency (EQE) is the ratio between extracted free charges and incident photons in a photovoltaic device. An EQE spectrum depends on the collection of free charges by the device and the absorption of the active layer. Ideally, an EQE spectrum would have a box shape, however, recombination of free charges decreases the efficiency. EQE spectra also take into account optical losses from transmission and reflection of the photovoltaic device. After the performance of the photovoltaic devices was measured, the devices were transferred to the EQE system, under nitrogen atmosphere. The EQE system is powered by a monochromatic light source, which scans the devices from 300 nm to 1000 nm at an interval of 5 nm.

Figure 2-13, as seen below, demonstrates a plot of the EQE data for three solar cell devices: a control device of P3HT:PC_{60}BM, a device of P3HT:PC_{60}BM containing 2.24 molar

percent of SiNc, and a device of P3HT:$PC_{60}BM$ with 10.3 molar percent of SiNc. The EQE data for the control device reaches a maximum of 75%, which is significantly higher than either device containing SiNc. A device that peaks at 75% demonstrates that the device has been highly optimized and that it has a large current density. The device with 2.24 molar percent of SiNc shows a decrease, as compared to the control device, in the region where $PC_{60}BM$ primarily absorbs (400-500 nm) and where P3HT absorbs the strongest (550-600 nm). This device has a decrease of nearly 20% in the $PC_{60}BM$ region and a decrease of 25% in the P3HT region, which demonstrates that the addition of SiNc is negatively affecting the interaction of light with P3HT and $PC_{60}BM$. The device containing 10.3 molar percent of SiNc also has a decrease in the P3HT and $PC_{60}BM$ regions, 25% for both areas. The decrease in these regions may be due to unfavorable aggregation of naphthalocyanine molecules.

Even though the devices with SiNc show a decrease in the EQE spectrum from 400 nm to 600 nm, there is a significant response in the Q-band, as seen in Figure 2-13. Interestingly, there is a second peak that appears at higher molar percents for SiNc. Both devices containing SiNc have a strong peak at 785 nm in the EQE spectrum, but the 10.3 molar percent SiNc device has a second Q-band peak at 825 nm. Both of these peaks have a significant response in the EQE response, reaching over 20% for the peak at 785 nm and 17% for the peak at 825 nm. Average values for the EQE spectrum are summarized in Table 2-7.

As mentioned in the previous section, the absorptance spectra for these devices did not have a second Q-band peak. Absorptance spectra were also taken for SiNc in neat P3HT and in neat $PC_{60}BM$, in order to determine if the second Q-band peak would appear. Figure 2-3 demonstrates that a second Q-band peak was not present, which concludes that there is no interaction between SiNc and neat P3HT or between SiNc and neat $PC_{60}BM$. A possible

explanation for the appearance of the second Q-band peak in the EQE spectrum of devices containing at least 10.3 molar percent of SiNc is the formation of aggregates in the bulk heterojunction. As the concentration of SiNc increases, SiNc molecules begin to interact with each other at a higher frequency, causing aggregates to form. These clusters of molecules may be J-aggregates or they could be forming through covalent interactions. However, there is no way to decisively prove these ideas, but they are possible explanations to an interesting phenomenon.

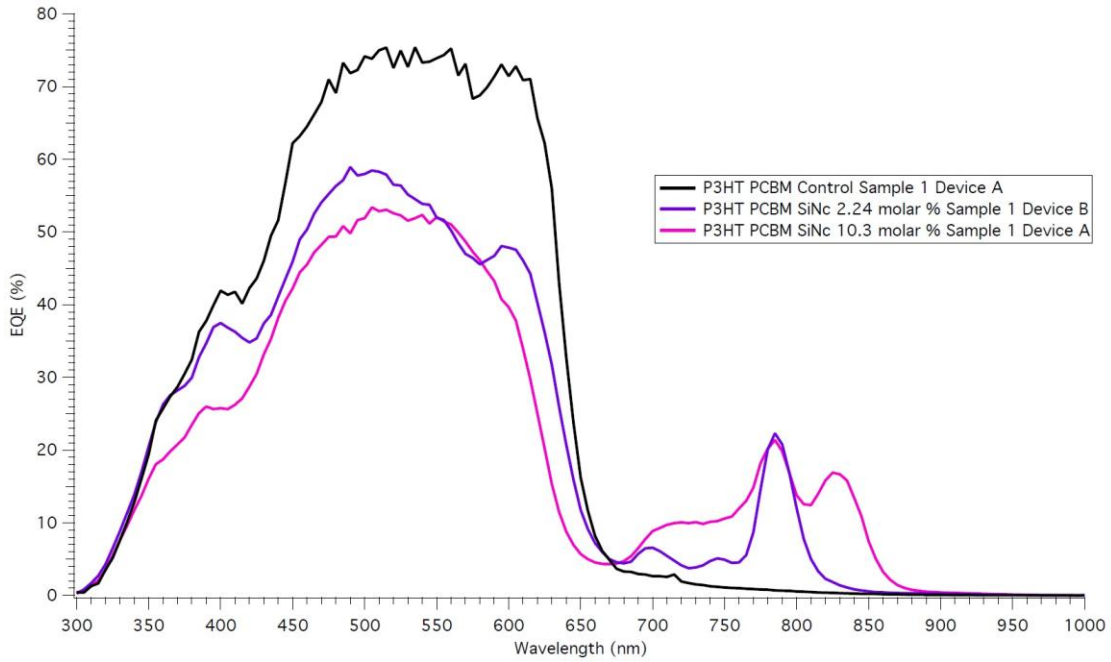

Figure 2-13. External quantum efficiency (EQE) spectra of P3HT:PC_{60}BM, P3HT:PC_{60}BM with SiNc (2.24 SiNc molar percent), and P3HT:PC_{60}BM with SiNc (10.3 SiNc molar percent) devices. The full set of spectra can be found in Figure B-1 in Appendix B.

SiNc Molar Conc. (%)	EQE at 500 nm (%)	EQE at 785 nm (%)	EQE at 800 nm (%)	EQE at 825 nm (%)
0	73.162	0.71815	0.57925	0.37028
2.24	58.088	21.709	11.198	1.7784
10.3	53.398	22.023	14.716	17.776

Table 2-7. Average values from the external quantum efficiency (EQE) data of P3HT:PC_{60}BM, P3HT:PC_{60}BM with SiNc (2.24 SiNc molar percent), and P3HT:PC_{60}BM with SiNc (10.3 SiNc molar percent) devices. The data for the specific devices can be found in Table B-1 in Appendix B.

SiNc was added to an idealized system containing PV 1000 photoactive ink, which is a highly optimized solution designed by Plexcore®. Figure 2-14 illustrates the EQE spectra of four devices that used PV 1000 ink in the active layer. The control device of the photoactive ink and the device with 2.24 molar percent of SiNc reached a maximum of 60%. However, devices containing higher concentrations of SiNc showed a slight decrease between 400 nm and 600 nm. The device with 10.3 molar percent of SiNc decreased from a maximum of 60% to 55%, compared to the control device. While the device containing 31.4 molar percent of SiNc decreased from a maximum of 60% to 53%. This is one of the main differences between devices with PV 1000 ink and P3HT:$PC_{60}BM$.

There is only one Q-band peak in the EQE spectra of devices that use the PV 1000 photoactive ink, even if the molar concentration of SiNc is increased to 31.4%. Even though there isn't a second Q-band peak, there is a much larger response at 785 nm, as compared to the EQE spectra of devices with P3HT:$PC_{60}BM$. Table 2-8 summarizes the average values for these devices. The lowest molar percent of SiNc already has a Q-band peak that surpasses the peak for the highest molar percent of SiNc in a device, in Figure 2-13. If the molar concentration of SiNc is increased to 10.3%, the Q-band peak nearly reaches 45%. However, when SiNc is increased to 31.4 molar percent, the Q-band peak decreases slightly to 37%. This may be due to the aggregation problem seen in devices that used P3HT and $PC_{60}BM$, or it may be due to a significant decrease in the absorption of the PV 1000 ink. The other main difference is the absence of a second Q-band peak in Figure 2-14. Even if SiNc is increased to 31.4 molar percent, a second Q-band peak does not appear in the EQE spectrum. This is most likely due to the additives in the PV 1000 photoactive ink that disrupt significant aggregation of SiNc molecules in the active layer.

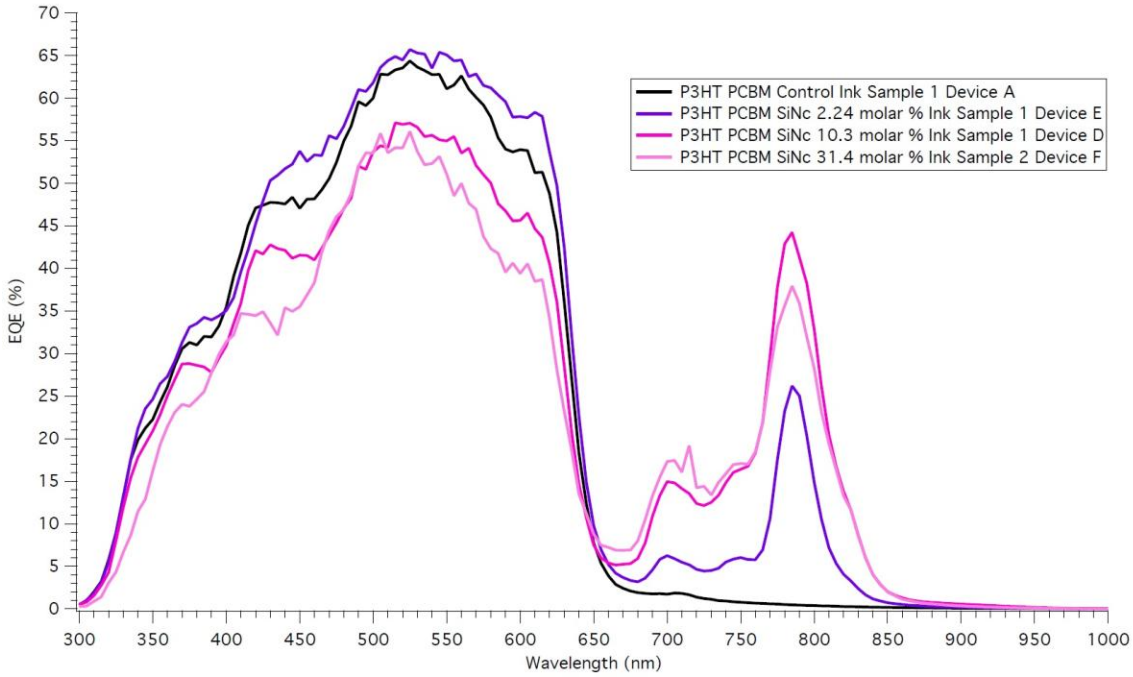

Figure 2-14. External quantum efficiency (EQE) spectra of P3HT:PC_{60}BM PV 1000 ink, P3HT:PC_{60}BM PV 1000 ink with SiNc (2.24 molar percent), P3HT:PC_{60}BM PV 1000 ink with SiNc (10.3 molar percent), and P3HT:PC_{60}BM PV 1000 ink with SiNc (31.4 molar percent) devices. The full set of spectra can be found in Figure B-2 in Appendix B.

SiNc Molar Conc. (%)	EQE at 500 nm (%)	EQE at 785 nm (%)	EQE at 800 nm (%)	EQE at 825 nm (%)
0	60.006	0.48290	0.38640	0.26725
2.24	62.540	25.430	14.574	3.2065
10.3	53.152	44.192	33.145	11.824
31.4	54.106	37.343	28.190	11.770

Table 2-8. Average values from the external quantum efficiency (EQE) of P3HT:PC_{60}BM PV 1000 ink, P3HT:PC_{60}BM PV 1000 ink with SiNc (2.24 molar percent), P3HT:PC_{60}BM PV 1000 ink with SiNc (10.3 molar percent), and P3HT:PC_{60}BM PV 1000 ink with SiNc (31.4 molar percent) devices. The data for the specific devices can be found in Table B-2 in Appendix B.

Figure 2-15 illustrates the EQE spectra of a control device and devices containing one of the phthalocyanine molecules. The control device reaches a maximum of 75% and does not have a Q-band peak, as expected. However, the devices with Pc1 or Pc2 only reach a maximum of 55%, significantly less than the control device. Devices with Pc3 are even lower, reaching a maximum of only 45%. Table 2-9 shows the average values for these devices. Even though

devices containing a phthalocyanine molecule have decreases in the P3HT and $PC_{60}BM$ regions, they have Q-band peaks at 785 nm. The response at 785 nm is not as significant as the response seen in devices with SiNc. However, the data seen below supports the theory that adding a small molecule into the bulk heterojunction will still result in a functioning device, if the energy levels of the molecule are appropriate.

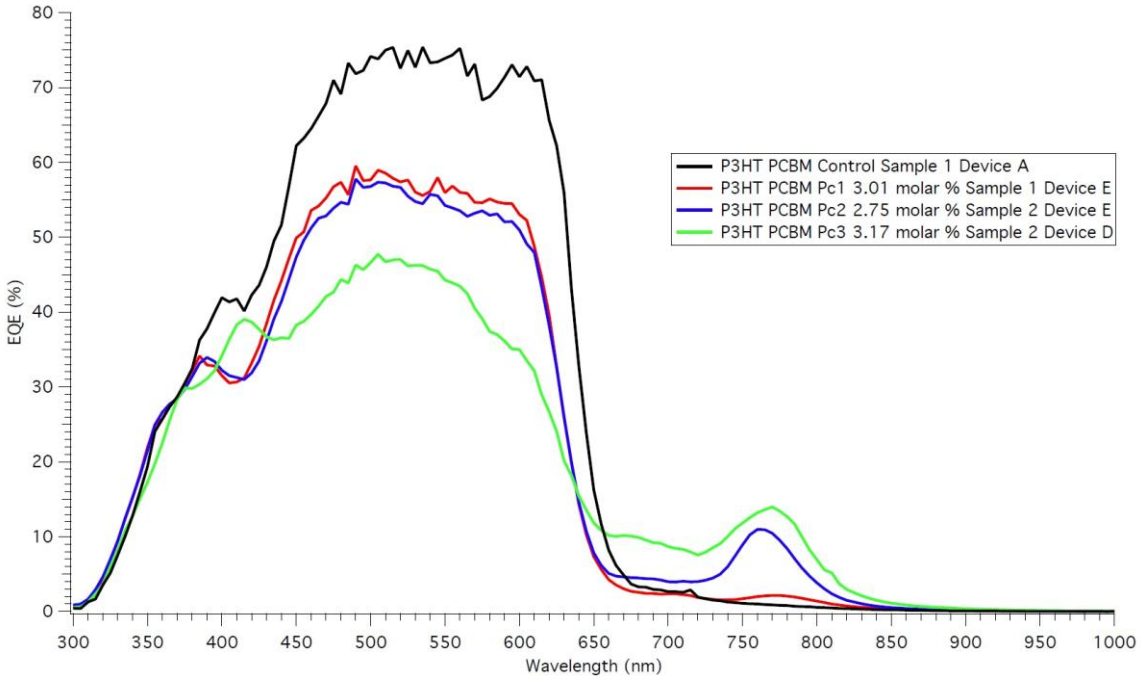

Figure 2-15. External quantum efficiency (EQE) spectra of P3HT:$PC_{60}BM$, P3HT:$PC_{60}BM$ with Pc1 (3.01 molar percent), P3HT:$PC_{60}BM$ with Pc2 (2.75 molar percent), and P3HT:$PC_{60}BM$ with Pc3 (3.17 molar percent) devices. The full set of spectra can be found in Figure B-3 in Appendix B.

Phthalocyanine Molar Conc.	EQE at 500 nm (%)	EQE at 785 nm (%)	EQE at 800 nm (%)	EQE at 825 nm (%)
Control (0 %)	74.161	0.71815	0.57925	0.37028
Pc1 (3.01%)	58.121	1.9591	1.4015	0.67073
Pc2 (2.75%)	56.170	7.0451	3.7554	1.2678
Pc3 (3.17%)	46.271	11.663	6.9514	2.5544

Table 2-9. Average values from the external quantum efficiency (EQE) of P3HT:$PC_{60}BM$, P3HT:$PC_{60}BM$ with Pc1 (3.01 molar percent), P3HT:$PC_{60}BM$ with Pc2 (2.75 molar percent),

and P3HT:$PC_{60}BM$ with Pc3 (3.17 molar percent) devices. The data for the specific devices can be found in Table B-3 in Appendix B.

2.4 Conclusion

To summarize, the addition of SiNc to the active layer results in a functioning solar cell device that performs slightly worse than a control device. The voltage, current density, and efficiency of devices with SiNc are less than the control device, comprised of P3HT:$PC_{60}BM$. However, adding SiNc to a device containing PV 1000 photoactive ink produces a device that has higher current density, voltage, and efficiency compared to a control device. Adding one of the three phthalocyanines to a device with P3HT:$PC_{60}BM$ decreases the performance, but still results in a functioning device.

The EQE data demonstrates that the performance decreases when SiNc is added to a device containing P3HT:$PC_{60}BM$ and shows that a second Q-band peak appears at high molar concentrations of SiNc. This second peak is most likely due to aggregation through the formation of J-aggregates or covalent interaction between SiNc molecules. However, the EQE data for the PV 1000 ink devices does not have a second Q-band peak, possibly due to the components in the photoactive ink. The EQE data for devices with one of the phthalocyanines illustrates that the performance decreases compared to the control device and that a Q-band peak appears at 785 nm.

The energy levels of SiNc, relative to those of P3HT and $PC_{60}BM$, can not only determine whether a solar cell device will function, but can describe the morphology of the active layer. Figure 2-16 shows SiNc positioned in a P3HT-rich area of the bulk heterojunction. If the SiNc molecule is photoexcited, an electron is promoted to the excited state of SiNc. Since an electron is excited, a hole sits in the ground state of SiNc. The hole is able to transfer to

P3HT, however, the electron in the excited state of SiNc is not able to transfer to a lower energy state. Therefore, SiNc acts as an electron trap in this situation. Figure 2-17 shows SiNc in a $PC_{60}BM$-rich area of the active layer. Once SiNc is excited by a photon, an electron is promoted to the excited state. Then, the electron can transfer to $PC_{60}BM$'s excited state, which is positioned at a lower energy. However, the hole on SiNc cannot be transferred to a higher energy state. In this case, SiNc acts as a hole trap. If SiNc was dispersed in a P3HT-rich or a $PC_{60}BM$-rich region in a solar cell device, then the device would not be functional. This is due to the fact that charges would not be able to reach their respective electrodes. Due to this reasoning, SiNc will most likely be positioned in the amorphous phase of P3HT and $PC_{60}BM$, since SiNc will be able to facilitate in the transport of electrons and holes in this environment.

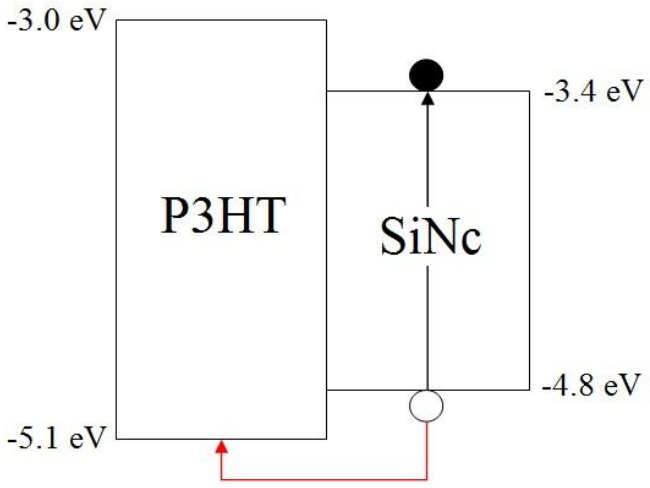

Figure 2-16. Energy level diagram for SiNc dispersed in P3HT. The black line represents photoexcitation, the filled circle represents an electron, the open circle represents a hole, and the red line represents the pathway for a hole. The oxidation and reduction potentials are reported vs. vacuum.[51,54,55]

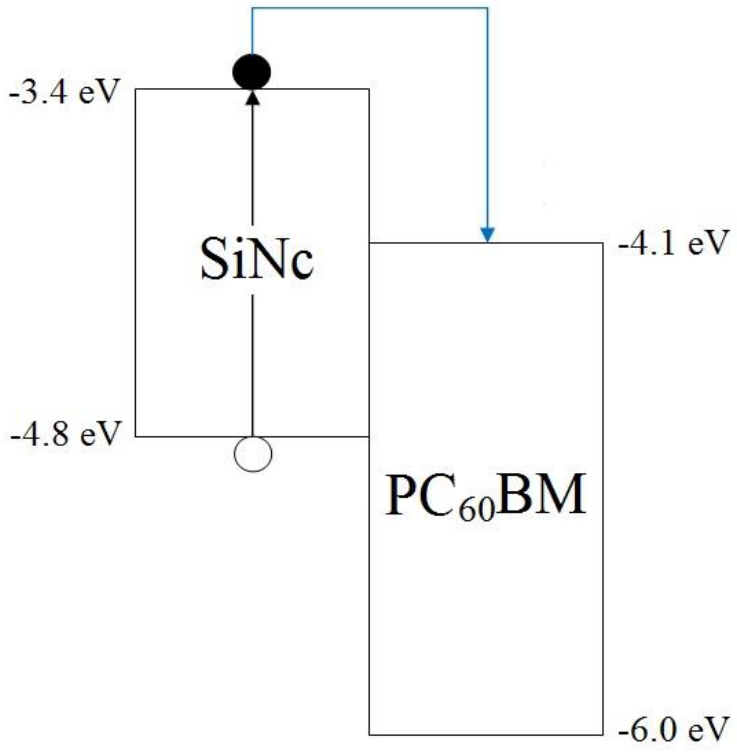

Figure 2-17. Energy level diagram for SiNc dispersed in $PC_{60}BM$. The black line represents photoexcitation, the filled circle represents an electron, the open circle represents a hole, and the blue line represents the pathway for an electron. The oxidation and reduction potentials are reported vs. vacuum.[51,54,55]

2.5 Experimental

2.5.1 Materials

The regio-regular sample of P3HT was purchased from Rieke Metals, Inc. (#4002-E, M_w=50,000 g/mol, regio-regularity of 93%). The sample of $PC_{60}BM$ was purchased from Nano-C (#KB121112, purity of 99.5%). The SiNc sample was obtained from Alan Sellinger, at the Colorado School of Mines, and the phthalocyanine samples (Pc1, Pc2, and Pc3) were acquired from Devens Gust, at Arizona State University. The Plexcore PV 1000 photoactive ink solution was purchased from Plextronics (#13-12864, 0.050 L). The 1,2-dichlorobenzene solution was

purchased from Sigma-Aldrich (#SHBC7846V, anhydrous, 99%). Tetrahydrofuran (THF) was obtained from Sigma-Aldrich (#SHBD6146V, anhydrous, ≥99.9%) and diethyl zinc (DEZ) solution was purchased from Sigma-Aldrich (#SHBC4865V). The standard indium-tin-oxide (ITO) on 1737 glass substrates were purchased from Thin Film Devices, Inc. Acetone was obtained from J.T. Baker (#53066, FW: 58.080) and isopropanol cleanroom LP (IPA) was purchased from KMG (#305BE3247). The Liquinox® detergent was purchased from Alconox (#1232). The molybdenum (VI) oxide (MoOx) sample was obtained from Strem Chemicals (#1313-27-5, FW: 143.95, 99.999%) and the silver sample (Ag) was purchased from R.D. Mathis Company, Evaporation Sources & Materials (#AG59659101, 99.99%, pellets). All of the samples were used as received.

2.5.2 Solar Cell Device Fabrication

Approximately 25.00 mg of P3HT and $PC_{60}BM$ were weighed out on a Sartorius digital scale (#CP255D, max 220g) and then transferred to a Fisherbrand vial (#03-339-21B, 15 mm x 45 mm). A Thermo Scientific Septa cap (#C4015-10, white virgin PTFE) was inserted into the lid of the Fisherbrand vial in order to create a better seal. A VWR® Spinbar® micro stir bar (#58948-353) was then added to the vial so the sample could be stirred on a Scilogex hot plate (#MS-H-Pro). The P3HT and $PC_{60}BM$ samples were dissolved in 1,2-dichlorobenzene to make a concentration of 50 mg/mL. A separate sample, containing SiNc, was dissolved in 1,2-dichlorobenzene to a concentration of 50 mg/mL as well. These solutions were kept on a hotplate in a MBRAUN glove box (Unilab, #UL03-121), stirring at 400 revolutions per minute (rpm) and 115 °C, overnight. The SiNc solution was then added to the P3HT:$PC_{60}BM$ solution in varying amounts in order to control the final concentration in the ternary blend. The ternary solution was left on a hot plate under nitrogen atmosphere, stirring at 400 rpm and 65°C, for two hours. A

solution of zinc oxide (ZnO) was prepared by mixing 3 mL of THF and 1 mL of DEZ. This solution was left on a hotplate in a Fisher Hamilton fume hood (Safeaire, #54-L), stirring at 800 rpm and 25°C, for at least two hours.

Organic solar cell devices were constructed using patterned indium-tin-oxide (ITO) on glass substrates. The substrates were cleaned with a solution of deionized (DI) water and Liquinox® detergent. The resistivity of the substrates was measured (Amprobe, #35XP-A) after the ITO was hand scrubbed with the water and detergent solution. The resistivity of each substrate was in the range of 30 to 40 Ohms (Ω). The substrates then went through a sonication process (Cole-Parmer, #8893) for 10 minutes in the water and detergent solution. The substrates were rinsed with DI water and then sonicated for 5 minutes in DI water. This process of rinsing and sonicating was repeated for a total of three times. The substrates were then dried with a pressured nitrogen stream before being put in acetone and sonicated for 20 minutes. Substrates were dried with nitrogen and placed in isopropanol and sonicated for 20 minutes. Afterwards, the substrates were dried with nitrogen again before being placed in the UV ozone plasma cleaner (Technics West Inc., #500-II) for 15 minutes.

The cleaned substrates were spin-coated with approximately 250 μL of ZnO at 5000 rpm for 60 seconds. Before the ZnO layer was allowed to dry completely, the ZnO was scratched off the six pixels and edges of the patterned ITO with a razor. This step ensures that the circuit is completed when the active layer is deposited. The previous steps were carried out in a laminar flow hood (Fisher Hamilton, Safeaire, #54-L). The substrates were then transferred to a nitrogen atmosphere and dried on a hot plate at 120 °C for 20 minutes. The active layer was deposited onto the ZnO layer by spin coating at 900 rpm for 45 seconds. The thickness of the active layer was measured on a Dektak 8 Advanced Development Profiler (Veeco). The active layers were all

approximately 250 nm thick. After the active layer was deposited, the substrates were left in a covered Petri dish to slowly dry overnight. When the samples were completely dry, the active layer was scraped off the edges and contacts of the ITO using a razor. Then the samples were annealed on a hot plate at 110 °C for 10 minutes. After annealing, the substrates were transferred to an Evovac-600 Vacuum Evaporation System - Glove box integrated (system 00660), made by Angstrom Engineering, in order to deposit the molybdenum oxide (MoOx) and silver (Ag) layers. The MoOx layer was deposited below $1x10^{-8}$ torr and was 10 nm thick. The subsequent Ag layer was deposited below $1x10^{-8}$ torr and was 150 nm thick. The finished devices were immediately transferred and stored under a nitrogen atmosphere.

2.5.3 Absorptance of Thin Films

The thin films, on quartz substrates, were placed in a Shimadzu UV-3600 UV-VIS-NIR Spectrophotometer with an external ISR-3100 integrating sphere attachment, in order to obtain the absorptance spectrum. A picture and diagram of the integrating sphere attachment is shown in Figure 2-18. The transmittance (T) and reflectance (R) of the thin film were measured in the integrating sphere so that the reflection of the sample can be separated from the absorptance. The reflection is due to the substrate and the composition of the thin film. In order to properly measure the absorptance of the thin film, there is a correction for the mirror inside the integrating sphere. After the reflectance is corrected, the following equation is used to calculate the absorptance (A):

$$A = 100 - T - R(corrected)\ . \quad (1)$$

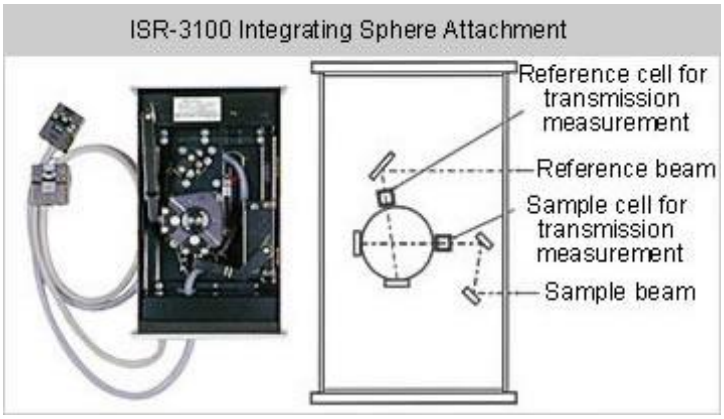

Figure 2-18. A picture and diagram of the integrating sphere used to calculate the absorptance of thin films through the measurement of trasmittance and reflectance.

2.5.4 Solar Cell Device Characterization

Characterization of the completed devices were carried out in a nitrogen atmosphere. A solar simulator, using AM1.5G solar spectrum from a xenon (Xe) arc lamp, was used in order to obtain the current density - voltage (JV) curves. A KG2-filtered Hamamatsu photodiode was used as a calibration, in order to minimize the spectral mismatch during characterization. After the JV curves were obtained, the external quantum efficiency (EQE) spectra were collected using a monochromatic light source and scanning at an interval of 5 nm.

The fitting procedure utilized to fit the JV curves from the solar simulator was first devised by Zhang et al.[53] The fitting procedure starts with the single-diode model, which gives an equation for the current and voltage, as seen below:

$$I = I_0 \left(exp \left(\frac{q(V - R_s I)}{n k_B T} \right) - 1 \right) + \frac{V - R_s I}{R_{sh}} - I_{ph} \quad (2)$$

where I_0 is the saturation current, q is the charge of an electron, V is the voltage, R_S is the series resistance, I is the current, n is the ideality factor (also known as the n factor), k_B is the Boltzmann constant, T is the temperature, R_{sh} is the shunt resistance, and I_{ph} is the photocurrent.

However, this equation is not analytically solvable. Therefore, Zhang et al. took advantage of the Lambert W function in order to make the equation solvable:

$$I = \frac{V}{R_s} - \frac{R_{sh}(R_s I_{ph} + R_s I_0 + V)}{R_s(R_{sh} + R_s)} + \frac{nk_BT}{qR_s} lambertw \times \left[\frac{qR_s I_0 R_{sh}}{(R_s + R_{sh})nk_BT} exp\left(\frac{R_{sh}q(R_s I_{ph} + R_s I_0 + V)}{nk_BT(R_s + R_{sh})}\right)\right] \quad (3)$$

where lambertw is the Lambert W function. This equation is able to be used because Equation 2 only has one exponential term, which made the derivation much simpler. However, Equation 3 cannot be used for the fitting procedure due to the large errors introduced by the difference between I_0 and I_{ph}.

Using initial conditions for current and voltage, Equations 4 and 5 can be derived from Equation 2. In order to derive Equation 4, the initial conditions are: I = - I_{SC} and V = 0. At these initial conditions, the device is said to be at short-circuit condition. Equation 5 is derived by using the initial conditions: I = 0 and V = V_{OC}. This is also known as the open-circuit condition.

$$-I_{SC} = I_0\left\{exp\left(\frac{qR_s I_{SC}}{nk_BT}\right) - 1\right\} + \frac{R_s I_{SC}}{R_{sh}} - I_{ph} \quad (4)$$

$$0 = I_0\left\{exp\left(\frac{qV_{OC}}{nk_BT}\right) - 1\right\} + \frac{V_{OC}}{R_{sh}} - I_{ph} \quad (5)$$

After Equations 4 and 5 have been determined, they can be combined to derive Equations 6 and 7, as seen below:

$$I_0 = \frac{\left(I_{SC} + \frac{R_s I_{SC} - V_{OC}}{R_{sh}}\right)exp\left(\frac{-qV_{OC}}{nk_BT}\right)}{1 - exp\left(\frac{q(R_s I_{SC} - V_{OC})}{nk_BT}\right)} \quad (6)$$

$$I_{ph} + I_0 = \frac{I_{SC} + \frac{R_s I_{SC} - V_{OC}}{R_{sh}}}{1 - exp\left(\frac{q(R_s I_{SC} - V_{OC})}{nk_BT}\right)} + \frac{V_{OC}}{R_{sh}} \ . \quad (7)$$

If the equations for I_0 and $I_{ph} + I_0$ are substituted into Equation 3, Equation 8 can be derived:

$$I = \frac{V}{R_s} - \frac{R_{sh}\left(R_s\frac{I_{SC}+\frac{R_sI_{SC}-V_{OC}}{R_{sh}}}{1-exp\left(\frac{q(R_sI_{SC}-V_{OC})}{nk_BT}\right)}+\frac{R_sV_{OC}}{R_{sh}}+V\right)}{R_s(R_s+R_{sh})} + \frac{nk_BT}{qR_s}lambertw\left[\frac{qR_s}{nk_BT}\frac{\left(I_{SC}-\frac{V_{OC}}{R_s+R_{sh}}\right)exp\left(\frac{-qV_{OC}}{nk_BT}\right)}{1-exp\left(\frac{q(R_sI_{SC}-V_{OC})}{nk_BT}\right)} \times \right.$$

$$\left. expRshqRsISC+RsISC-VOCRsh1-expqRsISC-VOCnkBT+RsVOCRsh+VnkBTRs+Rsh \right] . \quad (8)$$

Taking advantage of the short-circuit and open-circuit conditions, the number of unknown parameters has been reduced from five to three (n, R_s, and R_{sh}). Equation 8 is an exactly solvable equation, however, it can be simplified by the following assumption:

$$\Delta = exp\left(\frac{q(R_sI_{SC}-V_{OC})}{nk_BT}\right) \ll 1 . \quad (9)$$

If the assumption in Equation 9 is used, Equations 5 and 6 reduce to the following:

$$I_0 = \left(I_{SC} + \frac{R_sI_{SC}-V_{OC}}{R_{sh}}\right) exp\left(\frac{-qV_{OC}}{nk_BT}\right) \quad (10)$$

$$I_{ph} + I_0 = I_{SC} + \frac{R_sI_{SC}}{R_{sh}} . \quad (11)$$

This means that Equation 8 reduces to:

$$I = \frac{nk_BT}{qR_s}lambertw\left[\frac{qR_s}{nk_BT}\left(I_{SC} - \frac{V_{OC}}{R_s+R_{sh}}\right) exp\left(\frac{-qV_{OC}}{nk_BT}\right) \times exp\frac{q}{nk_BT}\left(R_sI_{SC} + \frac{R_{sh}V}{R_{sh}+R_s}\right)\right] + \frac{V}{R_s} -$$

$$I_{SC} - \frac{R_{sh}V}{R_s(R_{sh}+R_s)} . \quad (12)$$

Equation 12 was the fit used in the fitting procedure in order to determine the n factor, series resistance, and shunt resistance.

Chapter III: Time-Resolved Microwave Conductivity

3.1 Introduction

Time-resolved microwave conductivity (TRMC) is a contact-less technique that utilizes the pump-probe method. TRMC has been used to determine the properties of various solar energy samples, such as a wide range of donor molecules (P3HT, pBTTT, and PCPDTBT), various acceptor molecules ($PC_{60}BM$, single-walled carbon nanotubes, colloidal nanoparticles, and ZnO), quantum dots, and dye-sensitized solar cells. A sample is first pumped with a 4 ns wide laser pulse and then probed with a microwave source. The TRMC system used in the following experiments takes advantage of a Continuum Precision II Nd:YAG laser, which is sent through a Continuum Panther Optical Parametric Oscillator (OPO) in order to precisely control the wavelength of the laser pulse. The details of the TRMC setup will be discussed in the experimental section. TRMC is used to determine the yield mobility product ($\varphi\Sigma\mu$) of free charges, photogenerated by the laser pulse, in thin film samples. If the mobility of the charges are previously known or determined, then the yield of the sample can be easily calculated. There are two main TRMC methods: pulse-radiolysis and flash-photolysis. All of the experiments were carried out with the flash-photolysis method.

Figure 3-1 illustrates the basics of the flash-photolysis TRMC technique. First, the thin film substrate is placed in a resonant microwave cavity. The resonant microwave cavity has a grating on the side facing the laser and an iris on the side facing the microwave source, as seen below. The grating on the resonant microwave cavity ensures that microwaves cannot exit the cavity, due to the polarization of the grating. The iris has two main functions for the microwave cavity. First, the iris makes the microwave cavity resonant so that the voltage measured from the microwave source reaches a minimum point, as seen in Figure 3-34 in the experimental section.

Second, the iris also limits the wavelength of the microwave that can pass through the opening. After the sample has been placed in the resonant microwave cavity, it is excited by the 4 ns wide laser pulse. The laser pulse actually passes through neutral density filters in order to change the intensity of the pulse. The thin film on the quartz substrate absorbs the laser pulse, which generates excitons. If the excitons do not recombine, or eliminate each other through exciton-exciton annihilation, they can dissociate into free charge carriers.

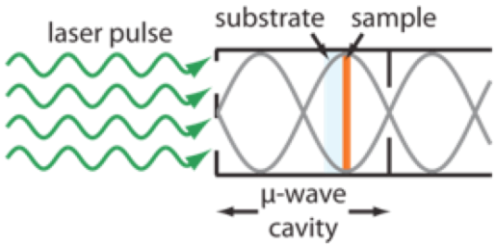

Figure 3-1. Illustration of the resonant microwave cavity used in the flash-photolysis time-resolved microwave conductivity (TRMC) experiments. Figure obtained from Nikos Kopidakis at NREL.

Flash-photolysis TRMC takes advantage of the fact that free charges absorb microwaves. As the charges absorb microwaves, the power from the microwave source decreases over time, which is measured through an oscilloscope. However, the number of free charge carriers decreases over time due to recombination or trap sites. Therefore, the microwave power increases and eventually reaches its baseline, which achieves the time-resolution of flash-photolysis TRMC. The change in microwave power is used to determine the photoconductance of the sample:

$$\frac{\Delta P}{P} = -K\Delta G \tag{13}$$

where ΔP is the change in microwave power, P is the initial microwave power, K is the sensitivity factor and it has the properties of the resonant microwave cavity, and ΔG is the

photoconductance. This is an important relationship between photoconductance and change in microwave power because the photoconductance is used to calculate the yield mobility product ($\varphi\Sigma\mu$):

$$\varphi\Sigma\mu = \frac{\Delta G}{\beta q_e I_0 F_A} \quad (14)$$

where β is the ratio between the dimensions of the resonant microwave cavity, q_e is the charge of an electron, I_0 is the initial photon flux, and F_A is the fraction of light absorbed. The yield mobility product ($\varphi\Sigma\mu$) is the most important value determined from flash-photolysis TRMC experiments. The details of the TRMC system will be discussed in the experimental section.

The experimental yield mobility product ($\varphi\Sigma\mu$) transients, obtained from the flash-photolysis TRMC system, were fitted in order to determine the yield mobility product at time zero (t=0 $\varphi\Sigma\mu$). The fits were extrapolated to the beginning of the laser pulse to determine this value. The yield mobility product at time zero is used to calculate the value of the yield mobility product at very low light intensities. These low intensities are not accessible in the TRMC system used for these experiments.

Figure 3-2 shows the batch fitting panel used to fit the yield mobility product transients. The procedure uses a double exponential equation to properly fit the transients. First, the highest intensity transient is fit to determine the initial parameters. The highest intensity transient is usually F0, as seen in Figure 3-3, which means no filter was applied since this is the total intensity of the laser pulse. Once the equation in the procedure has successfully fit the first transient, individual fits are applied to each transient in descending order of light intensity. As seen below, Equation 15 is the formula used in the fitting procedure:

$$\Delta G(t) = A_1 \exp\left(\frac{-t}{\tau_1}\right) + A_2 exp\left(\frac{-t}{\tau_2}\right) \quad (15)$$

where A_1 and A_2 are pre-exponential factors, t_1 and t_2 are time constants, and τ_1 and τ_2 are response times of the resonant microwave cavity. Figures 3-3 and 3-4 illustrate an example of the fits on yield mobility product transients for P3HT:$PC_{60}BM$ on a log and linear scale, respectively. Notice that an overlap occurs between the transients for F532 and F54 in Figure 3-4. This overlap happens due to the lack of consistency with the neutral density filters. The neutral density filters are not completely neutral at every wavelength and even though this is supposed to be corrected for, as discussed in the experimental section, sometimes transients of different intensities overlap.

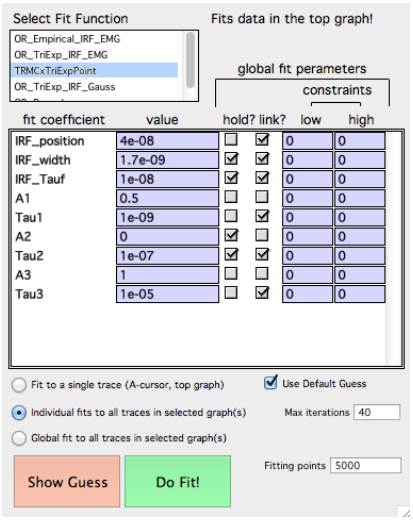

Figure 3-2. The batch fitting panel used to fit the yield mobility product (φΣμ) transients in Igor Pro.

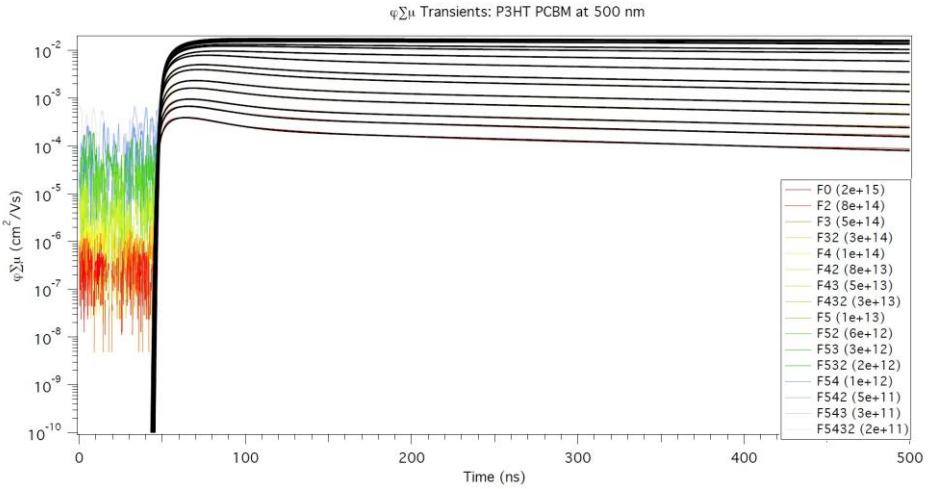

Figure 3-3. The fitted yield mobility product (φΣμ) transients of P3HT:$PC_{60}BM$ (on a quartz substrate), plotted on a log scale.

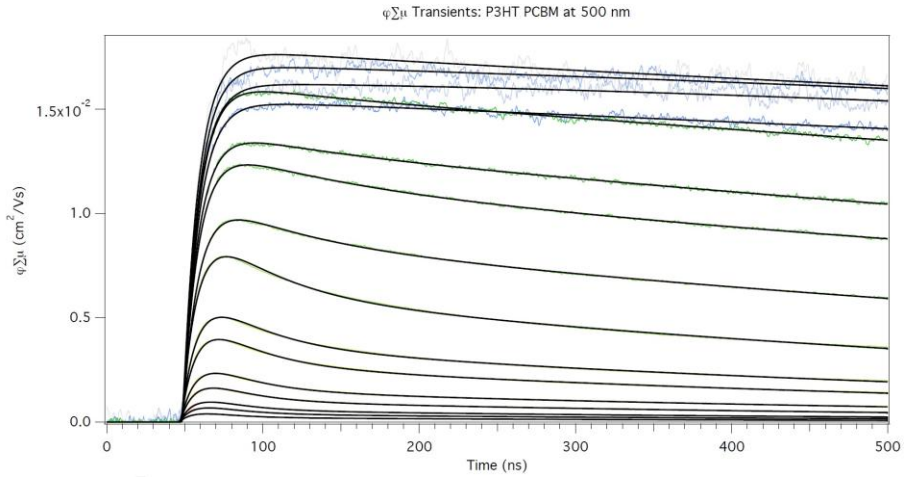

Figure 3-4. The fitted yield mobility product (φΣμ) transients of P3HT:$PC_{60}BM$ (on a quartz substrate), plotted on a linear scale.

The absorptance spectra were obtained, using a Shimadzu spectrophotometer with an integrating sphere attachment, in order to ascertain the values for the fraction of light absorbed (F_A). The fraction of light absorbed is needed to calculate the yield mobility product (φΣμ) as well as to properly fit the yield mobility product at time zero (t=0 φΣμ) plots using the modified

Dicker fit, discussed in the experimental section. Therefore, it is critical that the fraction of light is precisely calculated. The reflection of the sample needs to be factored out of the absorption, which is why the transmittance (T) and reflectance (R) of the thin film is experimentally determined. Since TRMC measurements were only taken at two wavelengths, 500 nm and 800 nm, the absorptance values at these wavelengths were determined from the spectra.

The absorptance spectra for P3HT:$PC_{60}BM$ and P3HT:$PC_{60}BM$ with SiNc (2.24 molar percent) can be seen in Figure 3-5. Notice the strong Q-band peak at 800 nm for the thin film containing SiNc. Figure 3-6 shows the absorptance spectra for thin films of neat P3HT, neat $PC_{60}BM$, neat P3HT with SiNc, and neat $PC_{60}BM$ with SiNc. Once again, there are Q-band peaks around 800 nm for the samples with SiNc. The values used for the fraction of light (F_A) are summarized in Table 3-1. The fraction of light (F_A) is also important in determining the absorbed flux for the yield mobility product at time zero ($t=0$ $\varphi\Sigma\mu$) plots, as seen in the following section.

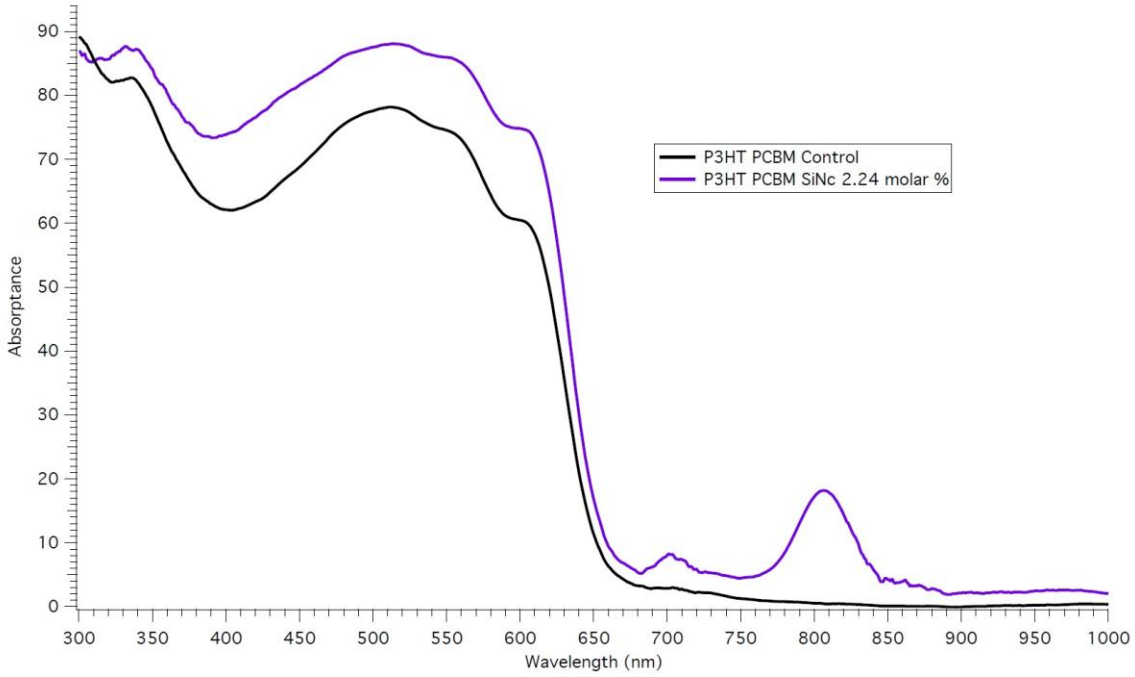

Figure 3-5. Absorptance spectra of P3HT:$PC_{60}BM$ and P3HT:$PC_{60}BM$ with SiNc (2.24 molar percent) on quartz substrates. The sample with SiNc has a Q-band peak of 17.202% at 800 nm.

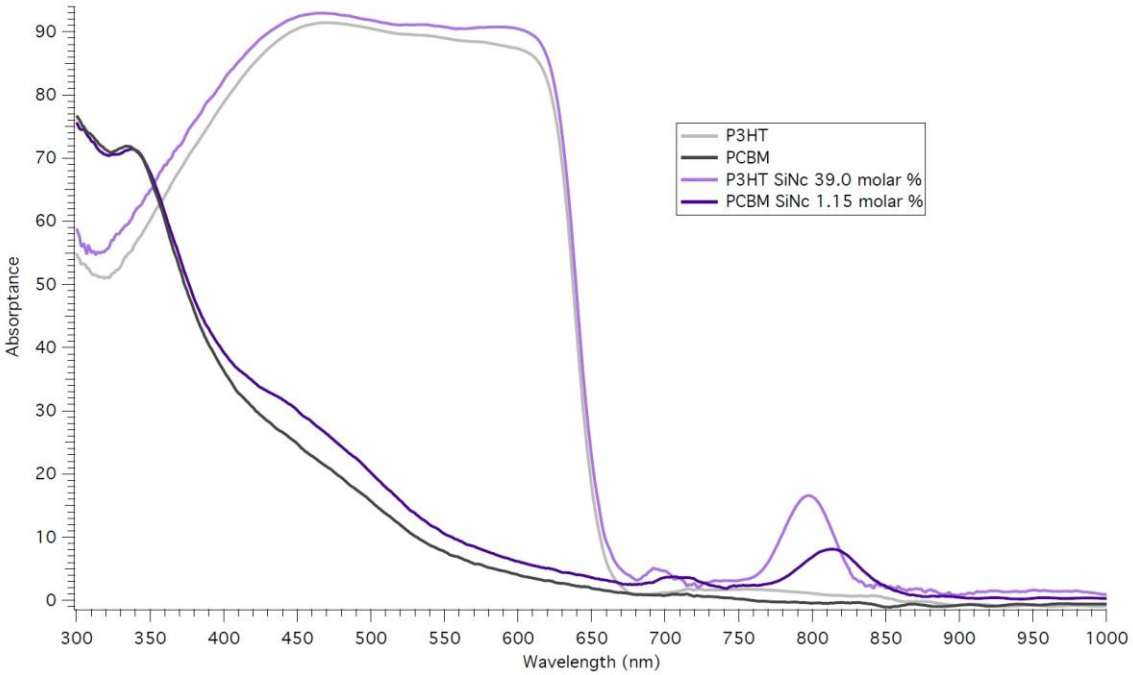

Figure 3-6. Absorptance spectra of neat P3HT, neat $PC_{60}BM$, neat P3HT with SiNc, and neat $PC_{60}BM$ with SiNc. Samples containing SiNc have Q-band peaks around 800 nm.

	Absorptance at 500 nm (%)	Absorptance at 800 nm (%)
P3HT:$PC_{60}BM$	77.573	0.53021
P3HT:$PC_{60}BM$ SiNc (2.24 molar %)	87.528	17.202
P3HT	90.513	1.1031
$PC_{60}BM$	15.737	0
P3HT SiNc (39.0 molar %)	91.847	16.424
$PC_{60}BM$ SiNc (1.15 molar %)	20.223	6.8746

Table 3-1. Summary of the absorptance values for the control samples and thin films containing SiNc. Only samples with SiNc have a significant Q-band peak around 800 nm.

Figures 3-7 and 3-8 illustrate the absorptance spectra for samples containing one of the three phthalocyanines, as well as control samples. Notice that only thin films with a phthalocyanine have a significant Q-band peak around 800 nm. Due to the strong peaks around

800 nm for samples with SiNc and the phthalocyanines, TRMC measurements were carried out at 800 nm in order to compare signals across all of the samples. The values used for the fraction of light absorbed (F_A) are summarized in Table 3-2. It is important to note that the neat $PC_{60}BM$ control sample does not absorb light at 800 nm, which means there will not be a TRMC signal at 800 nm for this thin film.

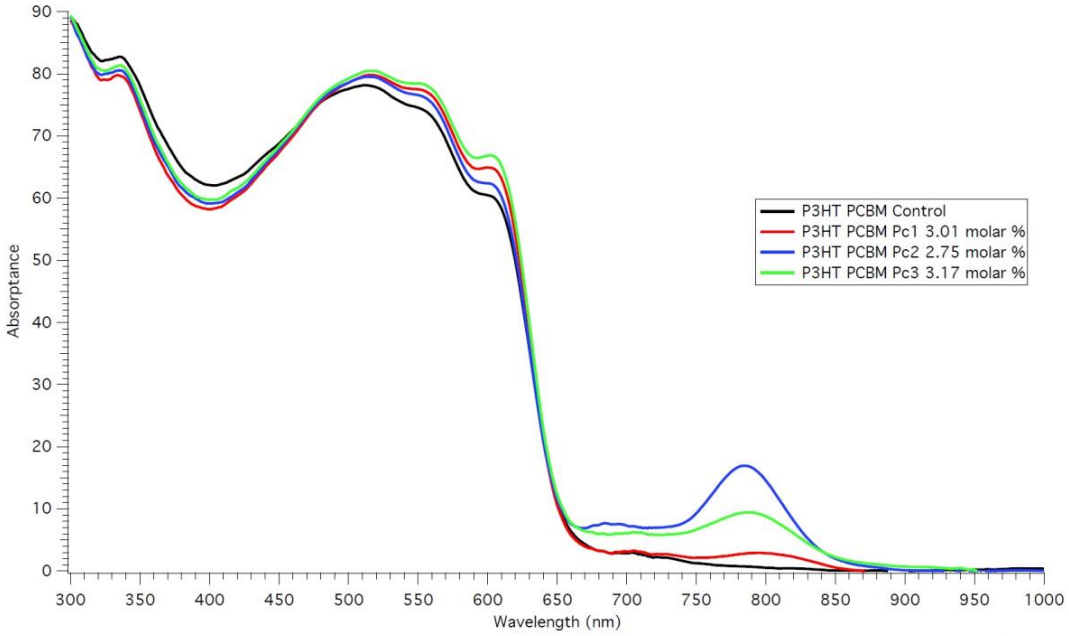

Figure 3-7. The absorptance spectra of P3HT:$PC_{60}BM$ and P3HT:$PC_{60}BM$ containing one of the phthalocyanines. There is a Q-band peak for thin films with a phthalocyanine.

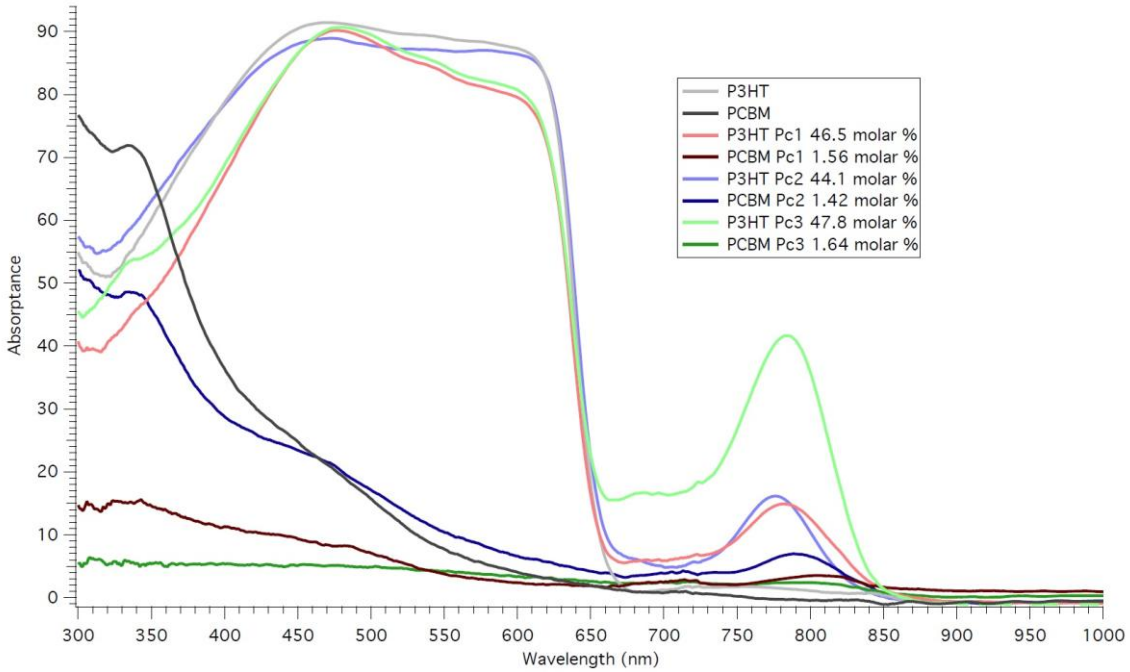

Figure 3-8. Absorptance spectra of neat P3HT, neat $PC_{60}BM$, neat P3HT with one of the phthalocyanines, and neat $PC_{60}BM$ containing one of the phthalocyanines.

	Absorptance at 500 nm (%)	Absorptance at 800 nm (%)
P3HT:$PC_{60}BM$	77.573	0.53021
P3HT:$PC_{60}BM$ Pc1 (3.01 molar %)	78.559	2.8756
P3HT:$PC_{60}BM$ Pc2 (2.75 molar %)	78.594	14.559
P3HT:$PC_{60}BM$ Pc3 (3.17 molar %)	79.234	8.7987
P3HT	90.513	1.1031
$PC_{60}BM$	15.737	0
P3HT Pc1 (46.5 molar %)	88.548	12.555
$PC_{60}BM$ Pc1 (1.56 molar %)	7.0907	3.5032
P3HT Pc2 (44.1 molar %)	87.792	10.412
$PC_{60}BM$ Pc2 (1.42 molar %)	17.124	6.5579
P3HT Pc3 (47.8 molar %)	89.496	35.780
$PC_{60}BM$ Pc3 (1.64 molar %)	4.8803	2.4122

Table 3-2. Summary of the absorptance values for control samples and thin films with one of the phthalocyanines.

3.2 Pulsing P3HT:$PC_{60}BM$ vs. Small Molecules

Flash-photolysis TRMC experiments were performed on thin film samples of P3HT:$PC_{60}BM$ and P3HT:$PC_{60}BM$ with SiNc (2.24 molar percent). The control sample of P3HT:$PC_{60}BM$ was excited at 500 nm with the 4 ns laser pulse. The P3HT:$PC_{60}BM$ with SiNc (2.24 molar percent) thin film was excited at both 500 nm and 800 nm, in order to compare to the control sample and to compare the excitation of P3HT:$PC_{60}BM$ to SiNc, respectively. The thin film samples were excited at 500 nm because this is the peak of the absorption for the blend of P3HT:$PC_{60}BM$, while 800 nm is the maximum in the absorptance spectra of SiNc, as seen in Figure 3-5. Therefore, when the sample is pulsed at 500 nm, only P3HT and $PC_{60}BM$ are excited. Since SiNc does not absorb at 500 nm, as seen in Figure 3-9, it will not contribute to the TRMC signal at this wavelength. Similarly, the blend of P3HT:$PC_{60}BM$ does not absorb at 800 nm, so when the sample containing SiNc is pulsed at 800 nm, only SiNc is excited. This rules out the possibility of the molecules contributing to different TRMC signals.

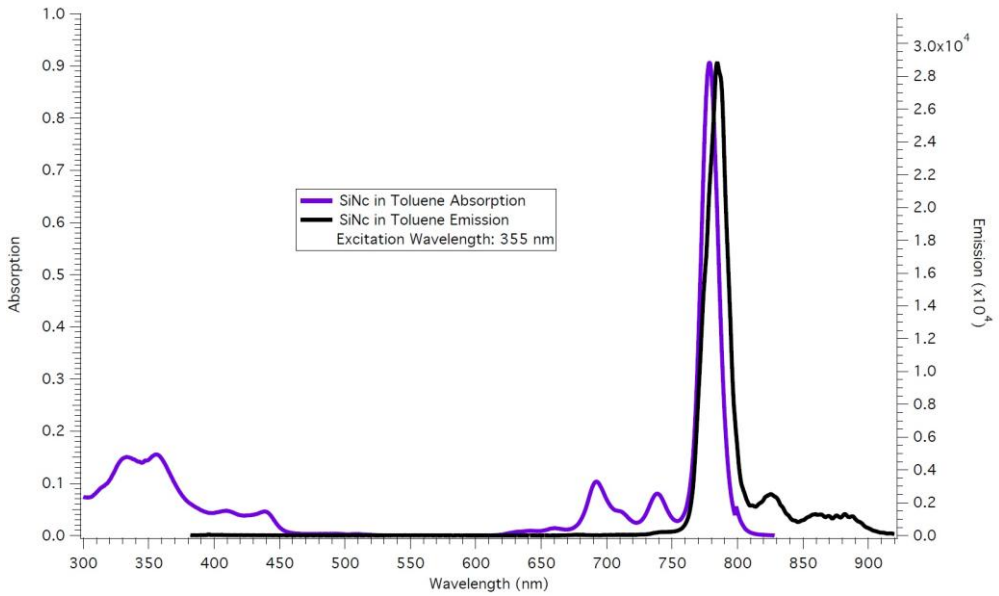

Figure 3-9. The absorption spectrum and emission spectrum of SiNc in toluene, excited at 355 nm. Notice that SiNc does not absorb light at 500 nm.

Photoconductance (ΔG) and yield mobility product (φΣμ) transients were obtained for the P3HT:PC_{60}BM control thin film and the sample containing SiNc (2.24 molar percent). The values for the maximum signal strength are summarized in Table 3-3. The strength of the photoconductance (ΔG) signal increases from the control sample to the thin film containing SiNc, when excited at 500 nm. The yield mobility product (φΣμ) transients increased in signal strength from the control to the SiNc sample as well. This indicates that the addition of SiNc to the thin film of P3HT:PC_{60}BM amplifies the TRMC signal when the sample is excited at 500 nm. SiNc must be positioned in such a way that enhances both the photoconductance and the yield mobility product transients. Ideally, SiNc would be located in the amorphous region of P3HT:PC_{60}BM, in order to transfer electrons from P3HT to PC_{60}BM and move holes from PC_{60}BM to P3HT. However, SiNc could be positioned in P3HT-rich and PC_{60}BM-rich regions, leading to decreases in the signal strength. These ideas will be discussed in the following sections. Also, it is important to note that free charges were still produced upon the excitation of the sample with SiNc, whether it was at 500 nm or 800 nm. Exciting SiNc directly resulted in free charge carriers, which means that electrons were moved from SiNc to PC_{60}BM and holes were transferred from SiNc to P3HT. Even though the signal strength for both photoconductance and yield mobility product transients decreased for the thin film sample containing SiNc, excited at 800 nm, free charge carriers were still created in the bulk heterojunction. The raw, experimental data can be found in Figures C-1 through C-3 and C-10 through C-12 in Appendix C.

	ΔG Signal Strength (S)	φΣμ Signal Strength ($cm^2/V \cdot s$)
P3HT:PC_{60}BM at 500 nm	2.1101e-7	1.8444e-2
P3HT:PC_{60}BM SiNc (2.24 molar %) at 500 nm	3.2029e-7	2.3081e-2

P3HT:PC_{60}BM SiNc (2.24 molar %) at 800 nm	1.7838e-7	1.6751e-2

Table 3-3. Summary of the signal strength for photoconductance (ΔG) and yield mobility product (φΣμ) transients of P3HT:PC_{60}BM and P3HT:PC_{60}BM with SiNc (2.24 molar percent) at 500 nm and 800 nm.

The photoconductance (ΔG) transients were normalized, as seen in Figures 3-10 and 3-11, in order to compare the decay of the signal as well as the light intensity dependence. Figure 3-10 shows the normalized photoconductance transients for the thin film of P3HT:PC_{60}BM and the thin film of P3HT:PC_{60}BM with SiNc (2.24 molar percent), excited at 500 nm. Notice that both plots demonstrate that the samples are dependent on the light intensity of the laser. Several normalized photoconductance plots, as seen in the next section, are independent of light intensity and are visually very different from the plots below. The decay rate of the photoconductance signal in both plots are nearly identical, which shows that exciting either sample results in free charge carriers that decay at the same rate. This also implies that the decay mechanism is very similar, if not identical, between the two samples. The normalized photoconductance plots for P3HT:PC_{60}BM, excited at 500 nm, and P3HT:PC_{60}BM with SiNc (2.24 molar percent), excited at 800 nm, are compared in Figure 3-11. Once again, the decay rates are nearly identical and both are light intensity dependent. Regardless of the excitation wavelength, the decay dynamics in all three samples are similar. This most likely means that it does not matter whether P3HT:PC_{60}BM or SiNc is excited because free charge carriers are still produced, the samples are dependent upon light intensity from the laser, and the decay mechanisms are practically the same.

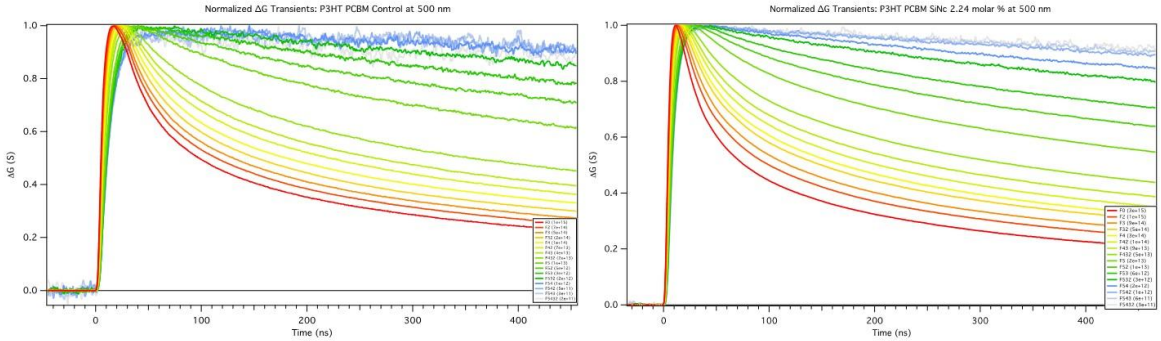

Figure 3-10. Normalized photoconductance (ΔG) transients for P3HT:PC_{60}BM and P3HT:PC_{60}BM with SiNc (2.24 molar percent) at 500 nm.

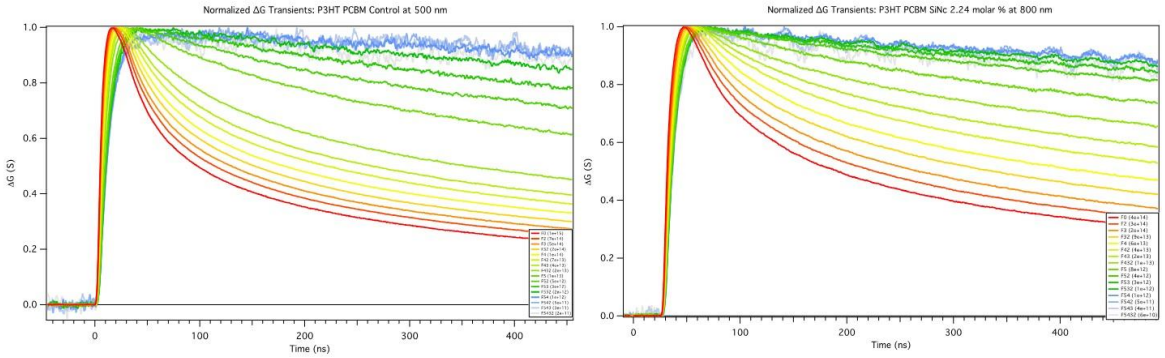

Figure 3-11. Normalized photoconductance (ΔG) transients for P3HT:PC_{60}BM and P3HT:PC_{60}BM with SiNc (2.24 molar percent) at 800 nm.

Yield mobility product at time zero (t=0 φΣμ) plots for the three samples are shown in Figure 3-12 below. It is important to note that the x-axis of the yield mobility product at time zero plots is absorbed flux. By using absorbed flux as the x-axis, the absorption of the thin films at the excitation wavelength are taken into account. This removes the fraction of light absorbed (F_A) as a variable in the plots. Recall that the modified Dicker fit, as represented by the solid line in the figure below, is used to properly estimate the yield mobility product at very low light intensities. These intensities are not accessible with the TRMC set-up used in these experiments.

Table 3-4 summarizes the Dicker A values, which are the values of the asymptotic line that the modified Dicker fit approaches.

First of all, the Dicker A value for the excitation of the P3HT:$PC_{60}BM$ with SiNc (2.24 molar percent) thin film, at 500 nm, is an order of magnitude higher than the value for the control sample. This means that the addition of SiNc molecules to the bulk heterojunction has significantly increased the yield of the sample, since the values for the mobilities are unchanged. The electron mobility on $PC_{60}BM$ and the hole mobility on P3HT are used in this discussion. Also, electrons and holes on SiNc will not contribute to the sum of mobilities for two reasons. One, if a SiNc molecule was positioned in its ideal location, in the amorphous region of P3HT:$PC_{60}BM$, then it will transfer an electron from P3HT to $PC_{60}BM$ and it will move a hole from $PC_{60}BM$ to P3HT. Therefore, a free charge will not be present on SiNc in this case. Two, if a SiNc molecule was located in a P3HT-rich or $PC_{60}BM$-rich region, it would act as an electron trap or as a hole trap, respectively.

The Dicker A values for the control sample and the thin film containing SiNc, excited at 800 nm, are nearly identical (within error of the system). This means that regardless of excitation wavelength or molecule being excited, charges are still produced at the same yield. This provides more evidence that the addition of SiNc to the bulk heterojunction significantly enhances the properties of the active layer. Finally, the curvature of the modified Dicker fits needs to be addressed. The modified Dicker fit for the thin film containing SiNc, excited at 800 nm, has a noticeably different shape compared to the other two fits. Notice that it does not drop off at high light intensities, while the other two fits are significantly lower. The yield mobility product at time zero plot is lower at high light intensities, which is counter-intuitive, because the large increase of free charges recombine before they can absorb the microwave power. Also, at low

light intensities, the 800 nm excited sample quickly plateaus, while the other two fits slowly approach the asymptotic line. The reason for the difference in curvature arises from the fact that SiNc acts as a trap in the bulk heterojunction when it is not positioned correctly. This phenomenon can be explained by looking at the energy levels of SiNc, P3HT, and $PC_{60}BM$. These ideas will be discussed in the following sections.

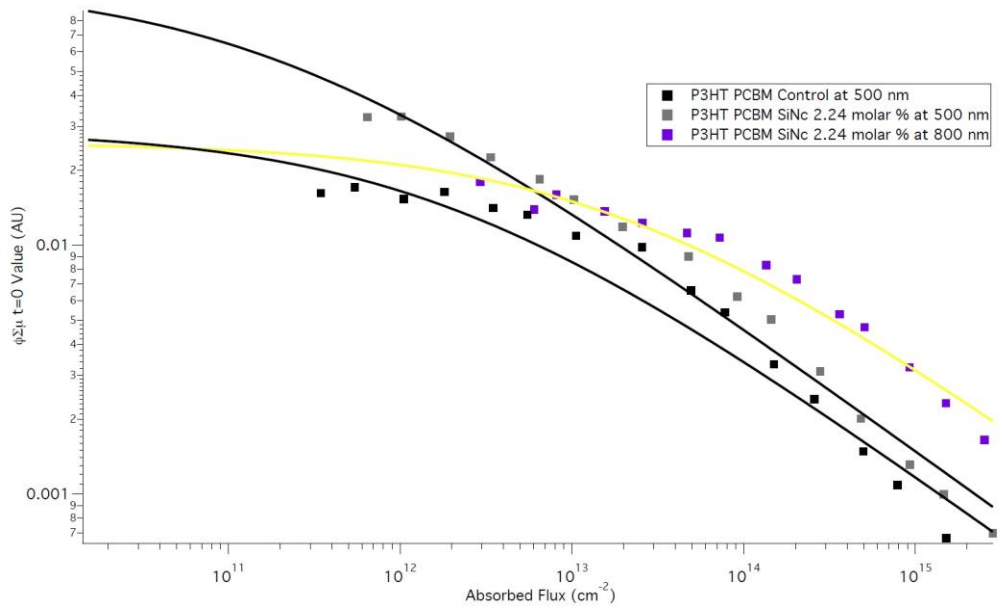

Figure 3-12. The yield mobility product at time zero (t=0 φΣμ) plots for P3HT:$PC_{60}BM$ and P3HT:$PC_{60}BM$ with SiNc (2.24 molar percent) at 500 nm and 800 nm. The squares represent the data points and the solid lines represent the modified Dicker fits.

	Dicker A Values ($cm^{-2}V^{-1}s^{-1}$)
P3HT:$PC_{60}BM$ at 500 nm	2.9003e-2
P3HT:$PC_{60}BM$ SiNc (2.24 molar %) at 500 nm	1.1292e-1
P3HT:$PC_{60}BM$ SiNc (2.24 molar %) at 800 nm	2.5861e-2

Table 3-4. Summary of the Dicker A values from the modified Dicker fits of the yield mobility at time zero (t=0 φΣμ) plots for P3HT:$PC_{60}BM$ and P3HT:$PC_{60}BM$ with SiNc (2.24 molar percent) at 500 nm and 800 nm.

Thin film samples of P3HT:$PC_{60}BM$ and P3HT:$PC_{60}BM$ with one of the phthalocyanines were excited with 4 ns laser pulses in order to obtain photoconductance (ΔG) and yield mobility product ($\varphi\Sigma\mu$) transients. The control sample of P3HT:$PC_{60}BM$ was pulsed at 500 nm, while the thin films containing one of phthalocyanines (Pc1, Pc2, or Pc3) were measured at both 500 nm and 800 nm. This way, all of the samples could be compared to the control sample's data and the signal strength, normalized photoconductance plots, and Dicker A values could be compared with the data from SiNc. The phthalocyanine samples were pulsed at 800 nm in order to excite only the phthalocyanine molecules. The same procedure was done with SiNc in the previous discussion. Figures 3-13 through 3-15, as seen below, illustrate the absorption and emission spectra of Pc1, Pc2, and Pc3 in toluene, respectively. Notice that all of the phthalocyanines have minimal absorption at 500 nm. This small absorption can be ignored when looking at TRMC data involving the excitation of P3HT:$PC_{60}BM$ at 500 nm. It is important to point out, in Figure 3-15, that there is a shoulder on the absorption spectrum for Pc3. This is actually a second peak in the absorption spectrum, which is not able to be completely resolved. There are two peaks in the Q-band because of the different energies for the NH-NH and N-N transition in the core of Pc3.

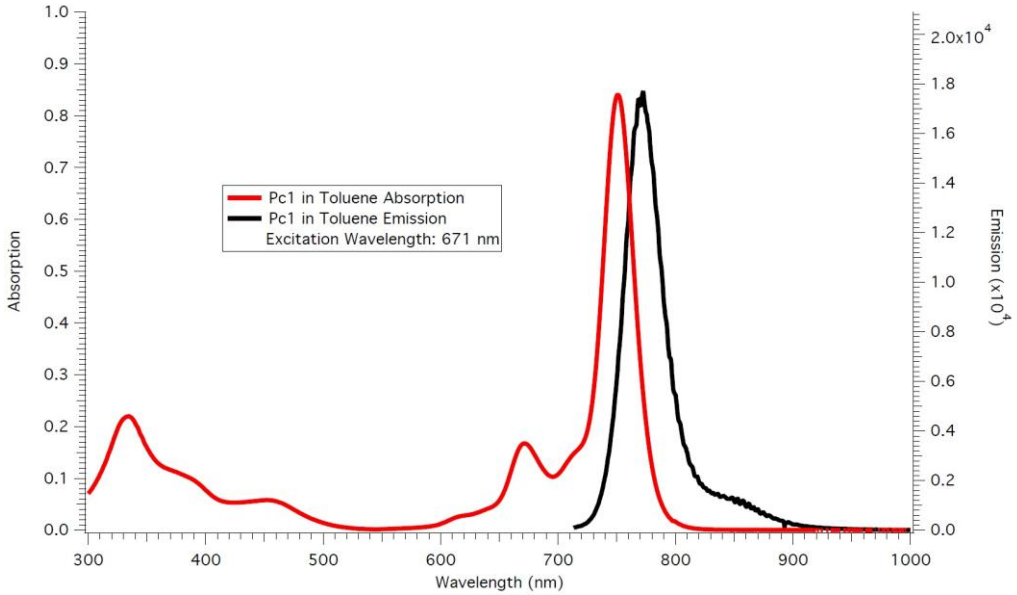

Figure 3-13. The absorption spectrum and emission spectrum of Pc1 in toluene, excited at 671 nm. Pc1 has a very small absorption at 500 nm, which will not affect the time-resolved microwave conductivity (TRMC) measurements at 500 nm.

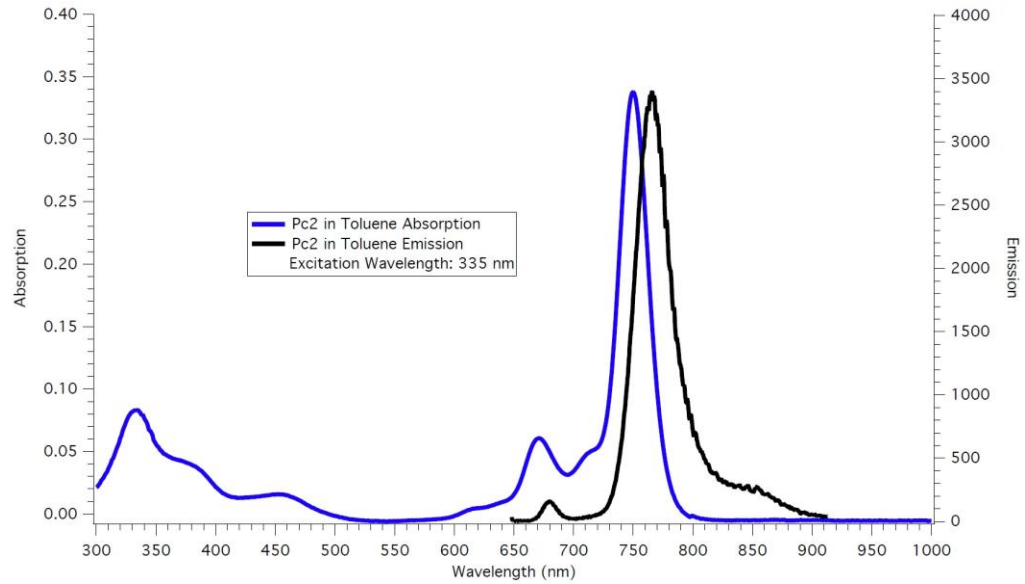

Figure 3-14. The absorption spectrum and emission spectrum of Pc2 in toluene, excited at 335 nm. Pc2 has minimal absorption at 500 nm, which will not affect the time-resolved microwave conductivity (TRMC) measurements at this wavelength.

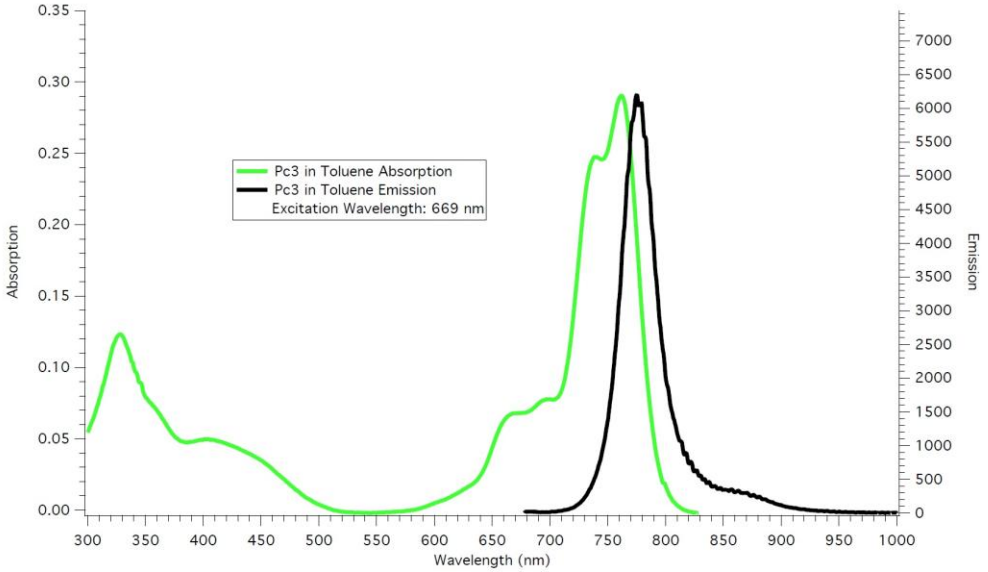

Figure 3-15. The absorption spectrum and emission spectrum of Pc3 in toluene, excited at 669 nm. Pc3 has a miniscule absorption at 500 nm, which means this can be ignored in the time-resolved microwave conductivity (TRMC) measurements at 500 nm.

Flash-photolysis TRMC data was collected for the control sample of P3HT:PC_{60}BM and thin films containing one of the phthalocyanines. The values of the signal strength of the photoconductance transients and the yield mobility product transients are summarized in Table 3-5. The signal strength for both photoconductance and yield mobility product are very similar for all four samples, when excited at 500 nm. The numbers are on the same order of magnitude and do not significantly fluctuate. This demonstrates that the addition of a phthalocyanine molecule to the bulk heterojunction does not impact the interaction of light with P3HT:PC_{60}BM, since the active layer is still producing a high yield of free charge carriers. Looking at the signal strength of the samples excited at 800 nm, it can be seen that the photoconductance values are an order magnitude smaller than the control thin film. However, the yield mobility product transients for P3HT:PC_{60}BM with Pc1 are on the same order of magnitude as P3HT:PC_{60}BM, excited at 500 nm. Thin films with Pc2 or Pc3 are an order of magnitude smaller than the control. These conclusions still provide further evidence that the addition of a small molecule to the bulk

heterojunction results in free charge carriers at a high yield. The experimental data can be found in Figures C-4 through C-9 and C-13 through C-18 in Appendix C.

	ΔG Signal Strength (S)	φΣμ Signal Strength ($cm^2/V \cdot s$)
P3HT:PC_{60}BM at 500 nm	2.1101e-7	1.8444e-2
P3HT:PC_{60}BM Pc1 (3.01 molar %) at 500 nm	1.6345e-7	1.9665e-2
P3HT:PC_{60}BM Pc2 (2.75 molar %) at 500 nm	1.7286e-7	1.8778e-2
P3HT:PC_{60}BM Pc3 (3.17 molar %) at 500 nm	1.3768e-7	1.3341e-2
P3HT:PC_{60}BM Pc1 (3.01 molar %) at 800 nm	8.3248e-8	1.0188e-2
P3HT:PC_{60}BM Pc2 (2.75 molar %) at 800 nm	9.2153e-8	9.2160e-3
P3HT:PC_{60}BM Pc3 (3.17 molar %) at 800 nm	6.7279e-8	8.2176e-3

Table 3-5. Summary of the signal strength for photoconductance (ΔG) and yield mobility product (φΣμ) transients of P3HT:PC_{60}BM, P3HT:PC_{60}BM with Pc1 (3.01 molar percent), P3HT:PC_{60}BM with Pc2 (2.75 molar percent), and P3HT:PC_{60}BM with Pc3 (3.17 molar percent). Samples with a phthalocyanine were measured at 500 nm and 800 nm.

Normalized photoconductance (ΔG) plots for thin films of P3HT:PC_{60}BM and P3HT:PC_{60}BM with one of the phthalocyanines are shown below. First, a comparison of the normalized photoconductance plots for samples pulsed at 500 nm are illustrated in Figure 3-16. Notice that all four plots show light intensity dependence and that they are nearly identical, visually. They also have the same decay rates since the transients reach roughly the same position in the 500 ns time window. This means that the decay dynamics of the free charge carriers are the same, which is a logical conclusion because all of the samples are pulsed at 500 nm. Since the samples were excited at 500 nm, only P3HT:PC_{60}BM should be involved in the generation of free charge carriers. Second, Figure 3-17 shows a comparison of normalized

photoconductance plots for thin films of P3HT:$PC_{60}BM$, excited at 500 nm, and thin films of Pc1, Pc2, and Pc3, excited at 800 nm. It is quickly apparent that the three plots containing one of the phthalocyanines are very different from the control normalized photoconductance plot. This is due to the fact that the samples pulsed at 800 nm are not as dependent upon the intensity of the laser as the control plot. In the following section, there are several normalized photoconductance plots that are completely independent of light intensity. However, the plots in Figure 3-17 are still slightly dependent on the laser intensity. There is also significantly more noise in the plots that are excited at 800 nm. Since the samples were pulsed at 800 nm, their decay dynamics have changed because now only the phthalocyanine molecules are excited by the laser. If the phthalocyanine molecules are ideally positioned in the amorphous region, free charges will transfer to the donor and acceptor molecules as they normally would in P3HT:$PC_{60}BM$. However, the phthalocyanines, just as SiNc, can act as traps in the bulk heterojunction, disrupting the decay mechanism seen in the control sample.

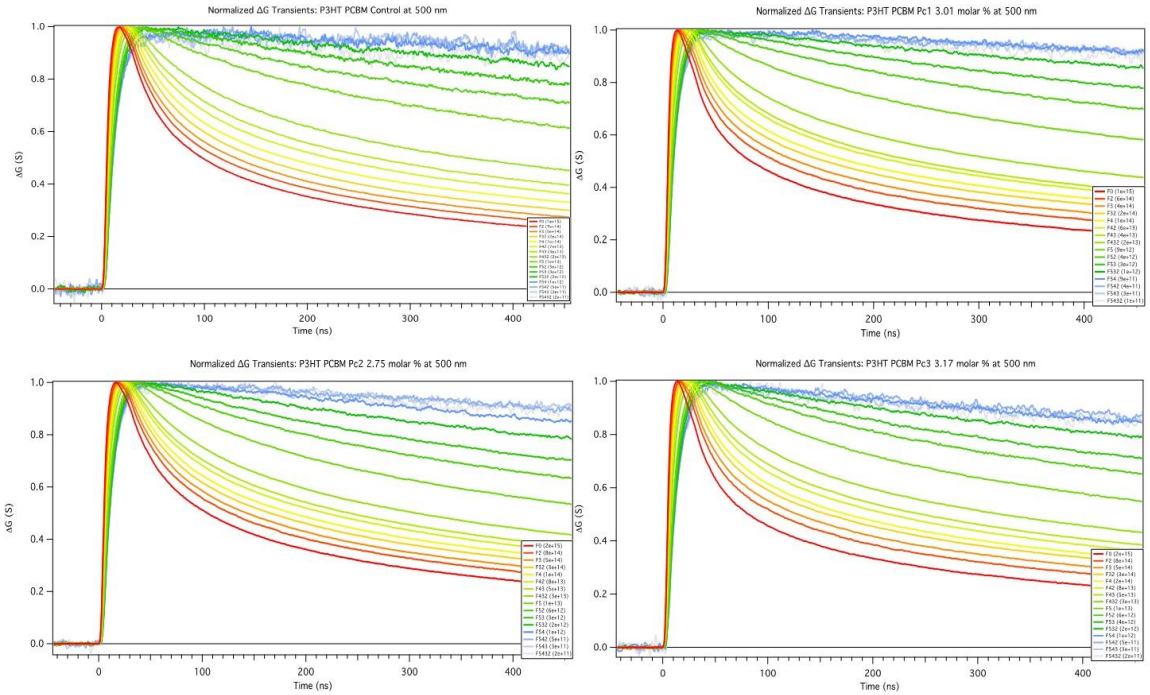

Figure 3-16. Normalized photoconductance (ΔG) transients for P3HT:$PC_{60}BM$, P3HT:$PC_{60}BM$ with Pc1 (3.01 molar percent), P3HT:$PC_{60}BM$ with Pc2 (2.75 molar percent), P3HT:$PC_{60}BM$ with Pc3 (3.17 molar percent) at 500 nm.

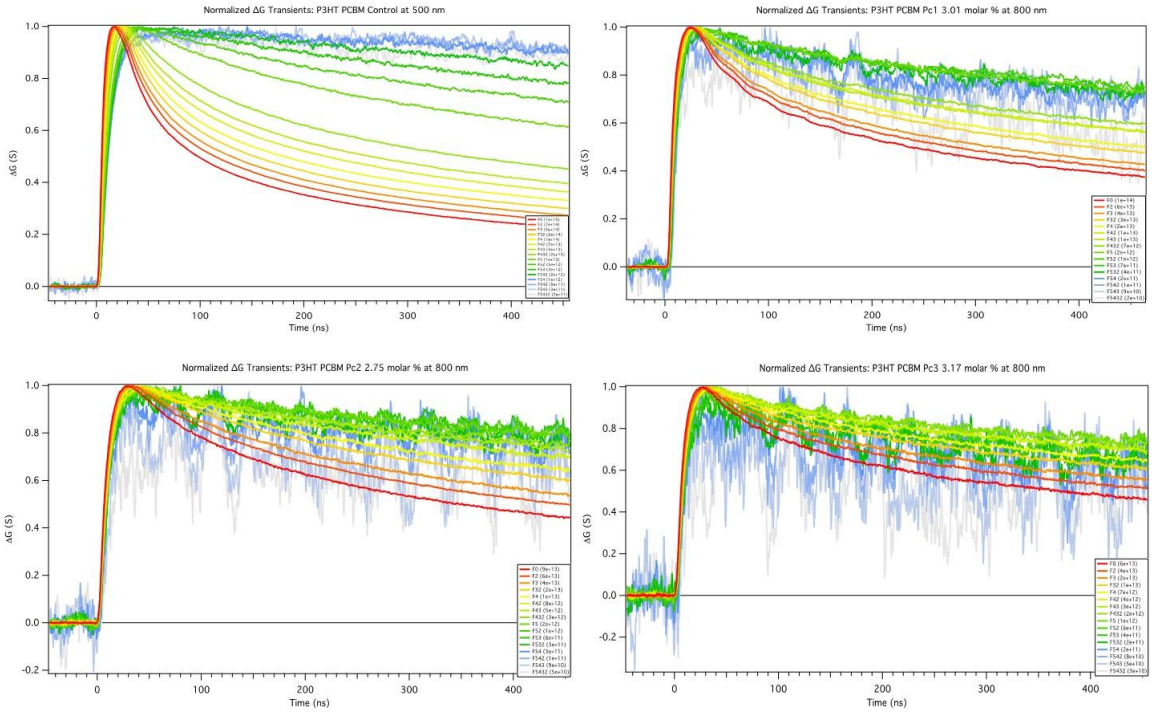

Figure 3-17. Normalized photoconductance (ΔG) transients for P3HT:PC_{60}BM, P3HT:PC_{60}BM with Pc1 (3.01 molar percent), P3HT:PC_{60}BM with Pc2 (2.75 molar percent), P3HT:PC_{60}BM with Pc3 (3.17 molar percent) at 800 nm.

The yield mobility product at time zero (t=0 φΣμ) plots are illustrated in Figures 3-18 through 3-20 and are separated into plots for each phthalocyanine and the control sample. Figure 3-21 shows all of the yield mobility product at time zero (t=0 φΣμ) plots on the same graph. The data points are represented by squares and the modified Dicker fits are represented by solid lines. Looking at the first three plots, it can be seen that the samples with Pc1 or Pc2, excited at 500 nm, have a larger Dicker A value compared to the control thin film of just P3HT:PC_{60}BM, which is summarized in Table 3-6. On the other hand, the sample containing Pc3, pulsed at 500 nm, has a very similar Dicker A value compared to the control and they are assumed to be the same, within the error of the TRMC system. This means that the addition of Pc1 and Pc2 to the bulk heterojunction actually enhanced the yield of the thin film, since the mobilities are the same, while Pc3 had the same yield as the control sample. Therefore, adding phthalocyanines to a thin film sample does not disrupt the interaction of P3HT:PC_{60}BM with light. When a phthalocyanine molecule is pulsed with the 4 ns laser, at 800 nm, the yield decreases compared to the control sample. However, this decrease is not very significant since the Dicker A value for Pc1, excited at 800 nm, is still on the same order of magnitude as the value for the control sample. The Dicker A values for Pc2 and Pc3, pulsed at 800 nm, are slightly lower, but these samples are still producing a large yield of free charge carriers. Once again, exciting a phthalocyanine, in the presence of P3HT and PC_{60}BM, results in free charges in the bulk heterojunction.

The shape of the yield mobility product at time zero (t=0 φΣμ) plots provide information about the mechanism of the photogeneration of free charges in the bulk heterojunction of phthalocyanines in P3HT:PC_{60}BM. The curvature of the modified Dicker fits for the samples

containing a phthalocyanine molecule, excited at 500 nm, are nearly identical to the fit for the control thin film. Both reach the same point at high light intensities, which makes sense because P3HT:$PC_{60}BM$ is excited in these cases. On the other hand, the modified Dicker fits for samples with Pc1, Pc2, or Pc3, excited at 800 nm, have significantly different curvatures. These fits plateau at lower light intensities much quicker than the fits for samples pulsed at 500 nm and they do not have the same yield mobility product at time zero ($t=0$ $\varphi\Sigma\mu$) values at high light intensities, as the samples at 500 nm. The reason for why the plots, at 800 nm, do not have the same values at high light intensities is due to the fact that the phthalocyanines, just as SiNc, act as electron and hole traps in the bulk heterojunction. If a phthalocyanine was located in a P3HT-rich region, it would be an electron trap, but if it was positioned in a $PC_{60}BM$-rich zone, it would act as a hole trap. This means that if an electron or hole is unable to recombine, the thin film still has residual free charges after a long period of time, which results in the change in the yield mobility product at time zero ($t=0$ $\varphi\Sigma\mu$) plot at high light intensities. Using flash-photolysis TRMC, one can probe the morphology of a bulk heterojunction in order to determine the location of specific molecules.

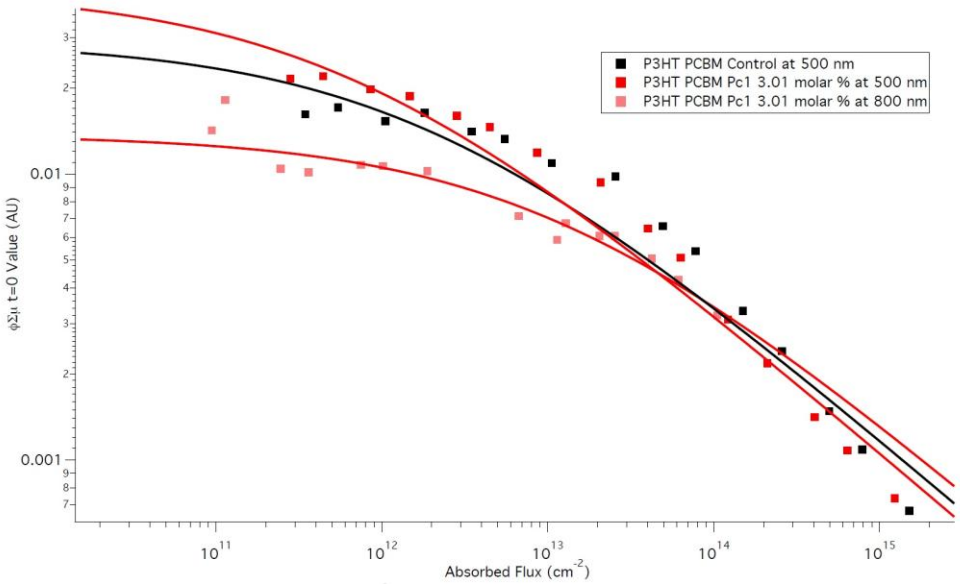

Figure 3-18. The yield mobility product at time zero (t=0 φΣμ) plots for P3HT:PC_{60}BM and P3HT:PC_{60}BM with Pc1 (3.01 molar percent) at 500 nm and 800 nm.

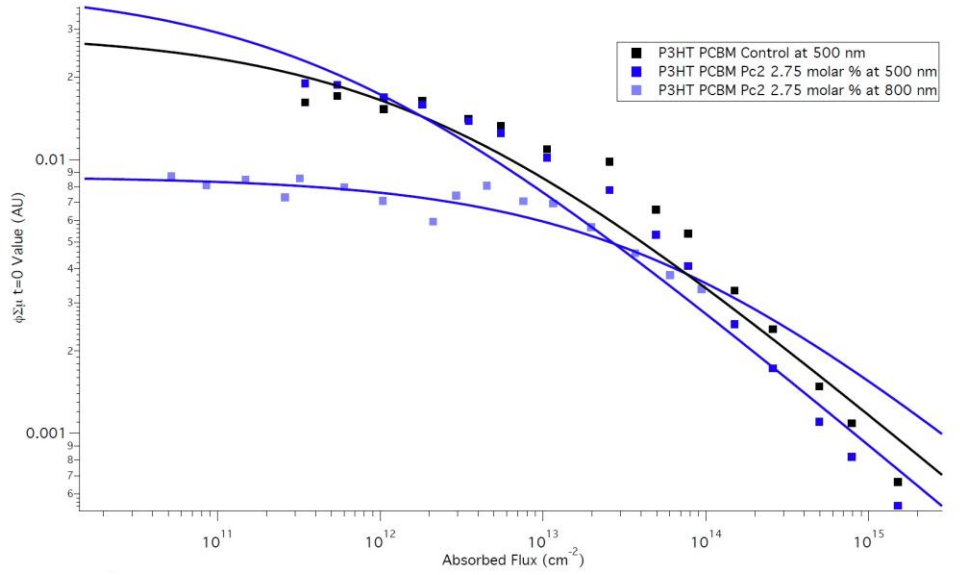

Figure 3-19. The yield mobility product at time zero (t=0 φΣμ) plots for P3HT:PC_{60}BM and P3HT:PC_{60}BM with Pc2 (2.75 molar percent) at 500 nm and 800 nm.

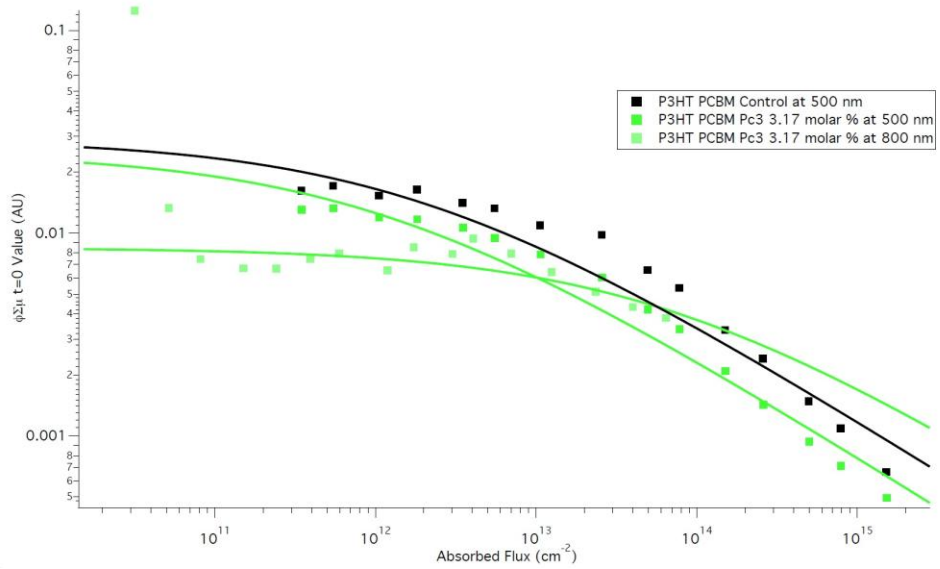

Figure 3-20. The yield mobility product at time zero (t=0 φΣμ) plots for P3HT:PC_{60}BM and P3HT:PC_{60}BM with Pc3 (3.17 molar percent) at 500 nm and 800 nm.

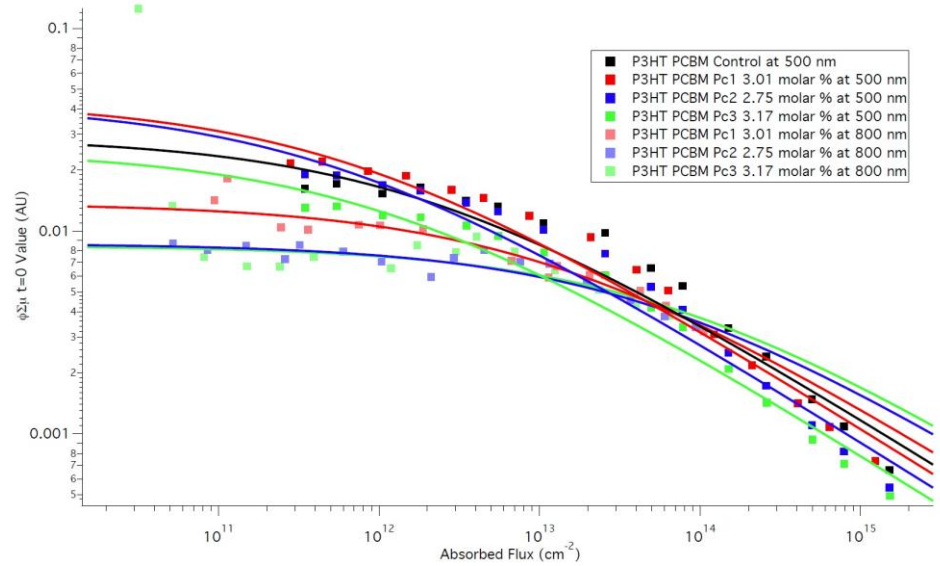

Figure 3-21. The yield mobility product at time zero (t=0 φΣμ) plots for P3HT:PC_{60}BM, P3HT:PC_{60}BM with Pc1 (3.01 molar percent), P3HT:PC_{60}BM with Pc2 (2.75 molar percent), and P3HT:PC_{60}BM with Pc3 (3.17 molar percent). The thin films with a phthalocyanine were measured at 500 nm and 800 nm.

	Dicker A Values ($cm^{-2}V^{-1}s^{-1}$)
P3HT:PC_{60}BM at 500 nm	2.9003e-2
P3HT:PC_{60}BM Pc1 (3.01 molar %) at 500 nm	4.3715e-2
P3HT:PC_{60}BM Pc2 (2.75 molar %) at 500 nm	4.2568e-2
P3HT:PC_{60}BM Pc3 (3.17 molar %) at 500 nm	2.4950e-2
P3HT:PC_{60}BM Pc1 (3.01 molar %) at 800 nm	1.3709e-2
P3HT:PC_{60}BM Pc2 (2.75 molar %) at 800 nm	8.6802e-3
P3HT:PC_{60}BM Pc3 (3.17 molar %) at 800 nm	8.4667e-3

Table 3-6. Summary of the Dicker A values from the modified Dicker fits of the yield mobility at time zero (t=0 $\varphi\Sigma\mu$) plots for P3HT:PC_{60}BM, P3HT:PC_{60}BM with Pc1 (3.01 molar percent), P3HT:PC_{60}BM with Pc2 (2.75 molar percent), and P3HT:PC_{60}BM with Pc3 (3.17 molar percent). Samples with a phthalocyanine were measured at 500 nm and 800 nm.

3.3 Ternary Blends vs. Neat Thin Films with Small Molecules

Thin film samples of neat P3HT, neat PC_{60}BM, neat P3HT with SiNc, and neat PC_{60}BM containing SiNc were spin-coated on quartz substrates. The procedure for constructing neat films is the same as the method for making ternary blend films, so that the number of variables between films is limited to the contents of the bulk heterojunction. Flash-photolysis TRMC was performed on these neat films in order to determine the yield mobility product ($\varphi\Sigma\mu$) and compare these to the values for the ternary blend samples. The raw, experimental data for these samples can be found in Figures C-19 through C-21 and C-28 through C-30 in Appendix C. The values for the signal strength of the photoconductance (ΔG) transients and the yield mobility product ($\varphi\Sigma\mu$) transients are shown in Table 3-7 below. Notice that there are not any values for the neat PC_{60}BM film, due to the fact that this thin film does not absorb light at 800 nm. The strength of the photoconductance signal increases by an order of magnitude from the neat P3HT sample to the samples containing SiNc. This result makes sense because both samples with SiNc

absorb significantly more light at 800 nm, compared to P3HT. The values for the absorption of these films can be seen in Table 3-1. Regardless, the addition of SiNc to a neat film of donor or acceptor molecules increased the photoconductance signal by a large margin.

Looking at the signal strength for the yield mobility product transients, the signal increases two orders of magnitude from the neat P3HT sample to the neat $PC_{60}BM$ with SiNc thin film. The reason the P3HT thin film has low signal strengths is due to the fact that P3HT is a donor molecule, meaning that the molecule donates electrons to an acceptor molecule. However, when an acceptor molecule is not present, P3HT molecules must have electrons and holes present, which leads to a higher chance of quick recombination. Even the neat P3HT containing SiNc samples have a yield mobility product signal strength that is an order of magnitude larger than the control sample. This means that exciting SiNc in a P3HT-rich or $PC_{60}BM$-rich environment results in a significant amount of free charges. Even though SiNc acts as an electron or hole trap in these films, free charge carriers are photogenerated and absorb microwave power.

If the values for the signal strength of the neat thin films are compared to the ternary blend samples, it can be seen that the ternary blend thin films have larger signals for both photoconductance and yield mobility product transients. P3HT:$PC_{60}BM$ containing SiNc, excited at 800 nm, has a signal strength of 1.7838e-7 S for the photoconductance transients and 1.6751e-2 $cm^2/V \cdot s$ for the yield mobility product transients. Table 3-3 summarizes the values for the signal strength of P3HT:$PC_{60}BM$ with SiNc. The photoconductance signal strength of P3HT:$PC_{60}BM$ containing SiNc is an order of magnitude larger than the neat thin films with SiNc. On the other hand, the neat $PC_{60}BM$ with SiNc sample has nearly the same yield mobility product signal strength as the ternary blend with SiNc. These results demonstrate that when SiNc molecules have the opportunity to be located in the amorphous region of P3HT:$PC_{60}BM$, the

photoconductance and yield mobility product transients increase by a significant amount. This is because the neat thin films only have P3HT-rich regions or $PC_{60}BM$-rich regions, therefore SiNc acts as an electron or hole trap, respectively.

	ΔG Signal Strength (S)	φΣμ Signal Strength ($cm^2/V \cdot s$)
P3HT at 800 nm	1.0287e-9	7.1231e-4
$PC_{60}BM$ at 800 nm	0	0
P3HT SiNc (39.0 molar %) at 800 nm	4.1037e-8	2.5002e-3
$PC_{60}BM$ SiNc (1.15 molar %) at 800 nm	1.0432e-8	1.2156e-2

Table 3-7. Values for the signal strength for photoconductance (ΔG) and yield mobility product (φΣμ) transients of neat P3HT, neat P3HT with SiNc (39.0 molar percent), and neat $PC_{60}BM$ containing SiNc (1.15 molar %) at 800 nm. Notice that there are not values for $PC_{60}BM$ because this molecule does not absorb at 800 nm.

A comparison of the normalized photoconductance transients for neat P3HT, neat P3HT with SiNc, and neat $PC_{60}BM$ containing SiNc is shown in Figure 3-22 below. The plot for the neat P3HT control sample is very noisy, which is due to the fact that P3HT does not absorb strongly at 800 nm. Neat P3HT is independent of light intensity as well, but there is a large amount of noise. The normalized photoconductance plot for neat P3HT with SiNc illustrates that this thin film is not very light intensity dependent, since the transients do not vary significantly with a change in laser intensity, and that the decay mechanisms of the free charge carriers are similar to those for neat P3HT. This is because the transients for both samples decay to the same position in the 500 ns time window and the normalized photoconductance plots have nearly identical shapes. Comparing the neat P3HT thin film's normalized photoconductance to that of neat $PC_{60}BM$ with SiNc, it can be seen that they are completely different in shape and in decay. First, neat $PC_{60}BM$ with SiNc is entirely independent of light intensity. Second, the

photoconductance transients decay to the baseline after 50 ns past the laser pulse, which is practically an immediate decay response. Therefore, the decay dynamics of the free charge carriers in neat $PC_{60}BM$ containing SiNc, exciting SiNc at 800 nm, are nothing like the decay of free charges in neat P3HT.

The normalized photoconductance plot for P3HT:$PC_{60}BM$ with SiNc, pulsed at 800 nm, is dependent upon the light intensity of the laser, as seen in Figure 3-11. Comparing the shape of the plot for P3HT:$PC_{60}BM$ containing SiNc to the plots for the neat samples, it can be seen that the neat samples are visually very different. The highest light intensity transient decays lower than 0.4 while the lowest light intensity barely decays and stays above 0.9 in the normalized photoconductance plot for P3HT:$PC_{60}BM$ with SiNc. However, the transient for F0 only reaches 0.4 and the transient for F5432 decays lower than 0.6 in the normalized photoconductance plot of neat P3HT containing SiNc. The plot of neat $PC_{60}BM$ with SiNc decays immediately after the laser pulse, therefore there are no similarities between these normalized transients and the plot for P3HT:$PC_{60}BM$ with SiNc. The significant difference between these plots demonstrates that the decay mechanisms of the ternary blend sample and the neat thin films are very different, due to the fact that SiNc is not located in an amorphous region of P3HT:$PC_{60}BM$ in the neat samples. These results continue to confirm the possibility of probing the morphology of bulk heterojunctions using flash-photolysis TRMC experiments.

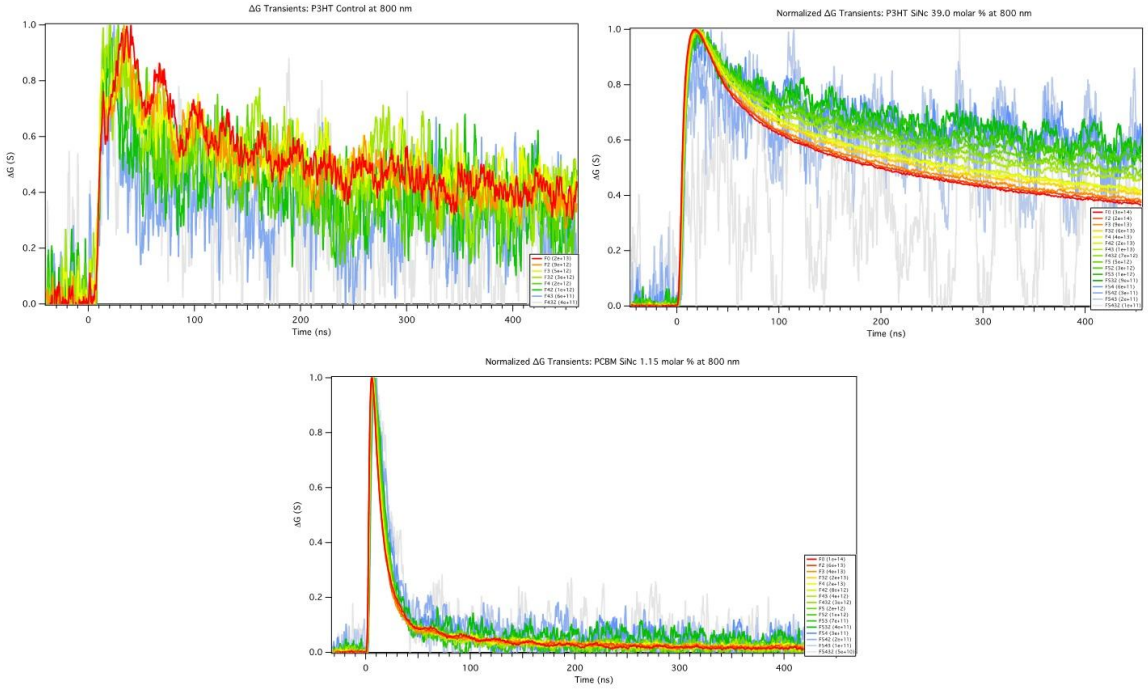

Figure 3-22. Normalized photoconductance (ΔG) transients for neat P3HT, neat P3HT with SiNc (39.0 molar percent), and neat $PC_{60}BM$ with SiNc (1.15 molar percent) at 800 nm.

After the yield mobility product (φΣμ) transients were fitted with the double exponential function, the yield mobility product at time zero (t=0 φΣμ) plots were obtained. Figure 3-23 shows the plots for neat P3HT, neat P3HT with SiNc, and neat $PC_{60}BM$ with SiNc. The data points are represented as squares and the modified Dicker fits are represented as solid lines. Once again, there is no data for the thin film of neat $PC_{60}BM$ since this sample does not absorb light at 800 nm. Table 3-8 summarizes the Dicker A values for the three samples, in which the neat $PC_{60}BM$ with SiNc sample has a larger value than that for neat P3HT. There are a limited number of data points for the yield mobility product at time zero plot for neat P3HT, due to large amount of noise when exciting P3HT at 800 nm. However, the upward trajectory of the modified Dicker fit makes it apparent that neat P3HT has a larger Dicker A value than the value for neat P3HT with SiNc. While neat $PC_{60}BM$ containing SiNc results in a larger yield, as compared to

the control P3HT sample, the thin film of neat P3HT with SiNc has a yield mobility product at time zero value an order of magnitude smaller than the control sample.

This is interesting because the addition of SiNc to a P3HT-rich environment decreased the yield of the bulk heterojunction, since the values for mobilities of electrons and holes are unchanged. Since SiNc acts as an electron trap in this P3HT-rich environment, an electron will be present on SiNc while a mobile hole will be located on P3HT. The electron is trapped on SiNc since it cannot be transferred to an acceptor molecule, such as $PC_{60}BM$. Therefore, the mobility that is being measured in neat P3HT with SiNc is the hole mobility on P3HT. Due to the fact that the hole mobility on P3HT is $2x10^{-8}$ $m^2V^{-1}s^{-1}$, which is significantly less than the electron mobility on $PC_{60}BM$, $3x10^{-7}$ $m^2V^{-1}s^{-1}$, the Dicker A value should be less for P3HT with SiNc.[40] The trapping and de-trapping processes in the P3HT with SiNc thin film are being measured in the yield mobility product at time zero plots as well. The plot for neat $PC_{60}BM$ with SiNc is actually measuring the electron mobility on $PC_{60}BM$ as well as the quick recombination of the trapped holes on SiNc and the electrons on $PC_{60}BM$. The fast recombination of free charges is apparent from the normalized photoconductance plot for this sample, as seen in Figure 3-22. There are no trap sites on $PC_{60}BM$,[56] therefore the yield mobility product at time zero plot will not measure the trapping or de-trapping of $PC_{60}BM$.

Looking at the shape of the yield mobility product at time zero plots in Figure 3-23, it is apparent that the data for neat P3HT with SiNc and neat $PC_{60}BM$ with SiNc are very similar. First of all, both traces seem to plateau at low intensities relatively quickly, while at high light intensities, the data points do not sharply drop off. This is due to the presence of electron or hole traps in the neat films, which disrupts the recombination of free charges. If the Dicker A values for neat films with SiNc are compared to the ternary blend of P3HT:$PC_{60}BM$ and SiNc, excited

at 800 nm, it can be seen that neat film of $PC_{60}BM$ and SiNc actually has a larger Dicker A value, 9.0058e-2 $cm^2/V{\cdot}s$, than the value for P3HT:$PC_{60}BM$ and SiNc, 2.5861e-2 $cm^2/V{\cdot}s$. This is most likely due to measurement of only the mobile electrons on $PC_{60}BM$ in the neat sample. On the other hand, the Dicker A value for the neat P3HT with SiNc sample is smaller than the value for the ternary blend. Also, the shapes of the plots for all three samples are nearly identical, which means that the decay process are similar. Therefore, it can be concluded that SiNc is positioned in P3HT-rich regions, $PC_{60}BM$-rich regions, and amorphous regions in a ternary blend of P3HT:$PC_{60}BM$.

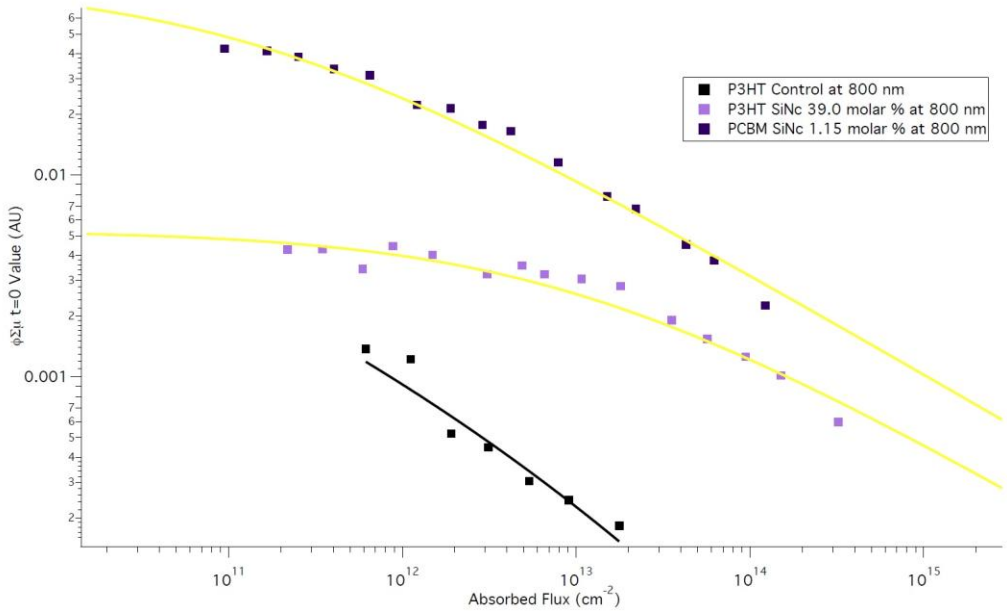

Figure 3-23. The yield mobility product at time zero (t=0 φΣμ) plots for neat P3HT, neat P3HT with SiNc (39.0 molar percent), and neat $PC_{60}BM$ with SiNc (1.15 molar percent) at 800 nm.

	Dicker A Values ($cm^{-2}V^{-1}s^{-1}$)
P3HT at 800 nm	2.6403e-2
$PC_{60}BM$ at 800 nm	0
P3HT SiNc (39.0 molar %) at 800 nm	5.3252e-3
$PC_{60}BM$ SiNc (1.15 molar %) at 800 nm	9.0058e-2

Table 3-8. Summary of the Dicker A values from the modified Dicker fits of the yield mobility at time zero (t=0 φΣμ) plots for neat P3HT, neat P3HT with SiNc (39.0 molar percent), and neat $PC_{60}BM$ with SiNc (1.15 molar percent) at 800 nm.

Flash-photolysis TRMC experiments were carried out on thin film samples of neat P3HT with a phthalocyanine and neat $PC_{60}BM$ containing one of the phthalocyanines, excited at 800 nm. The transients for photoconductance (ΔG) and yield mobility product (φΣμ) are in Figures C-22 through C-27 and C-31 through C-36 in Appendix C. Once again, there is no data for neat $PC_{60}BM$ due to the fact that the thin film sample that was spin-coated did not absorb light at 800 nm. Below, Table 3-9 summarizes the signal strength for the photoconductance and yield mobility product transients for neat P3HT, neat P3HT with Pc1, Pc2, or Pc3, and neat $PC_{60}BM$ with one of the phthalocyanines. Looking at the photoconductance signal strength, the neat P3HT samples with Pc1, Pc2, or Pc3 have a higher signal than the P3HT control sample, pulsed at 800 nm. The thin films with Pc1 or Pc2 have a signal that is an order of magnitude larger than the control sample. This result makes sense because the phthalocyanines absorb significantly more light at 800 nm, as compared to neat P3HT. These values are summarized in Table 3-2. There is more variation in the signal strength for the photoconductance transients of neat $PC_{60}BM$ thin films with one of the phthalocyanines. The yield mobility product signal strengths for the neat P3HT films with Pc1 or Pc2 are an order of magnitude larger than the control sample, however, the sample containing Pc3 has a smaller signal. On the other hand, neat films of $PC_{60}BM$ with Pc1 or Pc2 have large yield mobility product signals.

Comparing the signal strength for the transients for neat films to the ternary blend films, it can be shown that the ternary blend samples have larger signal strengths for photoconductance and yield mobility product. However, neat samples containing Pc2 have very similar values to the sample of P3HT:$PC_{60}BM$ with Pc2, as summarized in Table 3-5. Both the photoconductance

and yield mobility product signal strengths are on the same order of magnitude, which is very important because this demonstrates that the addition of Pc2 to a neat sample of P3HT or $PC_{60}BM$ can significantly increase experimental signals. The values for samples containing Pc1 or Pc3 vary quite a bit from the ternary blend samples, however, the addition of one of these phthalocyanines to a neat thin film sample does not destroy the sample, even though the small molecules act as electron or hole traps.

	ΔG Signal Strength (S)	φΣμ Signal Strength ($cm^2/V \cdot s$)
P3HT at 800 nm	1.0287e-9	7.1231e-4
$PC_{60}BM$ at 800 nm	0	0
P3HT Pc1 (46.5 molar %) at 800 nm	1.0654e-8	1.1114e-3
$PC_{60}BM$ Pc1 (1.56 molar %) at 800 nm	4.7274e-9	7.4610e-3
P3HT Pc2 (44.1 molar %) at 800 nm	3.0825e-8	1.6947e-3
$PC_{60}BM$ Pc2 (1.42 molar %) at 800 nm	1.0695e-8	6.8317e-3
P3HT Pc3 (47.8 molar %) at 800 nm	9.7063e-9	2.0710e-4
$PC_{60}BM$ Pc3 (1.64 molar %) at 800 nm	3.1354e-9	6.2876e-4

Table 3-9. Summary of the signal strength for photoconductance (ΔG) and yield mobility product (φΣμ) transients of neat P3HT, neat P3HT with one of the phthalocyanines, and neat $PC_{60}BM$ containing one of the phthalocyanines at 800 nm.

Comparing the normalized photoconductance transients can give insight into the decay mechanisms of the free charge carriers in the bulk heterojunction. Figure 3-24, as seen below, illustrates the plots for normalized photoconductance transients of neat P3HT, neat P3HT with Pc1, and neat $PC_{60}BM$ with Pc1, excited at 800 nm. It is important to note that all three samples are not dependent upon the light intensity of the laser, since the transients, in an individual plot,

decay with the same shape and to the same position in the 500 ns time window. Even though there is a significant amount of noise in each plot, the transients for higher light intensities lie on top of each other, indicating that a change in the neutral density filter does not affect the decay of the photoconductance signal. If the plots for neat P3HT with Pc1 and neat $PC_{60}BM$ with Pc1 are compared to the control sample of neat P3HT, it can be seen that neat P3HT sample containing Pc1 is nearly identical to the control thin film plot. Both sets of normalized photoconductance transients decay to the same position in the time window with a very similar curvature. This is interesting because it does not seem to matter what molecule is excited in a neat sample of P3HT since the neat P3HT with Pc1 thin film behaves the same as the neat P3HT thin film. On the other hand, the neat $PC_{60}BM$ sample with Pc1 behaves in a very different way. First of all, the signal for neat $PC_{60}BM$ containing Pc1 decays very rapidly, which means the curvature of the normalized transients is dissimilar to both the control P3HT sample and the neat P3HT sample with Pc1. Second, since neat $PC_{60}BM$ with Pc1 decays quickly, the positions of the transients in the 500 ns time window are much lower than the other two plots. This comparison demonstrates that the decay dynamics of neat P3HT and neat P3HT with Pc1 are identical while the decay of the free charge carries in neat $PC_{60}BM$ containing Pc1 is very different. This result makes sense because Pc1 is present in two environments, since P3HT is a donor molecule and $PC_{60}BM$ is an acceptor molecule and because these two molecules crystallize differently as well.

Now, the normalized photoconductance transients, as seen in Figure 3-17, for P3HT:$PC_{60}BM$ with Pc1 can be compared to the plots for neat P3HT with Pc1 and neat $PC_{60}BM$ with Pc1. P3HT:$PC_{60}BM$ with Pc1 is dependent on light intensity of the laser, since the transients decay to different positions and with different curvatures. The F0 transient decays to 0.4, while the lowest light intensity transient, F5432, decays to 0.8. The plot of the normalized

photoconductance transients for neat P3HT with Pc1 demonstrates that the highest light intensity and lowest light intensity transients decay to the same position of 0.4, while the transients for neat $PC_{60}BM$ with Pc1 decay to 0.15. Since the shape of the normalized photoconductance transients for neat P3HT with Pc1 and neat $PC_{60}BM$ with Pc1 are completely different from the plot of the transients for P3HT:$PC_{60}BM$ with Pc1, it can be concluded that the decay mechanisms in these three samples are not the same. This is due to the fact that Pc1 is located in an amorphous region of P3HT:$PC_{60}BM$ only in the ternary blend sample.

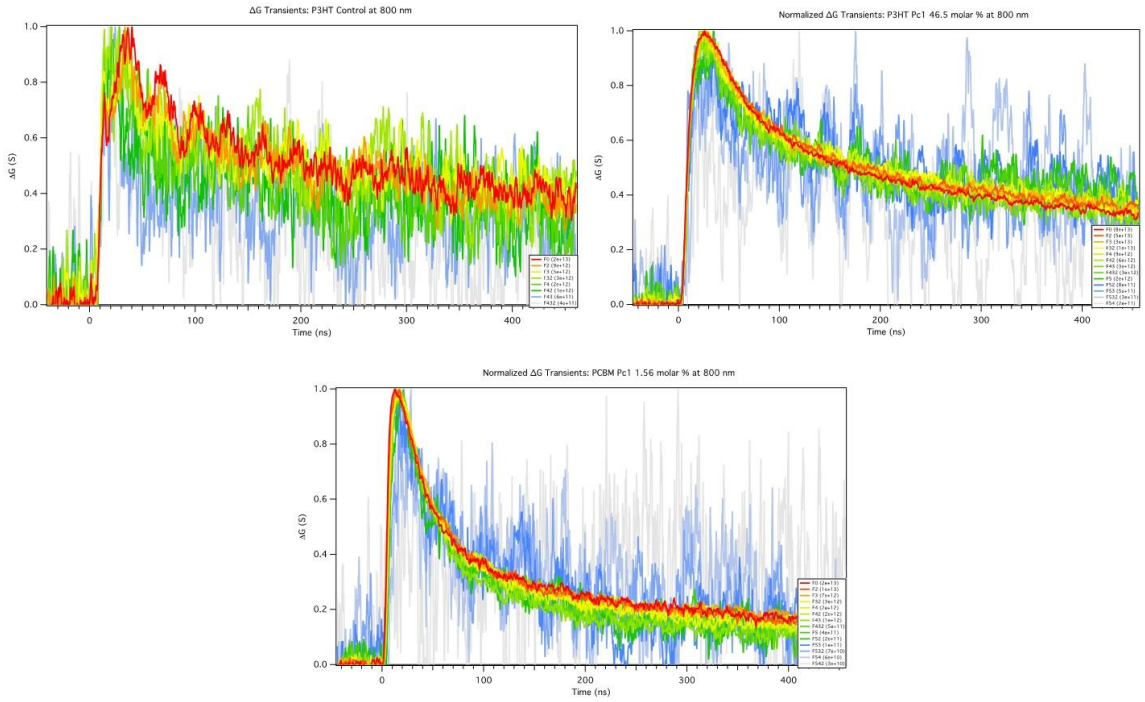

Figure 3-24. Normalized photoconductance (ΔG) transients for P3HT, neat P3HT with Pc1, and neat $PC_{60}BM$ containing Pc1 at 800 nm.

Figure 3-25 illustrates the normalized photoconductance transient plots for neat P3HT, neat P3HT with Pc2, and neat $PC_{60}BM$ with Pc2. All three samples were excited at 800 nm using the 4 ns wide laser pulse. Looking at the intensity dependence of each plot, it can be seen that the

samples are independent of the light intensity of the laser, however, there is a large amount of noise present. The shape and final positions of the neat P3HT and neat P3HT with Pc2 normalized transients are identical, which means that the free charges in these samples decay in the same manner. While neat P3HT with Pc2 behaves the same as the control sample, neat $PC_{60}BM$ with Pc2 decays very quickly in the 500 ns time window and reaches a much lower position than the other two plots. Therefore, the decay dynamics in neat $PC_{60}BM$ with Pc2 are different from the decay of free charges in neat P3HT and neat P3HT with Pc2. Comparing the neat samples to the ternary blend thin film samples, it can be concluded that the decay mechanisms in the ternary blend sample of P3HT:$PC_{60}BM$ with Pc2 are different from those in the neat thin films because the highest light intensity transient, F0, decays to 0.4, while the lowest light intensity transient, F5432, only decays to 0.8. However, the transients for the neat samples do not behave in this way. Also, the ternary blend sample is dependent on light intensity. In conclusion, free charges decay differently in neat P3HT, neat $PC_{60}BM$, and P3HT:$PC_{60}BM$ when Pc2 is present and excited at 800 nm. This is due to the very different environments of these three samples, however, more flash-photolysis TRMC analysis can shed light on the location of small molecules in thin film samples.

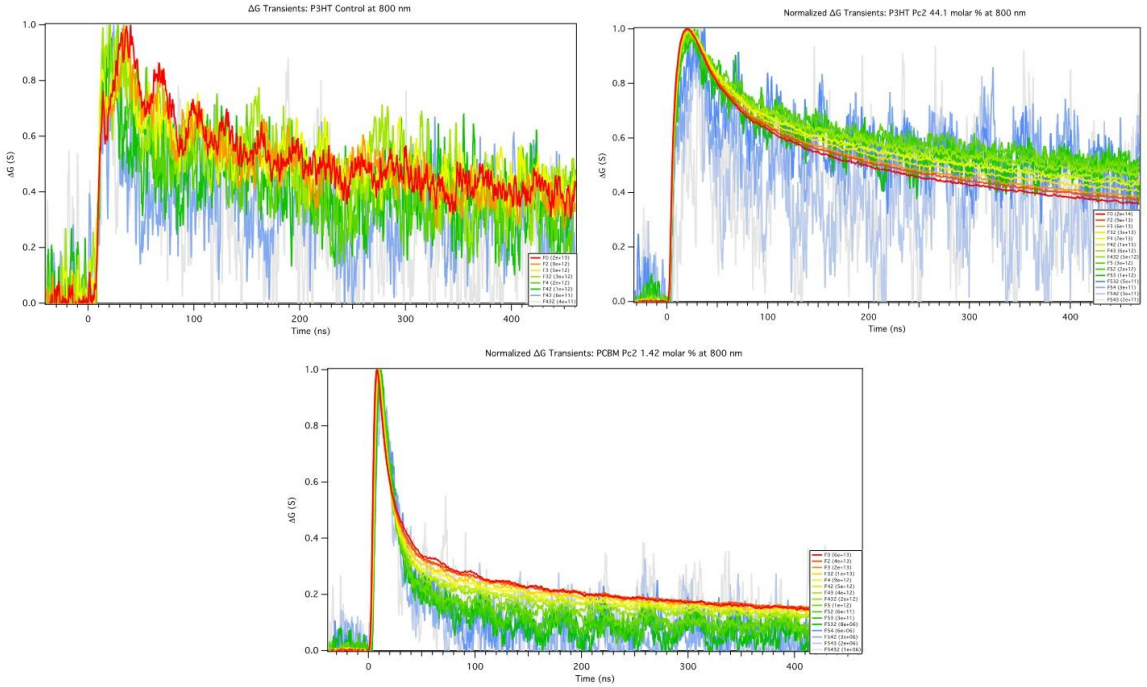

Figure 3-25. Normalized photoconductance (ΔG) transients for neat P3HT, neat P3HT containing Pc2, and neat $PC_{60}BM$ with Pc2 at 800 nm.

The normalized photoconductance transient plots for neat P3HT, neat P3HT with Pc3, and neat $PC_{60}BM$ with Pc3 are shown below in Figure 3-26. It is important to note that all three samples are not dependent upon the light intensity of the laser, even though there is a significant amount of noise. The shape and final position of the transients for neat P3HT and neat P3HT with Pc3 are the same, which means the decay mechanism of the free charges in these samples are the same. However, the plot for neat $PC_{60}BM$ with Pc3 is different since the signal decays rapidly, giving a sharp peak at the laser pulse and a lower position at the end of time window. The normalized plot for the photoconductance transients of P3HT:$PC_{60}BM$ with Pc3, as seen in Figure 3-17, decays to 0.4 for the highest intensity transient and 0.8 for the lowest intensity transient. This sample is also dependent upon the light intensity of the 4 ns wide laser pulse. Since the shape of the normalized photoconductance transients are different for the ternary blend

sample and the neat samples, it can be concluded that the decay mechanisms are not the same. This result makes sense because the environment of each sample is completely different and therefore, the behavior of free charges will be different.

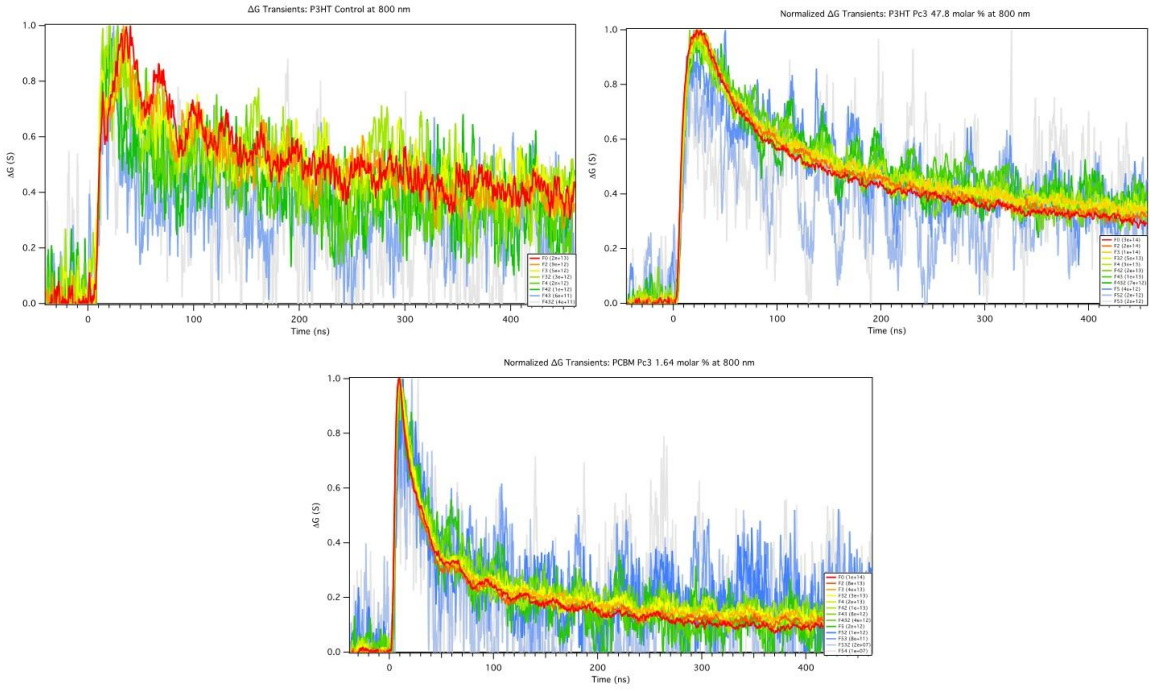

Figure 3-26. Normalized photoconductance (ΔG) transients for neat P3HT, neat P3HT with Pc3, and neat $PC_{60}BM$ containing Pc3 at 800 nm.

The yield mobility product at time zero (t=0 φΣμ) plots were obtained for the neat P3HT thin film, neat samples of P3HT with a phthalocyanine, and neat thin films of $PC_{60}BM$ with one of the phthalocyanines by extrapolating the double exponential fit of the yield mobility product transients to the beginning of the laser pulse. The plots are shown in Figures 3-27 through 3-29 below. It is important to note that there is no data for the thin film of neat $PC_{60}BM$, since this sample did not absorb any light at 800 nm. The Dicker A values for neat P3HT with Pc1 and neat P3HT with Pc2 are an order of magnitude less than the value for the control sample of neat

P3HT, while the value for neat P3HT with Pc3 is two orders of magnitude less. This means that exciting any of the phthalocyanines, in a neat P3HT environment, results in a smaller yield of free charge carriers in the bulk heterojunction. Therefore, the addition of a phthalocyanine and subsequent excitation of this small molecule, which means the phthalocyanine molecule must act as an electron trap resulting in lower yield of charges.

The Dicker A values for the neat $PC_{60}BM$ samples with one of the phthalocyanines vary a bit more than the neat P3HT thin film samples. Neat $PC_{60}BM$ with Pc1 has the same value as the neat P3HT control, within the error of the flash-photolysis TRMC system, while neat $PC_{60}BM$ with Pc2 has a Dicker A value that is slightly larger than the neat P3HT sample. However, neat $PC_{60}BM$ with Pc3 sample's Dicker A value is an order of magnitude smaller than the neat P3HT thin film. Even though the free charges in neat $PC_{60}BM$ samples have the shortest lifetimes, as shown in the normalized photoconductance transients, they have the largest yield in the yield mobility product at time zero ($t=0$ $\varphi\Sigma\mu$) plots. This is due to the fact that the mobility of electrons on $PC_{60}BM$ is larger than the mobility of holes on P3HT.[40] As seen in samples containing SiNc, the TRMC experiments are measuring the trapping and de-trapping process in P3HT thin films, while fast recombination of free charges are measured in $PC_{60}BM$ samples. The quick recombination in $PC_{60}BM$ thin films is most likely due to the high mobility of electrons on $PC_{60}BM$, since they have a strong possibility of interacting with a trapped hole on one of the phthalocyanines within the time window of the measurement. A summary of the Dicker A values is shown in Table 3-10.

The Dicker A values for the neat thin film samples can be compared to the values for the ternary blend samples in order to determine the effect of adding a phthalocyanine to the bulk heterojunction. Table 3-6 shows the Dicker A values for the ternary blends, excited at 800 nm.

The value for P3HT:$PC_{60}BM$ with Pc1 is 1.3709e-2 $cm^{-2}V^{-1}s^{-1}$, however, the Dicker A value for neat P3HT with Pc1 is an order of magnitude lower than this, while the value for neat $PC_{60}BM$ with Pc1 is very similar to the ternary blend's value. This comparison demonstrates that adding Pc1 to neat P3HT or neat $PC_{60}BM$ results in free charge generation. The lower value for neat P3HT with Pc1 can be attributed to the measurement of mobile holes on P3HT, which is less than the electron mobility on $PC_{60}BM$. The thin film sample of neat P3HT with Pc2 has a Dicker A value close to the value for P3HT:$PC_{60}BM$ with Pc2, 8.6802e-3 $cm^{-2}V^{-1}s^{-1}$. On the other hand, neat $PC_{60}BM$ with Pc2 has a Dicker A value that is an order of magnitude greater than the value for P3HT:$PC_{60}BM$ with Pc2. Interestingly, the addition of Pc2 to $PC_{60}BM$ increases the yield of free charge carriers, more so than mixing Pc2 with P3HT:$PC_{60}BM$. Comparing the Dicker A values for samples containing Pc3 is more difficult due to the large variation in values. However, it is evident that the addition of phthalocyanines to the bulk heterojunction of neat thin film samples results in a significant yield of free charges, upon excitation.

The shape of the yield mobility product at time zero (t=0 $\varphi\Sigma\mu$) plots can give insight into the decay processes of free charges in the thin films. The data points in Figures 3-27 through 3-29 reach the imaginary asymptotic line, represented by the Dicker A value, very quickly. At higher intensities, the data points do not sharply turn over, as seen in the plots for ternary blends of P3HT:$PC_{60}BM$ with one of the phthalocyanines, excited at 500 nm, in Figures 3-18 through 3-20. The shape of the plots for neat samples and ternary blend samples, excited at 800 nm, are very similar which means the decay mechanisms are nearly identical. This result makes sense because phthalocyanine molecules have the opportunity to be positioned in an amorphous region, in a P3HT-rich region, and in a $PC_{60}BM$-rich region when they are mixed with P3HT:$PC_{60}BM$. Since the shapes of the modified Dicker fits are similar, ternary blend samples must have three

regions in their morphology and phthalocyanine molecules can possibly be located in each environment.

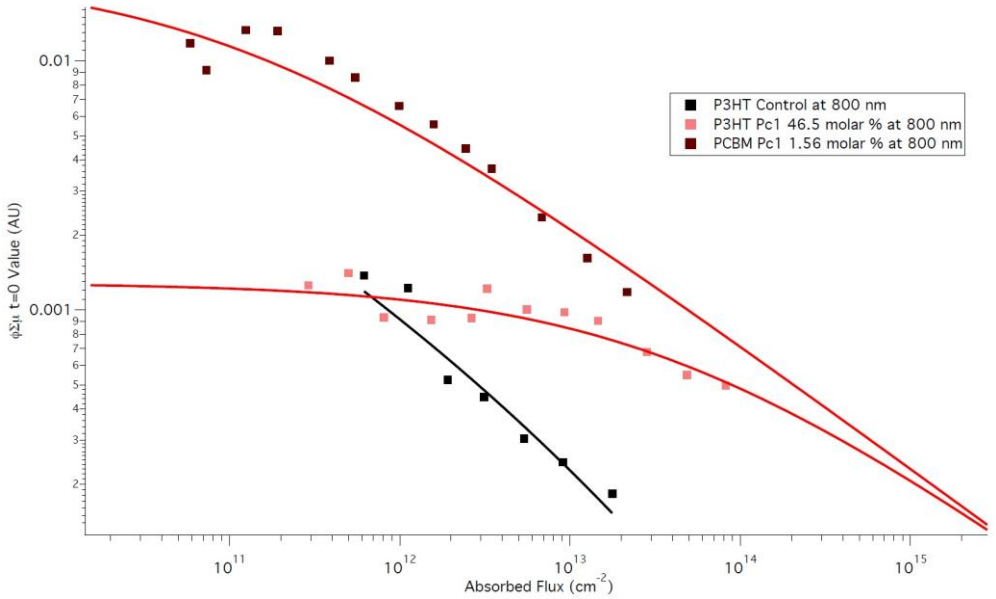

Figure 3-27. The yield mobility product at time zero (t=0 φΣμ) plots for neat P3HT, neat P3HT with Pc1 (46.5 molar percent), and neat $PC_{60}BM$ with Pc1 (1.56 molar percent) at 800 nm.

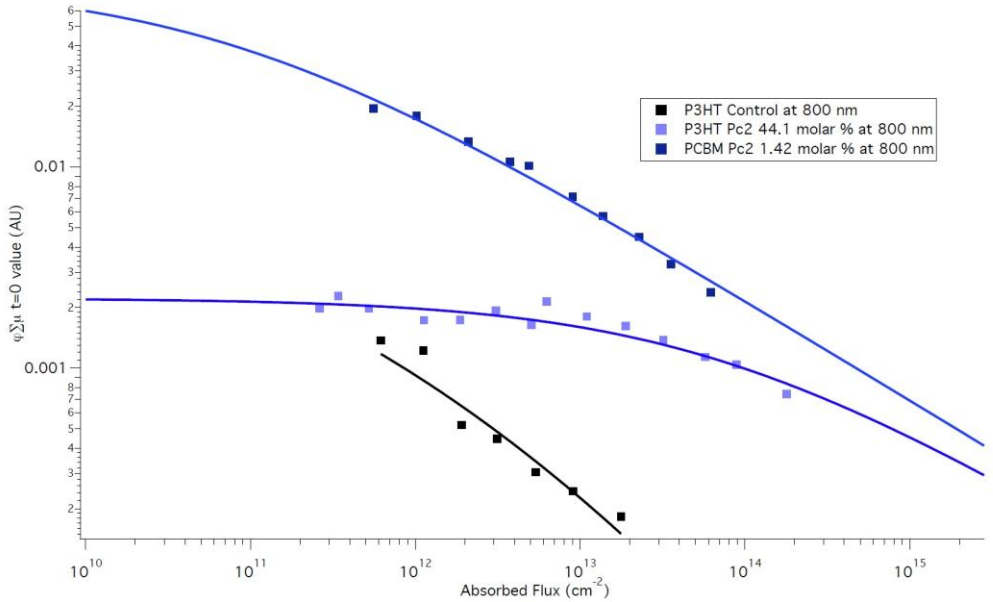

Figure 3-28. The yield mobility product at time zero (t=0 φΣμ) plots for neat P3HT, neat P3HT with Pc2 (44.1 molar percent), and neat $PC_{60}BM$ with Pc2 (1.42 molar percent) at 800 nm.

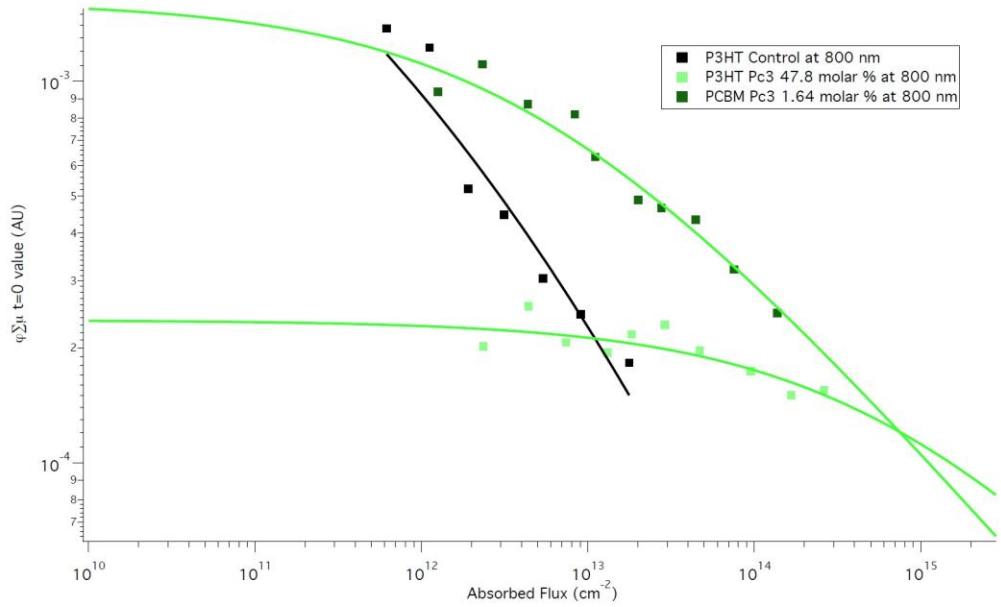

Figure 3-29. The yield mobility product at time zero (t=0 φΣμ) plots for neat P3HT, neat P3HT with Pc3 (47.8 molar percent), and neat $PC_{60}BM$ with Pc3 (1.64 molar percent) at 800 nm.

	Dicker A Values ($cm^{-2}V^{-1}s^{-1}$)
P3HT at 800 nm	2.6403e-2
$PC_{60}BM$ at 800 nm	0
P3HT Pc1 (46.5 molar %) at 800 nm	1.2829e-3
$PC_{60}BM$ Pc1 (1.56 molar %) at 800 nm	2.2595e-2
P3HT Pc2 (44.1 molar %) at 800 nm	2.2258e-3
$PC_{60}BM$ Pc2 (1.42 molar %) at 800 nm	8.1855e-2
P3HT Pc3 (47.8 molar %) at 800 nm	2.3646e-4
$PC_{60}BM$ Pc3 (1.64 molar %) at 800 nm	1.6193e-3

Table 3-10. Summary of the Dicker A values from the modified Dicker fits of the yield mobility at time zero (t=0 φΣμ) plots for neat P3HT, neat P3HT with one of the phthalocyanines, and neat $PC_{60}BM$ containing a phthalocyanine at 800 nm.

3.4 Energy Levels and Driving Force

As discussed in the previous chapter, photoexcitation of P3HT leads to an electron in the excited state of P3HT. This electron can undergo electron transfer to SiNc and then to $PC_{60}BM$,

while the hole moves in the opposite direction. Figure 3-30, as seen below, illustrates the energy level diagram for a ternary blend of P3HT:$PC_{60}BM$ with SiNc. In the diagram, P3HT is excited by a photon to generate an electron in the excited state. However, there is also the option of photoexciting SiNc and generating an electron-hole pair on the small molecule. In this case, an electron would move from SiNc to $PC_{60}BM$ and a hole would be transferred from SiNc to P3HT. The reduction and oxidation potentials for P3HT are -3.0 eV and -5.1 eV vs. vacuum, respectively, while the reduction and oxidation potentials for $PC_{60}BM$ are -4.1 eV and -6.0 eV vs. vacuum, respectively.[54,55] The energy levels for SiNc were measured against Fc^{+}/Fc, but were reported vs. vacuum.[51]

Figure 3-30 demonstrates that SiNc has energy levels that are ideally positioned in between the energy levels of the donor and acceptor molecules. The energy levels of SiNc provide the answer to why this small molecule is able to be placed in a blend with P3HT and $PC_{60}BM$ and still produce free charge carriers. The energy levels allow the transfer of electrons and holes to their intended targets, as if the small molecule wasn't there. Theoretically, if SiNc had a reduction potential that was less negative than the reduction potential of P3HT, electrons would not be able to transfer from P3HT to SiNc and then to $PC_{60}BM$. In this case, an electron would be trapped on P3HT. On the other hand, if SiNc had a more negative oxidation potential than the oxidation potential of $PC_{60}BM$, $PC_{60}BM$ would act as a hole trap. This theoretical thinking assumes that SiNc is ideally positioned in the amorphous region of P3HT:$PC_{60}BM$, which means the charges must go through SiNc.

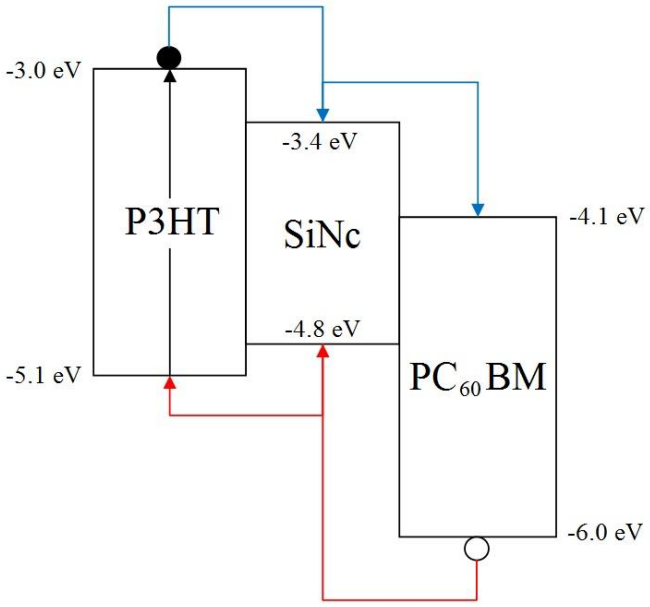

Figure 3-30. The energy level diagram for a ternary blend of P3HT:$PC_{60}BM$ with SiNc. The black arrow represents photoexcitation, the filled circle represents an electron, the open circle represents a hole, the blue arrows represent the electron pathways, and the red arrows represent the hole pathways. The oxidation and reduction potentials are reported vs. vacuum.

As seen below, Figure 3-31 is the energy level diagram for a ternary blend of P3HT:$PC_{60}BM$ with one of the phthalocyanines. Since the reported oxidation and reduction potentials for all three phthalocyanines were nearly identical,[52] they are assumed to be exactly the same in this discussion. In this case, the phthalocyanine molecules have energy levels that are ideally positioned between the energy levels of P3HT and $PC_{60}BM$. This is because electrons always transfer to reach a lower energy state, while holes move to a higher energy state. Since the oxidation potential of the phthalocyanines is more negative than the oxidation potential for P3HT, the hole will easily transfer from $PC_{60}BM$ to the phthalocyanine molecule and then to P3HT. Figure 3-31 illustrates that the addition of a phthalocyanine to a blend of P3HT:$PC_{60}BM$

will still allow the transfer of electrons and holes. This reasoning explains why solar cell devices with a phthalocyanine molecule were still functional and why TRMC studies on thin films containing a phthalocyanine molecule produced a large yield of free charge carriers. If it wasn't for the position of the phthalocyanine molecules' energy levels, these experiments would not have been successful.

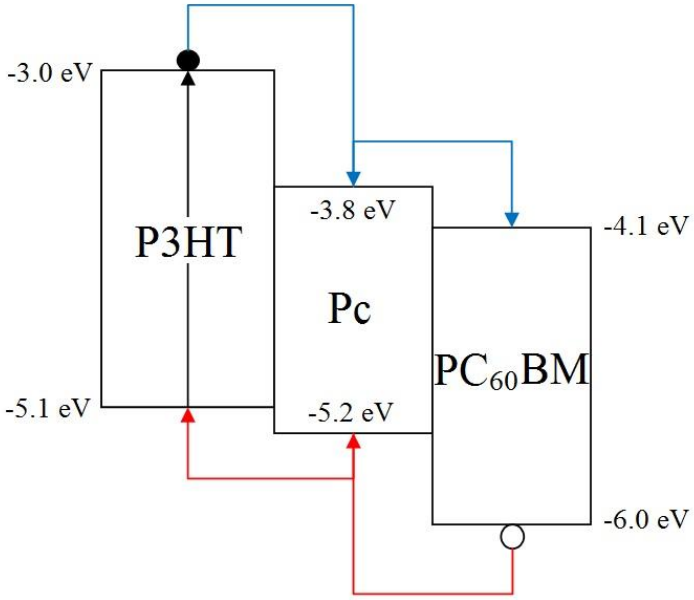

Figure 3-31. The energy level diagram for a ternary blend of P3HT:$PC_{60}BM$ with Pc1, Pc2 or Pc3. The black arrow represents photoexcitation, the filled circle represents an electron, the open circle represents a hole, the blue arrows represent the electron pathways, and the red arrows represent the hole pathways. The oxidation and reduction potentials are reported vs. vacuum.

Marcus theory explains the idea of a driving force for the photoinduced electron transfer in solar cell devices. Based upon Marcus theory, the most efficient photogeneration of free charge carriers occurs when the donor and acceptor energy level offset is similar to the sum of the exciton energy and the reorganization energy.[57] The reorganization energy, treated classically

by Marcus theory, is the energy associated with changing the configuration of the reactants into the configuration of the products.[58,59] This reorganization occurs through changing bond lengths and bond angles. The driving force, which is the change in Gibbs free energy (ΔG), increases as the yield of free charge carries is increased.[61] Equation 16 shows an adaptation of an equation for the driving force, which takes into account the oxidation and reduction potentials of the molecules:

$$\Delta G = (P_{oxidation} - P_{reduction}) - E_{exciton} \quad (16)$$

where $P_{oxidation}$ is the oxidation potential of the acceptor molecule, $P_{reduction}$ is the reduction potential of the donor molecule, and $E_{exciton}$ is the energy of an exciton.[61] The energy of an exciton is experimentally measured through spectroscopy and is estimated as the intersection of the absorption and emission spectra. The driving force can be increased to a peak position, but a greater force actually results in a decrease of charge generation. This phenomenon is known as the Marcus inverted region and it is caused by increasing the driving force to the point where the reorganization energy is too large.[57,58,60,61]

The values for the oxidation and reduction potentials used for the calculation of the driving force are the same as the numbers in Figures 3-30 and 3-31. The energy of the exciton for SiNc is 1.587 eV, since the intersection of the absorption and emission spectra, as seen in Figure 3-9, is 781.8 nm. The exciton energy for Pc1 is 1.631 eV. The intersection of the spectra, in Figure 3-13, is 760.7 nm. Even though Pc1 is used for the calculation, the energies of the exciton for the other two phthalocyanines are very similar. The driving force was calculated using P3HT as the donor molecule and the small molecule as the acceptor. Calculations were also carried out using the small molecule as the donor and $PC_{60}BM$ as the acceptor. Due to the use of neat thin films of both P3HT and $PC_{60}BM$, both of these calculations were necessary.

Table 3-11 summarizes the values used for the calculation and the associated driving forces. Notice that the driving force for P3HT and SiNc is positive, which means that the formation of free charge carriers should not occur in this thin film. This explains the low yield seen for this combination of donor and acceptor molecules. On the other hand, the three other driving forces are negative. The most negative driving forces are those with $PC_{60}BM$. This result helps to explain the very large yield seen in the yield mobility product at time zero plots. The calculation of the driving force is more evidence that the neat films with SiNc, or one of the phthalocyanines, still produces free charges.

	$P_{oxidation}$ (eV)	$P_{reduction}$ (eV)	$E_{exciton}$ (eV)	ΔG (eV)
P3HT/SiNc	5.1	3.4	1.587	+0.413
SiNc/$PC_{60}BM$	4.8	4.1	1.587	-0.887
P3HT/Pc	5.1	3.8	1.631	-0.331
Pc/$PC_{60}BM$	5.2	4.1	1.631	-0.531

Table 3-11. Summary of the values for the calculation of the driving force (ΔG) for SiNc and the phthalocyanine molecules.

3.5 Conclusion

Flash-photolysis time-resolved microwave conductivity (TRMC) experiments were carried out on ternary blend samples of P3HT, $PC_{60}BM$, and a small molecule. Neat thin films were also measured with this technique in order to compare the results to the ternary blends. Ternary blend films and neat films were manufactured exactly the same, so that the only variables between the samples were the contents of the bulk heterojunction. TRMC measurements were performed in order to determine the yield mobility product at time zero (t=0 $\varphi\Sigma\mu$) plots of the samples. This plot gives quantitative data for the yield of photogenerated free charge carriers and qualitative data for the decay mechanisms of the free charges. Normalized

photoconductance (ΔG) plots also give insight into the decay dynamics of the thin film samples as well as the light intensity dependence of the samples.

In conclusion, the addition of SiNc or one of the phthalocyanine molecules to the bulk heterojunction of P3HT:$PC_{60}BM$ results in the generation of a high yield of free charge carriers, after excitation from the 4 ns wide laser pulse. Not only is there a large yield of charges produced, but the yield is comparable to the control sample in several cases. These general results demonstrate that adding a small molecule to a blend of P3HT:$PC_{60}BM$ does not interrupt the interaction of light with P3HT or $PC_{60}BM$ and that the small molecule acts as an intermediary between the donor molecules and the acceptor molecules. As discussed in the previous section, the photogeneration of this high yield of free charges would not be possible if not for the appropriate energy levels of the small molecules. The energy levels hold the answer to why these samples produce free charges. If the energy levels of the small molecules were changed significantly, the small molecule would act as an electron or hole trap in any environment.

The neat thin film samples had similar results, however, the yield of free charges varied more than the ternary blend samples. That said, the neat $PC_{60}BM$ thin films with SiNc or one of the phthalocyanines had very high yields, which can be explained by the driving force calculation. Also, the high yield is due to the measurement of mobile electrons on $PC_{60}BM$. It is interesting to note that the lifetime of free charges in the neat $PC_{60}BM$ thin films was the shortest, while the yield was very large. This result is due to the quick recombination of mobile electrons on $PC_{60}BM$ and the trapped holes on the small molecule. On the other hand, neat P3HT thin films with one of the small molecules had relatively low yield of free charge carriers in the yield mobility product at time zero plots. The lower yield can be explained by the smaller driving

force associated with this neat film and the measurement of mobile holes on P3HT. In conclusion, adding a small molecule to a neat thin film results in this molecule acting as an electron or hole trap, but a significant amount of free charges are still produced.

3.6 Experimental

3.6.1 Materials

The regio-regular sample of P3HT was purchased from Rieke Metals, Inc. (#4002-E, M_w=50,000 g/mol, regio-regularity of 93%). The sample of $PC_{60}BM$ was purchased from Nano-C (#KB121112, purity of 99.5%). The SiNc sample was obtained from Alan Sellinger, from the Colorado School of Mines, and the phthalocyanine samples (Pc1, Pc2, and Pc3) were acquired from Devens Gust, from Arizona State University. The 1,2-dichlorobenzene solution was purchased from Sigma-Aldrich (#SHBC7846V, anhydrous, 99%). The quartz substrates were obtained from Allen Scientific Glass, Inc. (#ASG2073, 11mm x 24 mm x 1 mm). Helmanex® was purchased from Hellma (#190504). Acetone was obtained from J.T. Baker (#53066, FW: 58.080) and isopropanol cleanroom LP (IPA) was purchased from KMG (#305BE3247). The Liquinox® detergent was purchased from Alconox (#1232). The HPLC grade toluene used for solution-phase absorption was purchased from Fisher Chemical (#T290-1, 1 L). All of the samples were used as received.

3.6.2 Thin Film Fabrication

P3HT and $PC_{60}BM$ were weighed out on a Sartorius digital scale (#CP255D, Max 220 g). The P3HT and $PC_{60}BM$ samples were transferred to a Fisherbrand vial (#03-339-21B, 15 mm x 45 mm). A Thermo Scientific Septa cap (#C4015-10, White virgin PTFE) was inserted into the Fisherbrand vial lid in order to create a better seal. Afterwards, a VWR® Spinbar® micro stir bar

was added to the vial so the sample could be stirred on a Scilogex hot plate (#MS-H-Pro). The P3HT and $PC_{60}BM$ sample was made to a concentration of 50 mg/mL, dissolved in 1,2-dichlorobenzene. A solution containing SiNc was also made to a concentration of 50 mg/mL, dissolved in 1,2-dichlorobenzene. The two solutions were stirred on a hot plate, at 400 rpm and 115 °C, in a MBRAUN glove box (Unilab, #UL03-121), overnight. The SiNc solution was mixed with the P3HT:$PC_{60}BM$ solution. The ternary solution was stirred on a hot plate, at 400 rpm and 65°C, under nitrogen atmosphere, overnight.

Thin films were deposited on quartz substrates. The substrates were cleaned in a Fisher Hamilton fume hood (Safeaire, #54-L) with a 2% Helmanex in DI water solution. The substrates were sonicated (Cole-Parmer, #8893) in this detergent solution for 30 minutes and then dried with a pressured nitrogen stream. Afterwards, the substrates were sonicated in DI water for 20 minutes and dried with nitrogen. The substrates were then sonicated in IPA for 10 minutes and dried with nitrogen. The final sonication took place in acetone for 10 minutes. After the substrates were dried with nitrogen, they were placed in the UV ozone plasma cleaner (Technics West Inc., #500-II) for 15 minutes.

The cleaned quartz substrates were immediately placed in a nitrogen atmosphere. The ternary blend solution was spin coated onto the quartz substrates at 900 rpm for 45 seconds. This results in a layer that is approximately 250 nm thick. After the thin films were deposited, they were placed in a covered Petri dish in order to slowly dry overnight. When the samples were dry, they were annealed on a hot plate at 110 °C for 10 minutes. The samples were stored in a MBRAUN glove box (Labmaster SP, #10-257) until they were used for a flash-photolysis TRMC measurement.

3.6.3 Absorptance of Thin Films

The absorptance spectra of the thin film samples were measured on a Shimadzu UV-3600 UV-VIS-NIR Spectrophotometer, with an external ISR-3100 integrating sphere attachment. The details of this system are described in section 2.5.3.

3.6.4 Solution-Phase Absorption

The small molecules used in these experiments were dissolved in HPLC grade toluene and transferred to cuvettes in order to obtain the absorption spectra. HPLC grade toluene was used a blank. A Cary 500 Scan UV-Vis-NIR Spectrophotometer (Vairan EL00023134) was used to measure the absorption spectra of these molecules. The spectrophotometer took measurements from 300 nm to 1000 nm at an interval of 1 nm.

3.6.5 Photoluminescence

Photoluminescence (PL) is the emission of a photon after a molecule has absorbed light from a source, in this case a laser pulse. The molecule is photoexcited by the laser, resulting in an excited state. This excited state can relax to the ground state, a lower energy state, by emitting a photon. Emission measurements were determined using a Horiba Jobin Yvon Fluorolog-1039 with 300 lines per mm gratings, 5 nm slit widths, and a charge-coupled device (CCD) detector attached to a Horiba iHR320 Imaging Spectrometer. The samples used for solution-phase absorption were also used for photoluminescence measurements. The small molecules were dissolved in HPLC grade toluene and diluted to low concentrations so that both absorption and emission measurements could be taken. The excitation wavelength was chosen so that it did not interfere with the emission peak of the sample. Excitation wavelengths were primarily shifted to the blue, compared to the emission peak.

3.6.6 Flash-Photolysis Time-Resolved Microwave Conductivity

Time-resolved microwave conductivity (TRMC) is a contactless, transient absorption method which takes advantage of the pump-probe technique. The laser source is a Continuum Precision II Nd:YAG and its primary excitation is 10 Hz at 355 nm. After pulsing, the laser passes through the Continuum Panther Optical Parametric Oscillator (OPO), which tunes the primary excitation beam to any wavelength from 410 nm to 2600 nm. Then the laser beam passes through diffusers, in order to evenly diffuse the beam over the sample area. The laser also passes through neutral density filters, which vary the light intensity in order to create numerous transients, ranging from 10^{12} to 10^{14} photons/cm^2. Finally, the beam reaches the sample in the resonant microwave cavity, as diagramed in Figure 3-32. Before measurements were taken, an automated power reading calibration of the laser was taken. This step ensured that the correct power of the laser at each neutral density filter combination, since neutral density filters are not completely neutral at every wavelength.

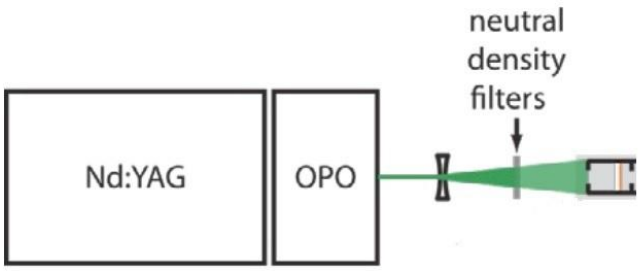

Figure 3-32. Diagram for the flash-photolysis time-resolved microwave conductivity (TRMC) laser setup. The TRMC system used for measurements consists of a Nd:YAG laser, an optimal parametric oscillator (OPO), diffusers, and neutral density filters. After the filters, the laser beam reaches the sample in the resonant microwave cavity.

The resonant microwave cavity is an X-band TE_{102} cavity. The probe is a microwave source that was tuned to 8.9 GHz, but this frequency depends on the thickness of the thin film and the dielectric constant of the sample. Figure 3-33, as seen below, outlines the general setup of the

TRMC system used in the experiments. The diffused laser pulse enters from the left hand side of the diagram and excites the thin film sample (2). The sample is positioned where the electric field is at its maximum. The resonant microwave cavity (1) has a quartz window facing the laser beam and metal grating. The purpose of the grating is to restrict the microwaves to the resonant cavity, since they are polarized in a particular direction, while the quartz window prevents photoionization of the thin film sample. A copper iris (3) sits in the resonant microwave cavity after the sample in order to restrict the wavelength of the microwaves in the cavity. As seen below, the circulator (4) directs microwaves from the source and into the resonant microwave cavity. The microwave source (5) is a Gunn diode which produces the X-band microwaves necessary for this experiment. After microwaves have been absorbed by the free charges in the thin film sample, the remaining microwave signal returns through the circulator and enters the microwave detector (6) and then the amplifier (7). The Tektronix oscilloscope (8) processes the data and follows the change in voltage during the experiment. Finally, the data is sent from the oscilloscope to the computer (9) which analyzes the data using Igor Pro.

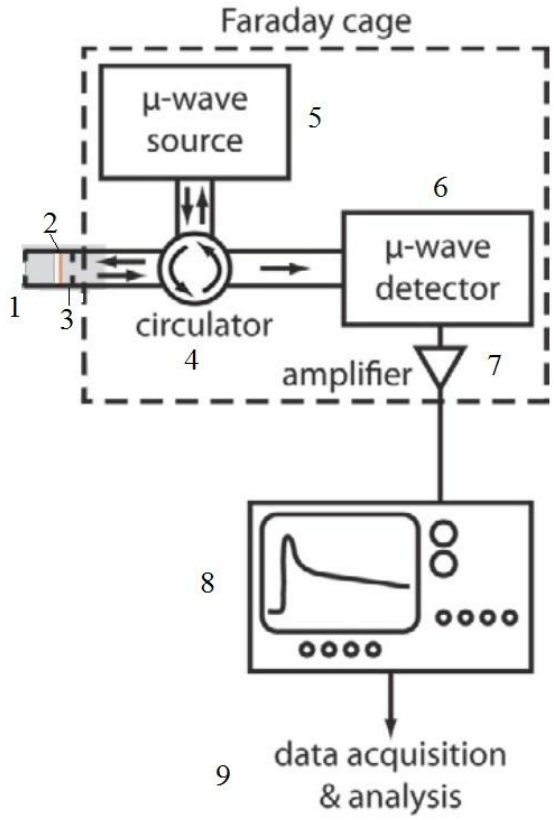

Figure 3-33. Diagram of the overall flash-photolysis time-resolved microwave conductivity (TRMC) system used for experimentation which includes: 1) the resonant microwave cavity, 2) the thin film sample on a quartz substrate, 3) copper iris, 4) circulator, 5) 8.9 GHz microwave source, 6) microwave detector, 7) amplifier, 8) Tektronix oscilloscope, and 9) computer with Igor Pro for recording and analyzing the data.

The laser pulse photo-generates excitons in the sample, which eventually dissociate into free charges. The microwave power is then absorbed by the free charges, which decreases the power output of the microwave. This decrease in the microwave power, ΔP(t), is proportional to the sample's photoconductance, ΔG(t). The change in the microwave power and the photoconductance are related by:

$$\frac{\Delta P(t)}{P_0} = -K \cdot \Delta G(t) \quad (17)$$

where P_0 is the initial microwave power and K is the sensitivity factor. K involves the dimensions and properties of the resonant microwave cavity, which will be discussed later.

Figure 3-34, below, illustrates the microwave power reflection coefficient, R, as a function of frequency. R is the ratio between the resonant microwave cavity's reflected power and shorting plate's reflected power. In Figure 3-34, the black circles represent the data points and the red line represents a Lorentzian fit to the data on the graph. Three values can be extracted from a plot of R vs. frequency: depth at the resonance (R_0), full width at half maximum (FWHM), and frequency at the resonance (f_0).

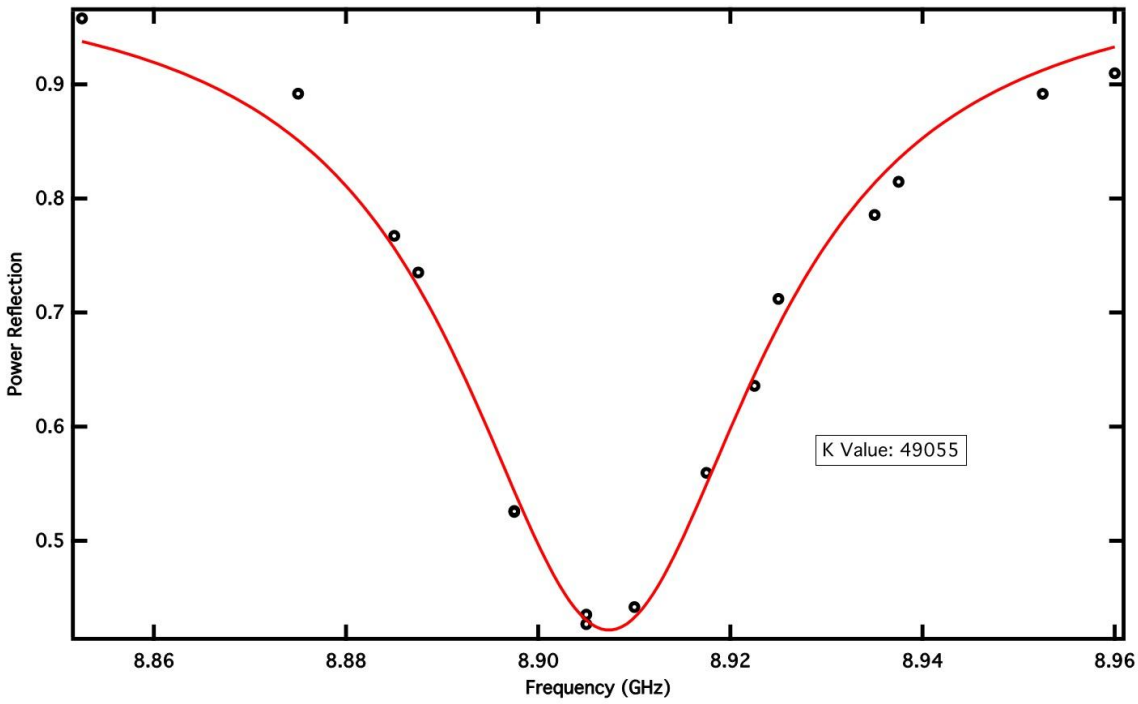

Figure 3-34. Resonance plot of the microwave cavity, using P3HT:PC_{60}BM with Pc1 (3.01 molar percent). The black circles represent the data points and the red line represents the Lorentzian fit to the data.

These values are used to determine the sensitivity factor (K) and the response time of the resonant microwave cavity (τ). The equation for τ is:

$$\tau = \frac{Q}{\pi \cdot f_0} \quad (18)$$

where Q is the quality factor of the resonant microwave cavity and f_0 is the frequency at the resonance. The equation for the quality factor, Q, is given by:

$$Q = \frac{f_0}{FWHM} \quad (19)$$

where f_0 is the frequency at the resonance and FWHM is the full width at half maximum of the resonance. The sensitivity factor, K, is calculated using the quality factor, Q, through the following formula:

$$-K = \frac{2Q\left(1 \pm \frac{1}{\sqrt{R_0}}\right)}{f_0 \varepsilon_r \varepsilon_0 d\left(\frac{a}{b}\right)\pi} \quad (20)$$

where Q is the quality factor, R_0 is the depth at the resonance, f_0 is the frequency at the resonance, ε_r is the dielectric constant of the sample, ε_0 is the permittivity of free space, d is the thickness of the sample, and a and b are the dimensions of the resonant microwave cavity. The value of d is approximately 100 nm since this is the thickness at which 90% of light is absorbed for the samples used in the experiments.

The equation for fitting the change in photoconductance of the sample as a function of time ($\Delta G(t)$) is shown below:

$$\Delta G(t) = A_1 \, exp\left(\frac{-t}{\tau_1}\right) + A_2 exp\left(\frac{-t}{\tau_2}\right) \quad (21)$$

where A_1 and A_2 are pre-exponential factors, t_1 and t_2 are time constants, and τ_1 and τ_2 are response times of the resonant microwave cavity. Equation 9 is a double exponential decay, which allows the fitting procedure to properly adjust for the rate of the photoconductance decay of the sample as well as the recombination or trapping of free charges.

The yield mobility product (φΣμ), which is one of the most important values to determine from experimental TRMC data, is calculated by using the formula below:

$$\varphi\Sigma\mu = \frac{\Delta G(t)}{\beta q_e I_0 F_A} \quad (22)$$

where φ is the yield, Σμ is the sum of mobilities, β is the ratio between the dimensions of the resonant microwave cavity, q_e is the charge of an electron, I_0 is the initial photon flux, and F_A is the fraction of light absorbed. The ratio of the dimensions of the microwave cavity used in these experiments is equal to 2.2.

The final step in analyzing the experimental TRMC data involves calculating the yield mobility product at time zero (t=0 φΣμ). This is determined by extrapolating the double exponential fits of the photoconductance (ΔG(t)) to the beginning of the laser pulse (t=0). After the values are calculated, a fitting procedure, first developed by Dicker et al.,[62] estimates the yield mobility product at low light intensities. The fit approaches an asymptote at very low light intensities. The fitting procedure is a necessary step because the TRMC system cannot access these low light intensities. The equation for the modified Dicker fit is given by:

$$\varphi\Sigma\mu = \frac{A}{1+\sqrt{B \cdot \frac{I_0 F_A}{d}}} \quad (23)$$

where A and B are coefficients for fitting, I_0 is the initial photon flux, F_A is the fraction of light absorbed by the sample, and d is the thickness of the sample.

Chapter IV: Conclusion

Organic solar cell devices were made using a ternary blend of P3HT:PC_{60}BM with SiNc or one of the phthalocyanine molecules as the active layer. All of the photovoltaic devices were constructed using the same procedure in order to limit the variables between different samples. Solar cell devices containing P3HT:PC_{60}BM with SiNc (2.24 and 10.3 molar percent) had an average efficiency of 1.4566% and 2.4315%, respectively. The average efficiency of the control devices of just P3HT:PC_{60}BM was 2.8600%. Even though the efficiency decreased, the fill factor of the current density - voltage (JV) curves increased with an increase in the molar percent of SiNc. Clearly, the addition of SiNc to the bulk heterojunction resulted in a solar cell device that did not function as well as the control device. However, the device with 10.3 molar percent of SiNc has performance values that approach those of the control device. Photovoltaic devices were also made with PV 1000 photoactive ink and SiNc. The control devices had an average efficiency of 2.8459%, which is relatively high for a sample of only P3HT:PC_{60}BM. Adding SiNc (2.24 molar percent and 10.3 molar percent) to the bulk heterojunction significantly increased the efficiency from 3.0454% to 3.1400%, respectively. Even devices containing one of the phthalocyanine molecules resulted in a functioning device. The average efficiencies for these devices were around 1.0000%.

The external quantum efficiency (EQE) spectra for these devices give information about the spectral response of the sample. The samples with P3HT:PC_{60}BM and SiNc exhibited a decrease in the region of P3HT and PC_{60}BM while there was a significant response in the Q-band at 785 nm. If the molar percent of SiNc was increased to 10.3, a second Q-band peak formed in the EQE spectra at 825 nm. This peak can be attributed to the possibility of J-aggregate formation or covalent interaction between the naphthalocyanine cores. Samples with

the photoactive ink and SiNc did not have a second Q-band peak in the EQE spectra, but they did have a very large response at 785 nm, reaching nearly 45%. This large Q-band peak can explain the increase in the efficiency of devices as the molar percent of SiNc was increased. The lack of a second peak at 825 nm is possibly due to the components of the PV 1000 photoactive ink that restrict the formation of J-aggregates or covalent interactions between SiNc molecules. Photovoltaic devices with Pc1, Pc2, or Pc3 did not have a second Q-band peak either. These samples also had a smaller response around 800 nm in the EQE spectra, but this makes sense because these devices did not perform as well as the others. In conclusion, the addition of SiNc or one of the phthalocyanines to the active layer of organic solar cell devices results in functioning devices and in some cases high performance devices. This is a very significant result because these small molecules do not completely interrupt the interaction of light with P3HT and $PC_{60}BM$.

Flash-photolysis time-resolved microwave conductivity (TRMC) measurements were carried out on ternary blend samples of P3HT:$PC_{60}BM$ with SiNc or one of the phthalocyanines, neat thin films of P3HT with a small molecule, and neat $PC_{60}BM$ with one of the small molecules. The shape and light intensity dependence of normalized photoconductance (ΔG) plots give insight into the decay mechanisms of the free charge carriers in these samples. Exciting P3HT:$PC_{60}BM$ with SiNc (2.24 molar percent) at 800 nm results in nearly identical normalized photoconductance plots as exciting the sample at 500 nm. This means that it does not matter if P3HT:$PC_{60}BM$ or SiNc is excited because free charges are still created and they decay in the same way. Interestingly, the yield mobility product at time zero ($t=0$ $\varphi\Sigma\mu$) plots for this sample asymptotically approach nearly the same value. This value, known as the Dicker A value, is an order of magnitude greater for P3HT:$PC_{60}BM$ with SiNc, excited at 500 nm, as compared to the

control sample. While P3HT:$PC_{60}BM$ with SiNc, excited at 800 nm, has a Dicker A value that is the same as the control sample's value, within the error of the system.

Ternary blend samples of one of the phthalocyanines with P3HT:$PC_{60}BM$ have normalized photoconductance plots that are the same for the samples excited at 500 nm. However, when the thin films were pulsed at 800 nm, which excites the small molecule instead of P3HT and $PC_{60}BM$, the resulting normalized plots were only slightly dependent on the light intensity of laser resulting in visually different plots. This means that the decay mechanism is different for these samples excited at 800 nm. The Dicker A values for the samples excited at 500 nm were on the same order of magnitude as the control, while the thin films with Pc2 or Pc3 had Dicker A values that were an order of magnitude lower. Regardless, the addition of a small molecule to a blend of P3HT:$PC_{60}BM$ results in the generation of a high yield of free charge carriers.

The data from neat thin films of P3HT with a small molecule and $PC_{60}BM$ containing one of the small molecules was also analyzed. The normalized photoconductance plots for neat P3HT with SiNc were nearly identical to the control sample of neat P3HT, even though there was a significant amount of noise in both samples. However, the normalized photoconductance plots for neat $PC_{60}BM$ with SiNc had very short lifetimes and were not dependent on the light intensity of the laser. This means that the decay mechanism of free charges in this sample is completely different from the other two thin films. The Dicker A values from the yield mobility product at time zero plots for neat $PC_{60}BM$ with SiNc were on the same order of magnitude as the control sample. The normalized plots for the neat thin films with one of the phthalocyanines had very similar shapes and light intensity dependence as the SiNc samples, since all the neat $PC_{60}BM$ thin films had very short lifetimes. The Dicker A values for neat $PC_{60}BM$ with Pc1 or

Pc2 were on the same order of magnitude as the control's value, while neat $PC_{60}BM$ with Pc3 had a Dicker A value that was an order of magnitude lower than the control's value. The shapes of the yield mobility product at time zero plots were nearly the same for all the samples excited at 800 nm. These plots quickly plateau at low intensities while the high intensity values did not significantly drop off. The reason for the different shapes of these plots is due to the fact that the small molecules act as electron or hole traps, depending on their environment. The ternary blend sample plots even had these characteristics, which means that flash-photolysis TRMC has the potential to probe the morphology of a bulk heterojunction.

The energy levels of SiNc and the phthalocyanine molecules, as seen in Figures 3-30 and 3-31, explain the results seen in the solar cell device data and the TRMC data. Since SiNc and the phthalocyanine molecules have energy levels that perfectly line up with the energy levels of P3HT and $PC_{60}BM$, they can transport charges from P3HT to $PC_{60}BM$ and from $PC_{60}BM$ to P3HT. These small molecules are able to act as a "middle-man" between the donor and acceptor molecules, facilitating the transport of charges. However, when a small molecule is located in a P3HT-rich region or a $PC_{60}BM$-rich region, the molecule behaves as an electron or a hole trap, respectively. As discussed above, flash-photolysis TRMC has the capability of probing these regions since the results from the yield mobility product at time zero plots have characteristic features. Hopefully, future experiments can delve into the possibilities of using this method to understand different morphological environments and give insight into the optimization of bulk heterojunctions as the active layer in organic solar cell devices.

Appendix

A. Current Density - Voltage Experimental Data

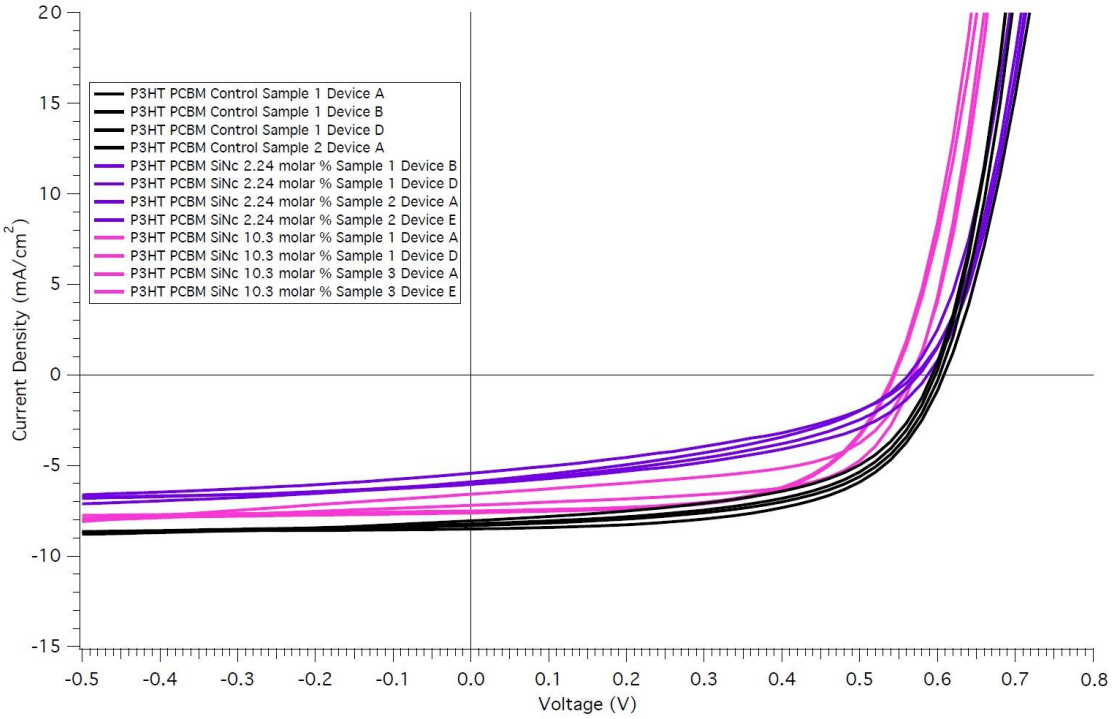

Figure A-1. Current density - voltage (JV) curves of organic solar cell devices: P3HT:$PC_{60}BM$, P3HT:$PC_{60}BM$ SiNc (2.24 molar percent), and P3HT:$PC_{60}BM$ SiNc (10.3 molar percent).

SiNc Molar Conc. (%)	V_{OC} (V)	J_{SC} (mA/cm^2)	Fill Factor (%)	Efficiency (%)	Mismatch Factor
0 (S1A)*	0.60260	10.556	58.209	2.9207	1.0436
0 (S1B)	0.59720	10.288	57.314	2.8157	1.0437
0 (S1D)	0.59297	10.595	55.312	2.6418	1.0431
0 (S2A)	0.60826	10.244	59.159	3.0620	1.0437
2.24 (S1B)*	0.58733	8.4203	46.368	1.6457	1.0162
2.24 (S1D)	0.57573	8.3792	44.341	1.5202	1.0165
2.24 (S2A)	0.57047	8.2215	41.402	1.2824	1.0177
2.24 (S2E)	0.56269	8.1000	41.455	1.3780	1.0164
10.3 (S1A)*	0.56988	8.0620	63.401	2.6012	1.0105
10.3 (S1D)	0.56698	7.4867	56.738	2.1188	1.0127
10.3 (S3A)	0.54296	9.0219	60.900	2.4857	1.0112
10.3 (S3E)	0.54490	9.0227	60.738	2.5202	1.0111

Table A-1. Data from the current density - voltage (JV) curves of the organic solar cell devices: P3HT:PC_{60}BM, P3HT:PC_{60}BM SiNc (2.24 molar percent), and P3HT:PC_{60}BM SiNc (10.3 molar percent).
*The set of data represented in Figure 2-10.

SiNc Molar Conc. (%)	n Factor	R_{shunt} (kΩ · cm^2)	R_{series} (kΩ · cm^2)
0 (S1A)	3.0137 ± 0.0392	2.0884 ± 0.0318	4.6474e-7 ± 8.69e-9
0 (S1B)	2.8626 ± 0.0377	1.1409 ± 0.0341	7.3955e-7 ± 1.23e-8
0 (S1D)	2.8484 ± 0.0494	0.69062 ± 0.0255	4.0796e-6 ± 9.47e-7
0 (S2A)	3.275 ± 0.0219	2.4983 ± 0.149	3.1965e-6 ± 1.67e-7
2.24 (S1B)	3.3837 ± 0.0944	0.89367 ± 0.0192	2.5478e-7 ± 5.17e-9
2.24 (S1D)	4.3732 ± 0.129	0.77991 ± 0.00598	2.0615e-7 ± 2.07e-9
2.24 (S2A)	3.9505 ± 0.165	0.48614 ± 0.0234	1.3864e-6 ± 8.1e-8
2.24 (S2E)	4.4326 ± 0.198	0.5793 ± 0.0363	3.158e-6 ± 8.78e-7
10.3 (S1A)	2.2586 ± 0.0174	0.56558 ± 0.00711	5.6367e-6 ± 8.12e-7
10.3 (S1D)	2.1706 ± 0.0168	0.3193 ± 0.0029	3.6574e-6 ± 1.25e-7
10.3 (S3A)	2.8128 ± 0.0175	1.464 ± 0.0113	8.0802e-7 ± 4.64e-9
10.3 (S3E)	2.8917 ± 0.0144	1.2419 ± 0.00896	7.1695e-7 ± 5.13e-9

Table A-2. Data from the fitting procedure of the current density - voltage (JV) curves of the solar cell devices: P3HT:PC_{60}BM, P3HT:PC_{60}BM SiNc (2.24 molar percent), and P3HT:PC_{60}BM SiNc (10.3 molar percent).

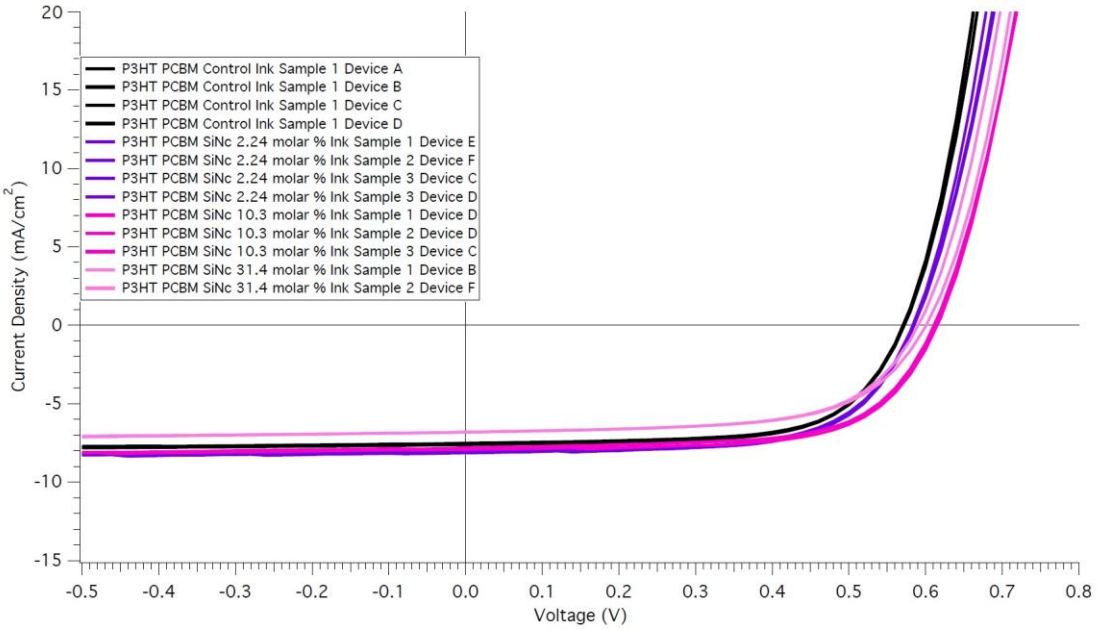

Figure A-2. Current density - voltage (JV) curves of organic solar cell devices: P3HT:PC_{60}BM PV 1000 ink, P3HT:PC_{60}BM SiNc PV 1000 ink (2.24 molar percent), P3HT:PC_{60}BM SiNc PV 1000 ink (10.3 molar percent), and P3HT:PC_{60}BM SiNc PV 1000 ink (31.4 molar percent).

SiNc Molar Conc. (%)	V_{OC} (V)	J_{SC} (mA/cm^2)	Fill Factor (%)	Efficiency (%)	Mismatch Factor
0 (S1A)†	0.57222	8.4900	66.020	2.8538	1.0433
0 (S1B)	0.57173	8.4647	65.738	2.8220	1.0436
0 (S1C)	0.57039	8.5671	65.715	2.8443	1.0434
0 (S1D)	0.57037	8.5979	65.846	2.8633	1.0442
2.24 (S1E)†	0.58310	9.8396	65.012	3.0499	1.0116
2.24 (S2F)	0.58473	9.9021	65.109	3.0078	1.0124
2.24 (S3C)	0.58446	9.8678	65.483	3.0405	1.0119
2.24 (S3D)	0.58487	9.6656	64.778	3.0835	1.0127
10.3 (S1D)†	0.61506	9.5236	65.707	3.1999	0.97853
10.3 (S2D)	0.61056	9.6761	65.137	3.1166	0.97815
10.3 (S3C)	0.61363	9.4320	64.802	3.1034	0.97685
31.4 (S1B)	0.60071	8.8837	62.527	2.5567	0.98409
31.4 (S2F)†	0.59005	8.9002	62.870	2.5270	0.98358

Table A-3. Data of the current density - voltage (JV) curves of the organic solar cell devices: P3HT:PC_{60}BM PV 1000 ink, P3HT:PC_{60}BM SiNc PV 1000 ink (2.24 molar percent), P3HT:PC_{60}BM SiNc PV 1000 ink (10.3 molar percent), and P3HT:PC_{60}BM SiNc PV 1000 ink (31.4 molar percent).
†The set of data represented in Figure 2-12.

SiNc Molar Conc. (%)	n Factor	R_{shunt} (kΩ · cm^2)	R_{series} (kΩ · cm^2)
0 (S1A)	2.6230 ± 0.0126	3.2033 ± 0.117	1.2759e-5 ± 2.34e-6
0 (S1B)	2.5328 ± 0.0113	2.8002 ± 0.106	2.7353e-5 ± 4.1e-6
0 (S1C)	2.6412 ± 0.0148	3.0116 ± 0.154	3.9331e-5 ± 9.12e-6
0 (S1D)	2.5654 ± 0.0117	3.0156 ± 0.132	1.0256e-5 ± 1.86e-6
2.24 (S1E)	2.7643 ± 0.0144	2.6394 ± 0.0909	1.0196e-5 ± 2.52e-6
2.24 (S2F)	2.8519 ± 0.0151	2.6605 ± 0.0364	3.176e-6 ± 7.41e-6
2.24 (S3C)	2.8557 ± 0.0213	2.8331 ± 0.202	1.7089e-5 ± 3.01e-6
2.24 (S3D)	2.9251 ± 0.0209	3.5403 ± 0.311	1.0575e-5 ± 1.6e-6
10.3 (S1D)	2.8007 ± 0.0147	2.6168 ± 0.102	1.0279e-5 ± 1.7e-6
10.3 (S2D)	2.8854 ± 0.0215	2.2836 ± 0.0583	1.9706e-6 ± 4.24e-8
10.3 (S3C)	2.7761 ±0.0215	1.7069 ± 0.0509	2.5617e-5 ± 7.23e-6
31.4 (S1B)	2.8785 ±0.0114	1.7501 ± 0.00646	8.1401e-7 ± 4e-8
31.4 (S2F)	2.7288 ± 0.0098	1.4534 ± 0.0125	1.8627e-6 ± 2.06e-8

Table A-4. Data from the fitting procedure of the current density - voltage (JV) curves of the solar cell devices: P3HT:PC_{60}BM PV 1000 ink, P3HT:PC_{60}BM SiNc PV 1000 ink (2.24 molar percent), P3HT:PC_{60}BM SiNc PV 1000 ink (10.3 molar percent), and P3HT:PC_{60}BM SiNc PV 1000 ink (31.4 molar percent).

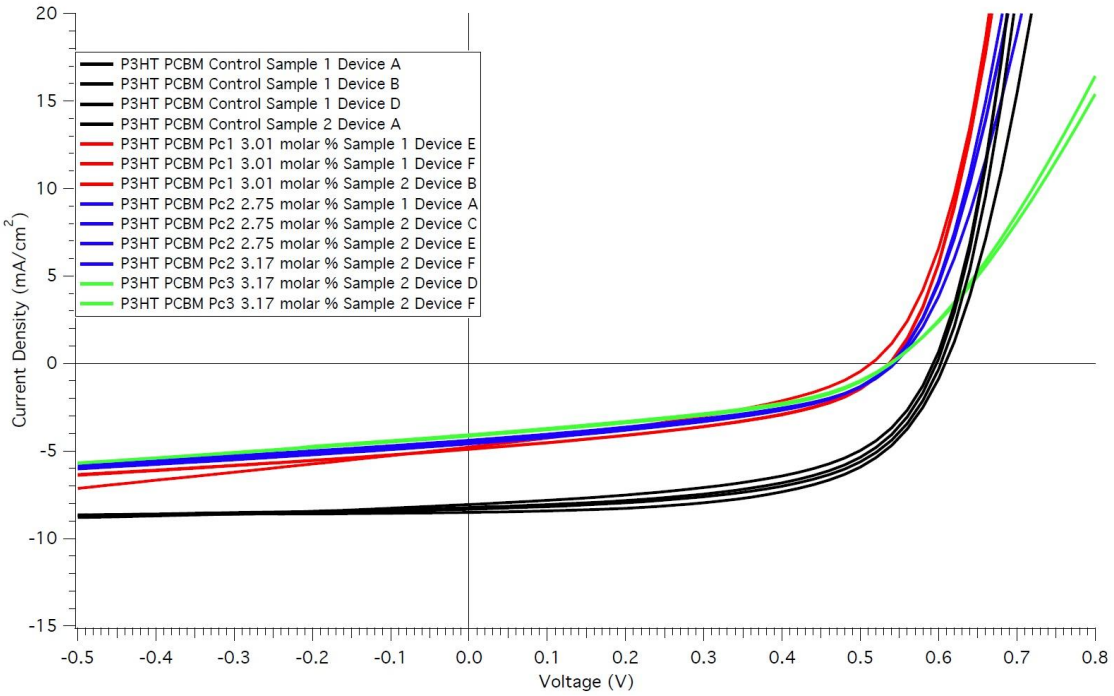

Figure A-3. Current density - voltage (JV) curves of organic solar cell devices: P3HT:PC_{60}BM, P3HT:PC_{60}BM Pc1 (3.01 molar percent), P3HT:PC_{60}BM Pc2 (2.75 molar percent), and P3HT:PC_{60}BM Pc3 (3.17 molar percent).

	V_{OC} (V)	J_{SC} (mA/cm^2)	Fill Factor (%)	Efficiency (%)	Mismatch Factor
Control (S1A)‡	0.60260	10.556	58.209	2.9207	1.0436
Control (S1B)	0.59720	10.288	57.314	2.8157	1.0437
Control (S1D)	0.59297	10.595	55.312	2.6418	1.0431
Control (S2A)	0.60826	10.244	59.159	3.0620	1.0437
Pc1 (S1E)‡	0.53630	7.9883	44.272	1.1621	1.0431
Pc1 (S1F)	0.51357	7.8710	37.197	0.91263	1.0434
Pc1 (S2B)	0.53813	8.1152	44.618	1.1734	1.0436
Pc2 (S1A)	0.54353	7.9760	42.732	1.0185	1.0302
Pc2 (S2C)	0.54033	8.0792	42.992	1.0501	1.0314
Pc2 (S2E)‡	0.54012	8.1665	43.151	1.0497	1.0315
Pc2 (S2F)	0.53960	8.1187	43.252	1.0711	1.0314
Pc3 (S2D)‡	0.53917	7.2891	42.433	0.94979	1.0213
Pc3 (S2F)	0.53790	7.2773	41.836	0.91656	1.0212

Table A-5. Data from the current density - voltage (JV) curves of the organic solar cell devices: P3HT:PC_{60}BM, P3HT:PC_{60}BM Pc1 (3.01 molar percent), P3HT:PC_{60}BM Pc2 (2.75 molar percent), and P3HT:PC_{60}BM Pc3 (3.17 molar percent).
‡The set of data represented in Figure 2-13.

	n Factor	R_{shunt} (kΩ · cm^2)	R_{series} (kΩ · cm^2)
Control (S1A)	3.0137 ± 0.0392	2.0884 ± 0.0318	4.6474e-7 ± 8.69e-9
Control (S1B)	2.8626 ±0.0377	1.1409 ± 0.0341	7.3955e-7 ± 1.23e-8
Control (S1D)	2.8484 ± 0.0494	0.69062 ± 0.0255	4.0796e-6 ± 9.47e-7
Control (S2A)	3.275 ± 0.0219	2.4983 ± 0.149	3.1965e-6 ± 1.67e-7
Pc1 (S1E)	2.6348 ± 0.0451	0.35053 ± 0.00506	6.1239e-7 ± 1.22e-8
Pc1 (S1F)	2.5937 ± 0.0266	0.20801 ± 0.00111	6.246e-7 ± 6.38e-9
Pc1 (S2B)	2.5312 ± 0.042	0.35798 ± 0.00544	5.0797e-7 ± 1.02e-8
Pc2 (S1A)	2.9394 ± 0.0454	0.37584 ± 0.00508	7.0434e-7 ± 9.73e-9
Pc2 (S2C)	2.6778 ± 0.0326	0.35018 ± 0.00435	7.5245e-7 ±8.53e-9
Pc2 (S2E)	2.8064 ± 0.0379	0.36871 ± 0.00466	6.1714e-7 ± 1.22e-8
Pc2 (S2F)	2.8574 ± 0.0397	0.36335 ± 0.00578	7.0112e-7 ± 1.17e-8
Pc3 (S2D)	5.6609 ± 0.0895	0.41172 ± 0.0119	5.6262e-7 ± 1.53e-8
Pc3 (S2F)	5.7408 ± 0.107	0.38064 ± 0.00967	6.8169e-7 ± 1.54e-8

Table A-6. Data from the current density - voltage (JV) curves of the organic solar cell devices: P3HT:PC_{60}BM, P3HT:PC_{60}BM Pc1 (3.01 molar percent), P3HT:PC_{60}BM Pc2 (2.75 molar percent), and P3HT:PC_{60}BM Pc3 (3.17 molar percent).

B. External Quantum Efficiency Experimental Data

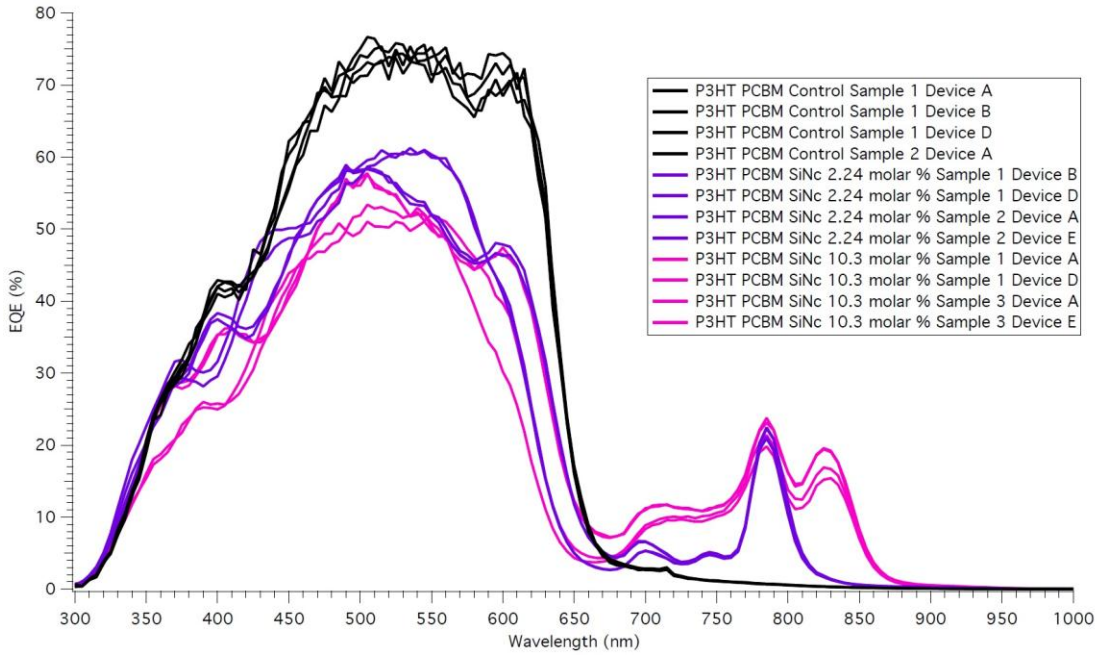

Figure B-1. External quantum efficiency (EQE) spectra of organic solar cell devices: P3HT:PC_{60}BM, P3HT PC_{60}BM SiNc (2.24 molar percent), and P3HT:PC_{60}BM SiNc (10.3 molar percent).

SiNc Molar Conc. (%)	EQE at 500 nm (%)	EQE at 785 nm (%)	EQE at 800 nm (%)	EQE at 825 nm (%)
0 (S1A)*	74.161	0.71300	0.56830	0.34970
0 (S1B)	72.167	0.73170	0.61280	0.37640
0 (S1D)	75.063	0.73690	0.58010	0.38170
0 (S2A)	71.255	0.69100	0.55580	0.37330
2.24 (S1B)*	57.996	22.319	12.041	1.8561
2.24 (S1D)	58.249	22.475	11.893	1.8645
2.24 (S2A)	58.803	21.137	10.365	1.6890
2.24 (S2E)	57.303	20.903	10.494	1.7038
10.3 (S1A)*	51.914	21.379	13.804	16.903
10.3 (S1D)	49.618	19.827	12.675	15.200
10.3 (S3A)	56.056	23.777	16.155	19.430
10.3 (S3E)	56.003	23.109	16.228	19.570

Table B-1. Data from the external quantum efficiency (EQE) spectra of the organic solar cell devices: P3HT:PC_{60}BM, P3HT:PC_{60}BM SiNc (2.24 molar percent), and P3HT:PC_{60}BM SiNc (10.3 molar percent).
*The set of data represented in Figure 2-14.

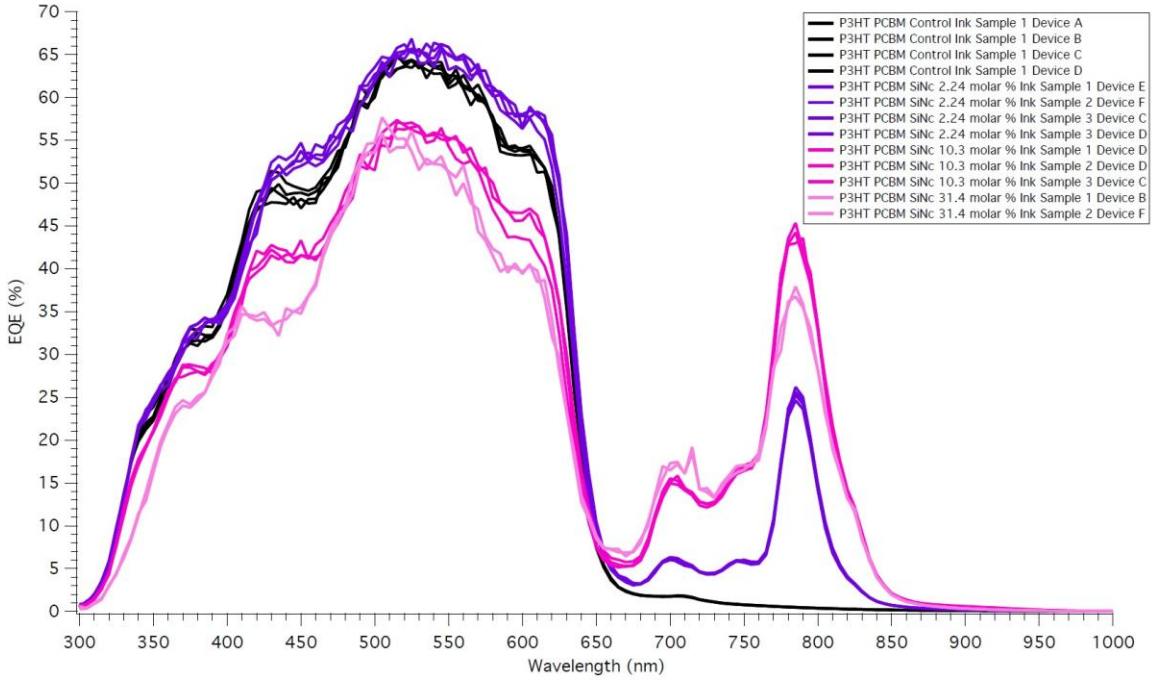

Figure B-2. External quantum efficiency (EQE) spectra of organic solar cell devices: P3HT:PC_{60}BM PV 1000 ink, P3HT:PC_{60}BM SiNc PV 1000 ink (2.24 molar percent), P3HT:PC_{60}BM SiNc PV 1000 ink (10.3 molar percent), and P3HT:PC_{60}BM SiNc PV 1000 ink (31.4 molar percent).

SiNc Molar Conc. (%)	EQE at 500 nm (%)	EQE at 785 nm (%)	EQE at 800 nm (%)	EQE at 825 nm (%)
0 (S1A)†	60.006	0.48290	0.39450	0.26720
0 (S1B)	60.855	0.50630	0.38040	0.26810
0 (S1C)	61.612	0.47980	0.39640	0.26610
0 (S1D)	61.673	0.48690	0.37430	0.26760
2.24 (S1E)†	61.813	26.200	14.871	3.2733
2.24 (S2F)	63.514	25.620	14.861	3.2535
2.24 (S3C)	62.703	25.252	14.375	3.1934
2.24 (S3D)	62.129	24.646	14.189	3.1056
10.3 (S1D)†	53.715	44.231	32.836	11.613
10.3 (S2D)	54.246	42.988	33.150	12.184
10.3 (S3C)	51.495	45.357	33.449	11.676
31.4 (S1B)	54.670	36.750	28.126	11.914
31.4 (S2F)†	53.542	37.936	28.253	11.625

Table B-2. Data from the external quantum efficiency (EQE) spectra of the organic solar cell devices: P3HT:PC_{60}BM PV 1000 ink, P3HT:PC_{60}BM SiNc PV 1000 ink (2.24 molar percent), P3HT:PC_{60}BM SiNc PV 1000 ink (10.3 molar percent), and P3HT:PC_{60}BM SiNc PV 1000 ink (31.4 molar percent).
†The set of data represented in Figure 2-15.

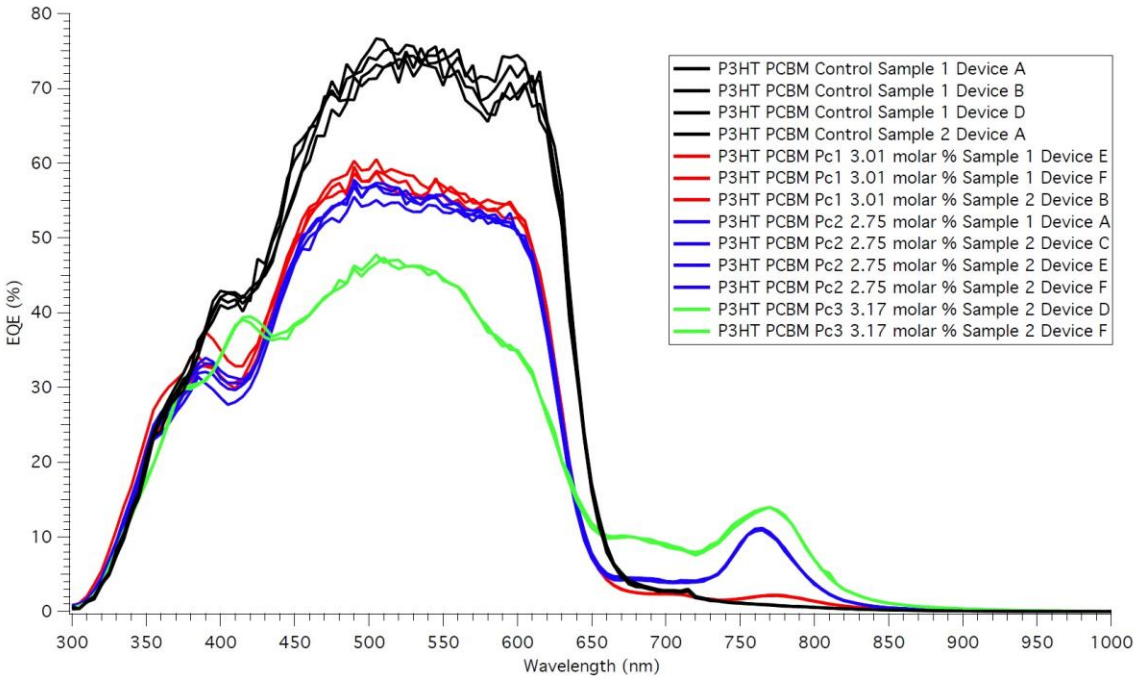

Figure B-3. External quantum efficiency (EQE) spectra of organic solar cell devices: P3HT:PC_{60}BM, P3HT:PC_{60}BM Pc1 (3.01 molar percent), P3HT:PC_{60}BM Pc2 (2.75 molar percent), and P3HT:PC_{60}BM Pc3 (3.17 molar percent).

	EQE at 500 nm (%)	EQE at 785 nm (%)	EQE at 800 nm (%)	EQE at 825 nm (%)
Control (S1A)‡	74.161	0.71300	0.56830	0.37330
Control (S1B)	72.167	0.73170	0.61280	0.37640
Control (S1D)	75.063	0.73690	0.58010	0.38170
Control (S2A)	71.255	0.69100	0.55580	0.34970
Pc1 (S1E)‡	57.668	1.9563	1.3997	0.66190
Pc1 (S1F)	57.530	1.9381	1.3827	0.66600
Pc1 (S2B)	59.166	1.9829	1.4220	0.68430
Pc2 (S1A)	54.440	7.0811	3.8233	1.2660
Pc2 (S2C)	56.641	6.9071	3.7347	1.2492
Pc2 (S2E)‡	56.789	7.0684	3.8354	1.2818
Pc2 (S2F)	56.811	7.1237	3.6283	1.2743
Pc3 (S2D)‡	46.630	11.677	6.9296	2.5357
Pc3 (S2F)	45.912	11.649	6.9732	2.5730

Table B-3. Data from the external quantum efficiency (EQE) spectra of the organic solar cell devices: P3HT:$PC_{60}BM$, P3HT:$PC_{60}BM$ Pc1 (3.01 molar percent), P3HT:$PC_{60}BM$ Pc2 (2.75 molar percent), and P3HT:$PC_{60}BM$ Pc3 (3.17 molar percent).
‡The set of data represented in Figure 2-16.

C. Time-Resolved Microwave Conductivity Experimental Data

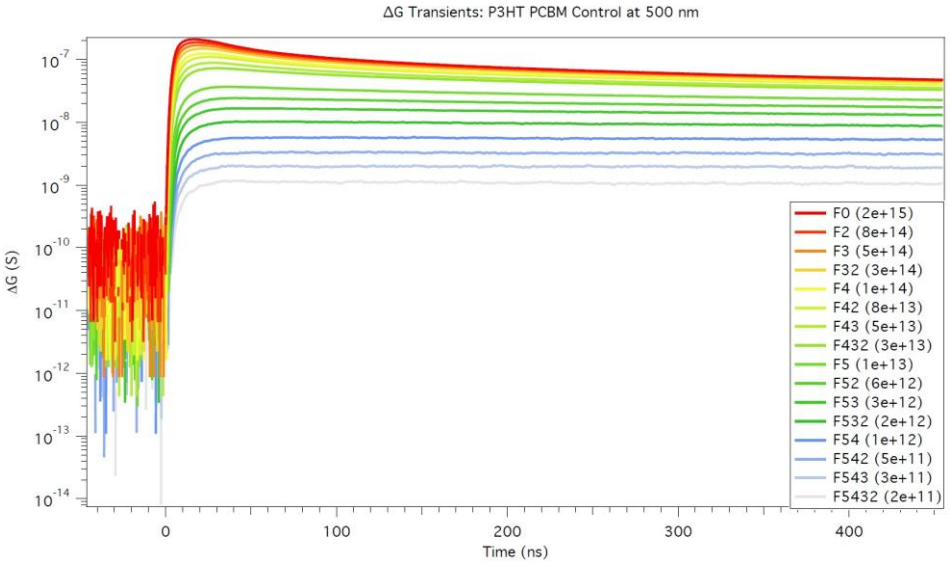

Figure C-1. Experimental photoconductance (ΔG) transients for a thin film sample of P3HT:$PC_{60}BM$, spin-coated on quartz and excited at 500 nm.

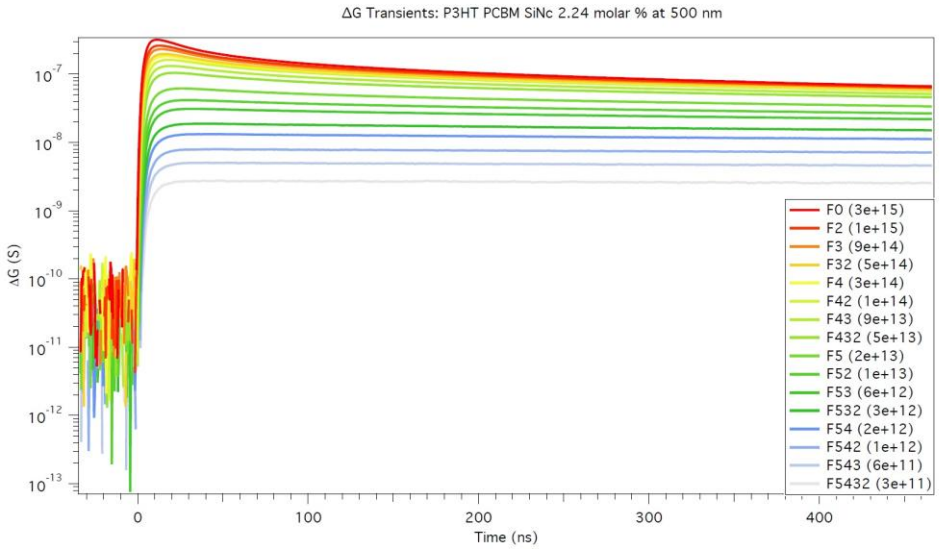

Figure C-2. Experimental photoconductance (ΔG) transients for a thin film sample of P3HT:$PC_{60}BM$ with SiNc (2.24 molar percent), spin-coated on quartz and excited at 500 nm.

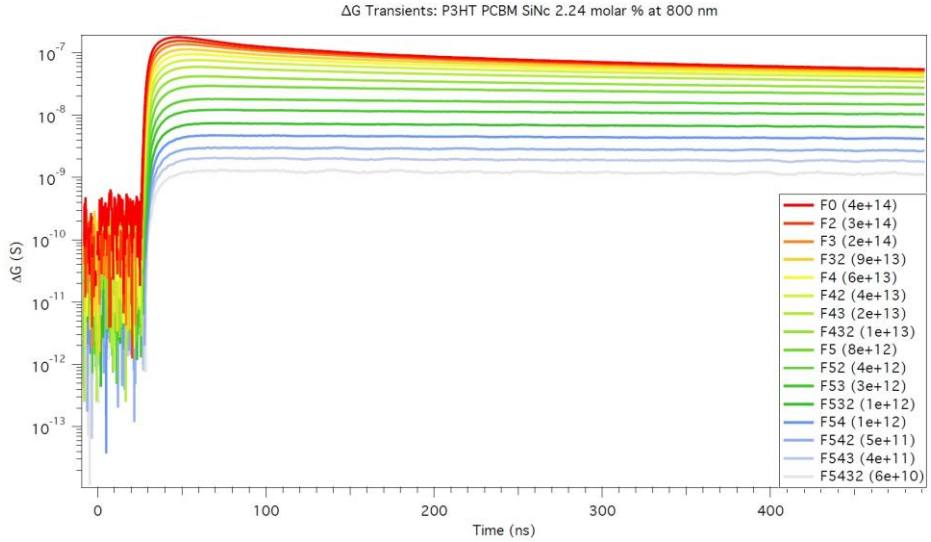

Figure C-3. Experimental photoconductance (ΔG) transients for a thin film sample of P3HT:$PC_{60}BM$ with SiNc (2.24 molar percent), spin-coated on quartz and excited at 800 nm.

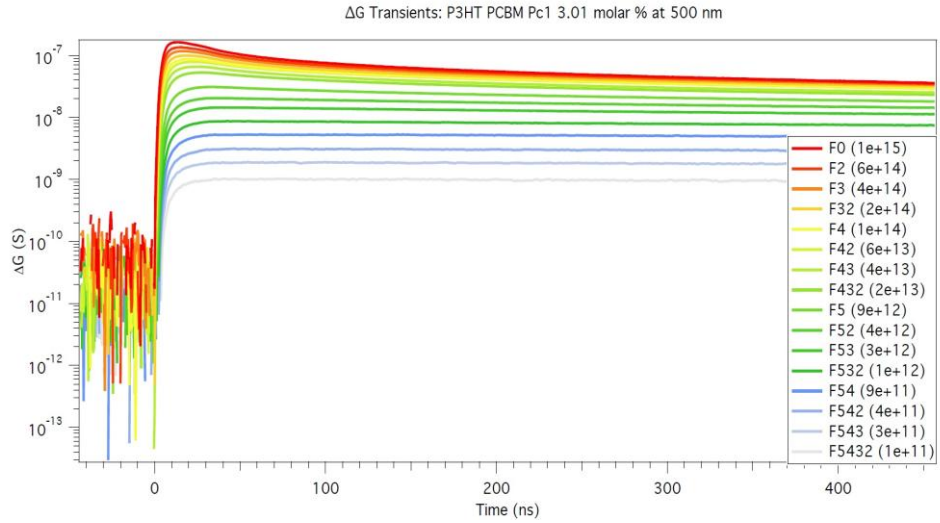

Figure C-4. Experimental photoconductance (ΔG) transients for a thin film sample of P3HT:$PC_{60}BM$ with Pc1 (3.01 molar percent), spin-coated on quartz and excited at 500 nm.

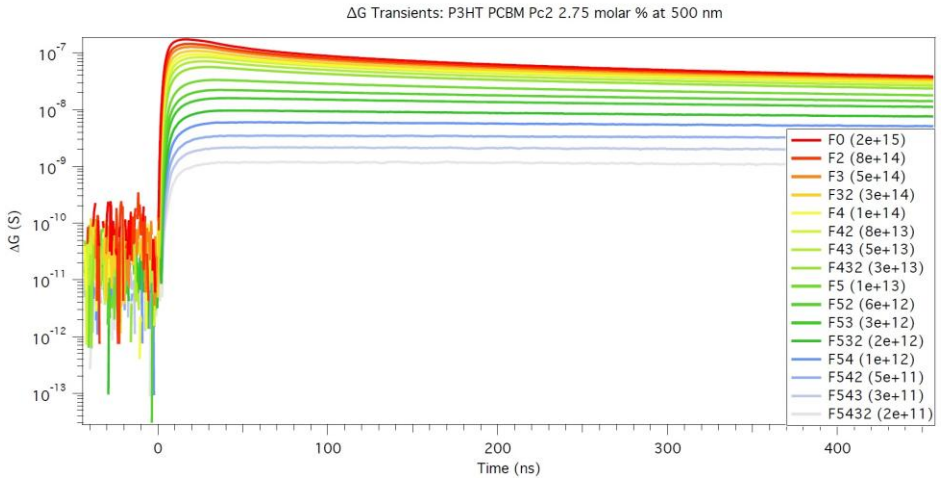

Figure C-5. Experimental photoconductance (ΔG) transients for a thin film sample of P3HT:$PC_{60}BM$ with Pc2 (2.75 molar percent), spin-coated on quartz and excited at 500 nm.

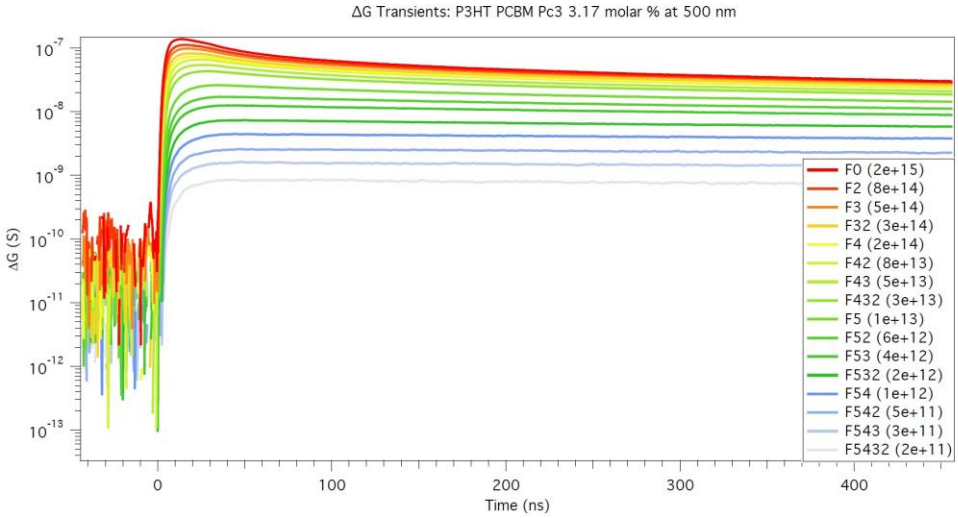

Figure C-6. Experimental photoconductance (ΔG) transients for a thin film sample of P3HT:$PC_{60}BM$ with Pc3 (3.17 molar percent), spin-coated on quartz and excited at 500 nm.

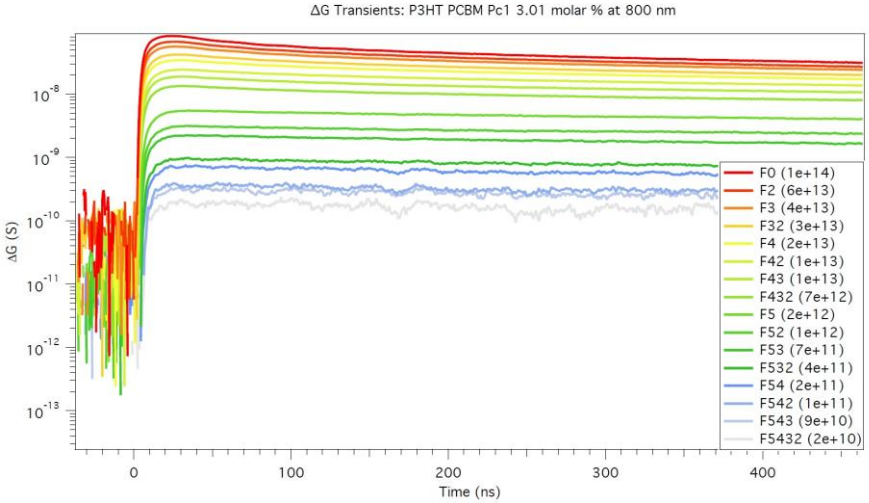

Figure C-7. Experimental photoconductance (ΔG) transients for a thin film sample of P3HT:$PC_{60}BM$ with Pc1 (3.01 molar percent), spin-coated on quartz and excited at 800 nm.

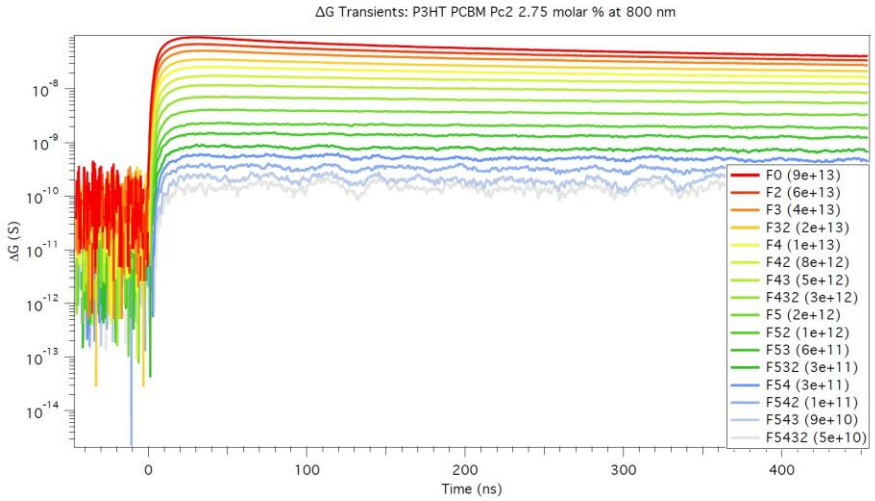

Figure C-8. Experimental photoconductance (ΔG) transients for a thin film sample of P3HT:$PC_{60}BM$ with Pc2 (2.75 molar percent), spin-coated on quartz and excited at 800 nm.

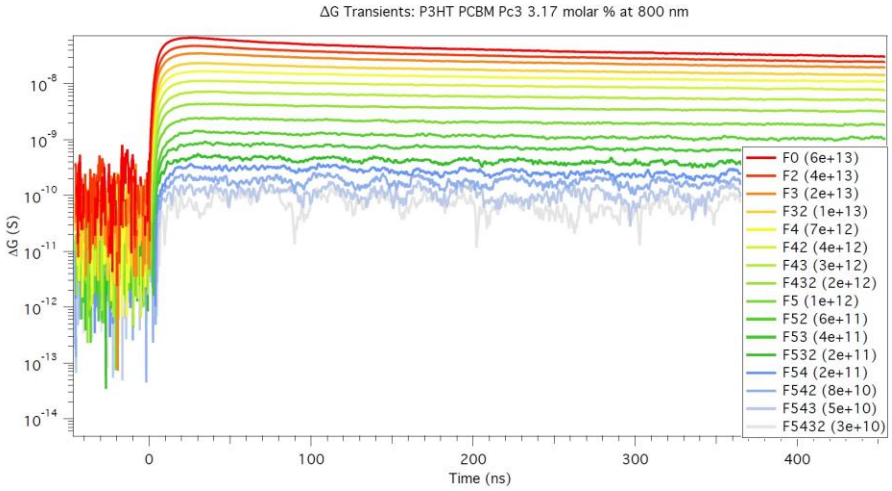

Figure C-9. Experimental photoconductance (ΔG) transients for a thin film sample of P3HT:$PC_{60}BM$ with Pc3 (3.17 molar percent), spin-coated on quartz and excited at 800 nm.

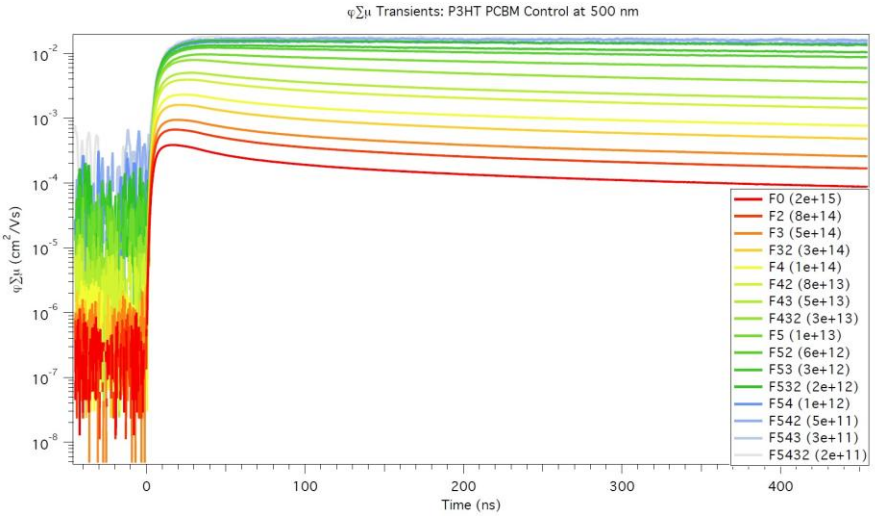

Figure C-10. Experimental yield mobility product (φΣμ) transients for a thin film sample of P3HT:$PC_{60}BM$, spin-coated on quartz and excited at 500 nm.

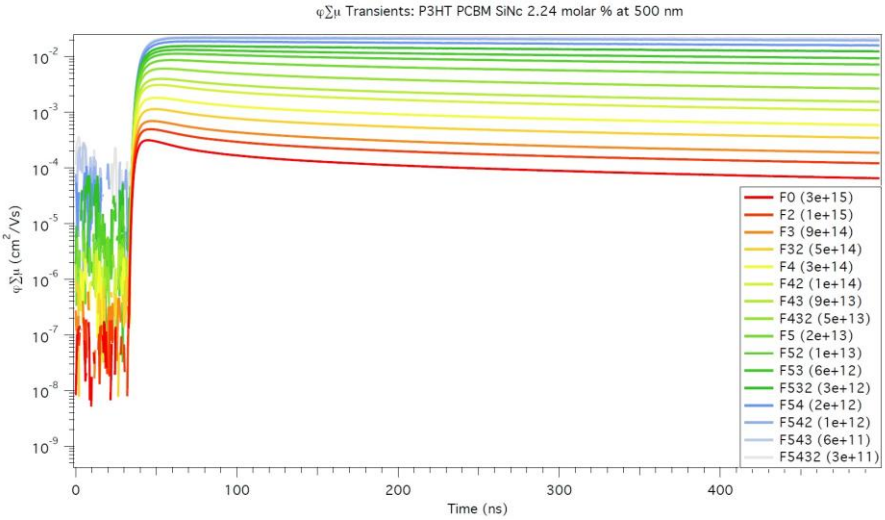

Figure C-11. Experimental yield mobility product (φΣμ) transients for a thin film sample of P3HT:$PC_{60}BM$ with SiNc (2.24 molar percent), spin-coated on quartz and excited at 500 nm.

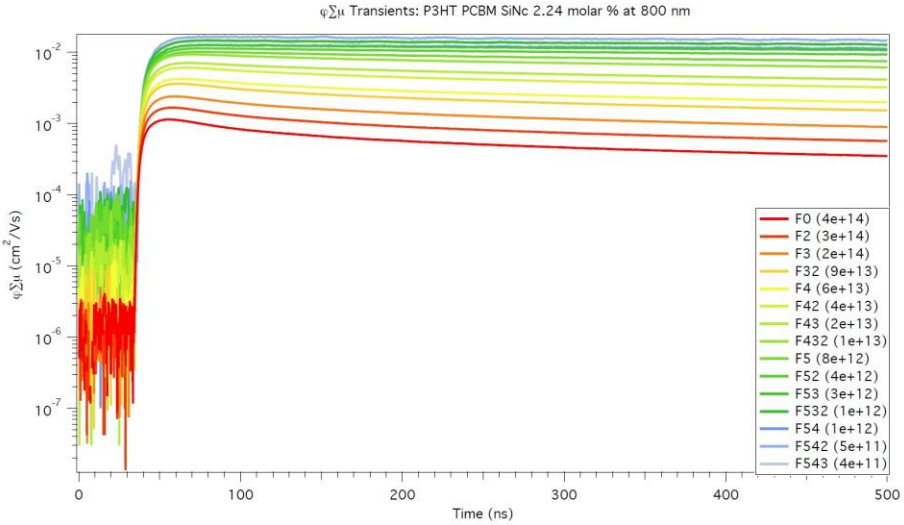

Figure C-12. Experimental yield mobility product (φΣμ) transients for a thin film sample of P3HT:PC_{60}BM with SiNc (2.24 molar percent), spin-coated on quartz and excited at 800 nm.

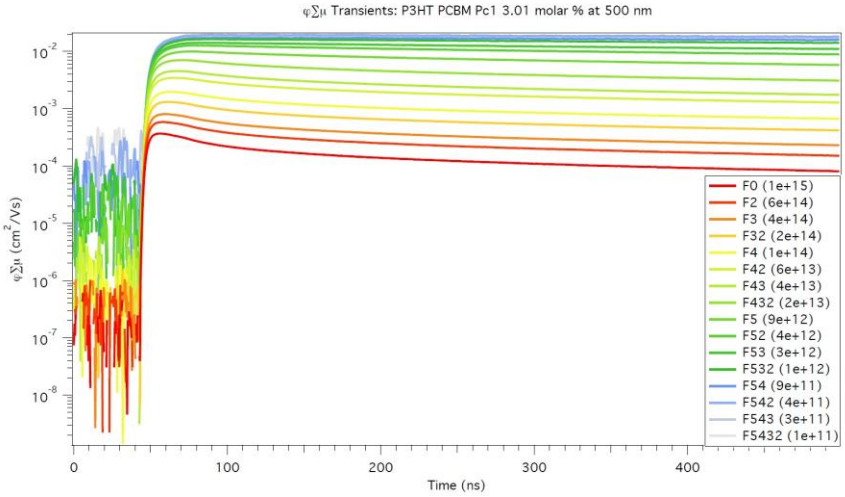

Figure C-13. Experimental yield mobility product (φΣμ) transients for a thin film sample of P3HT:PC_{60}BM with Pc1 (3.01 molar percent), spin-coated on quartz and excited at 500 nm.

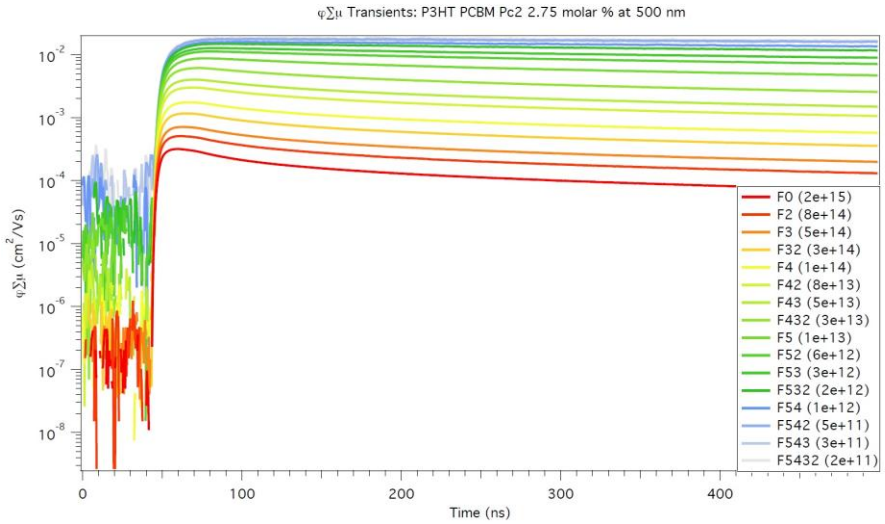

Figure C-14. Experimental yield mobility product (φΣμ) transients for a thin film sample of P3HT:$PC_{60}BM$ with Pc2 (2.75 molar percent), spin-coated on quartz and excited at 500 nm.

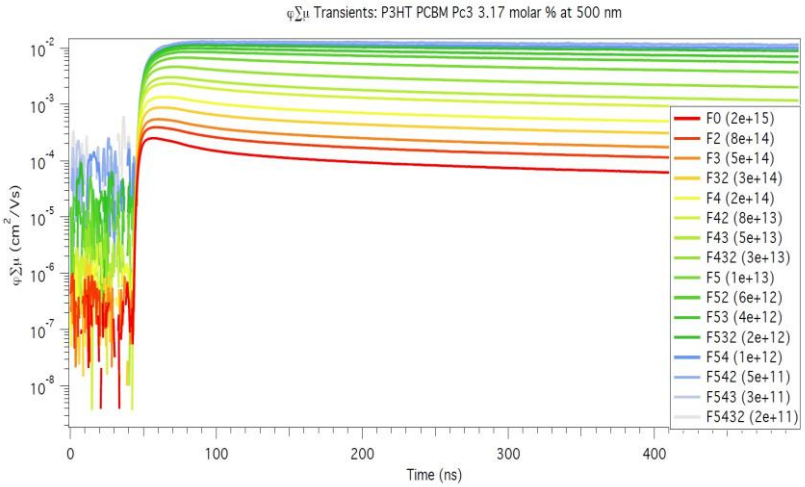

Figure C-15. Experimental yield mobility product (φΣμ) transients for a thin film sample of P3HT:$PC_{60}BM$ with Pc3 (3.17 molar percent), spin-coated on quartz and excited at 500 nm.

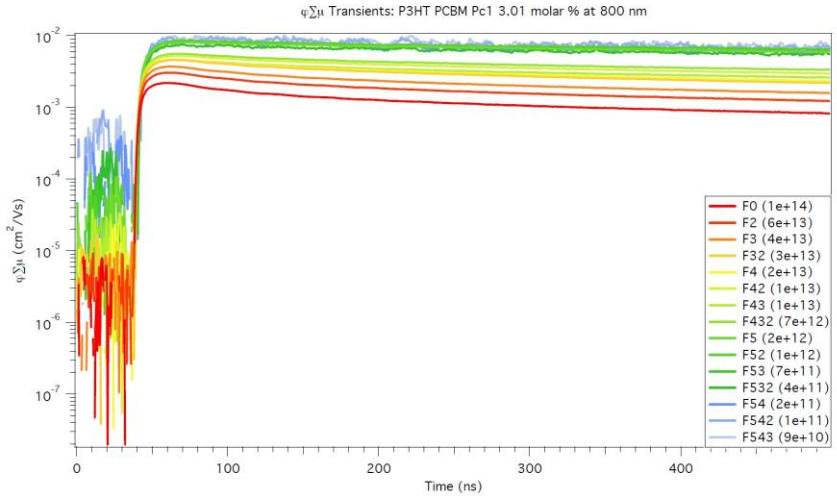

Figure C-16. Experimental yield mobility product (φΣμ) transients for a thin film sample of P3HT:$PC_{60}BM$ with Pc1 (3.01 molar percent), spin-coated on quartz and excited at 800 nm.

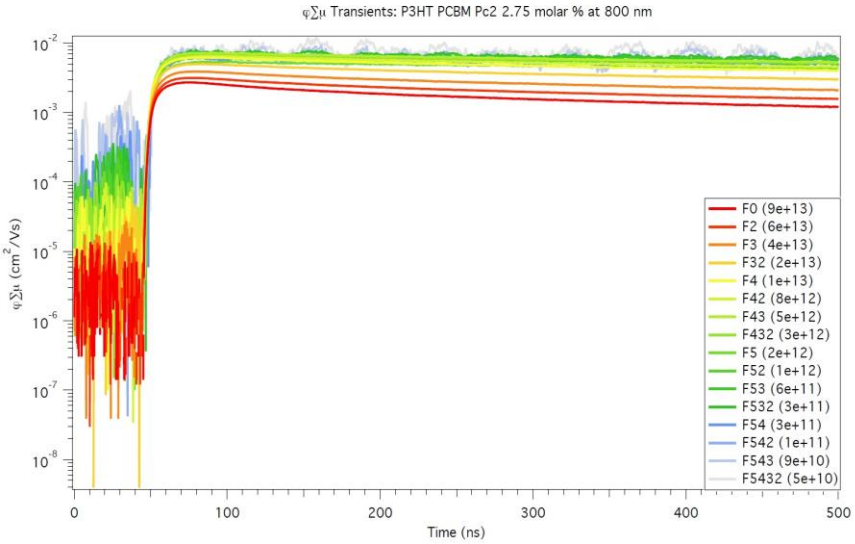

Figure C-17. Experimental yield mobility product (φΣμ) transients for a thin film sample of P3HT:$PC_{60}BM$ with Pc2 (2.75 molar percent), spin-coated on quartz and excited at 800 nm.

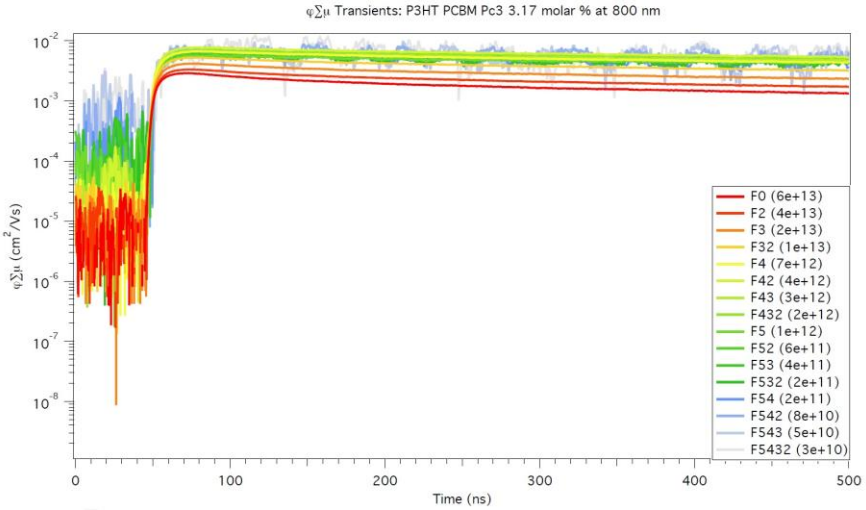

Figure C-18. Experimental yield mobility product (φΣμ) transients for a thin film sample of P3HT:$PC_{60}BM$ with Pc3 (3.17 molar percent), spin-coated on quartz and excited at 800 nm.

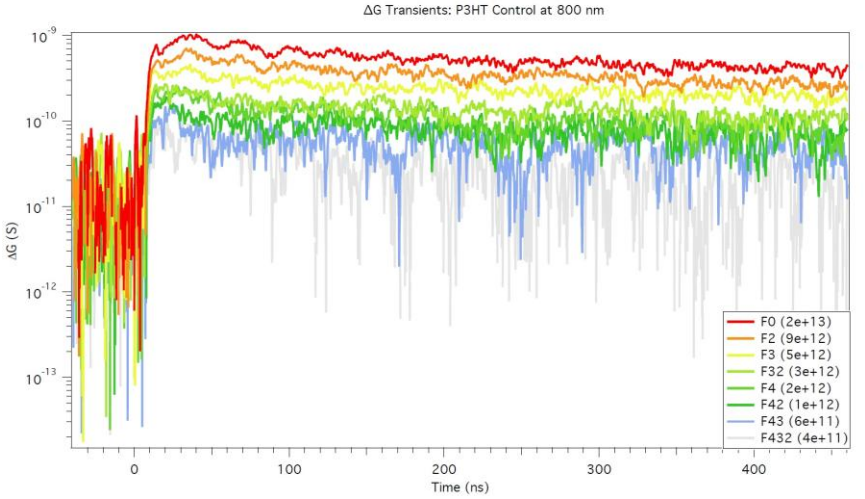

Figure C-19. Experimental photoconductance (ΔG) transients for a thin film sample of neat P3HT, spin-coated on quartz and excited at 800 nm.

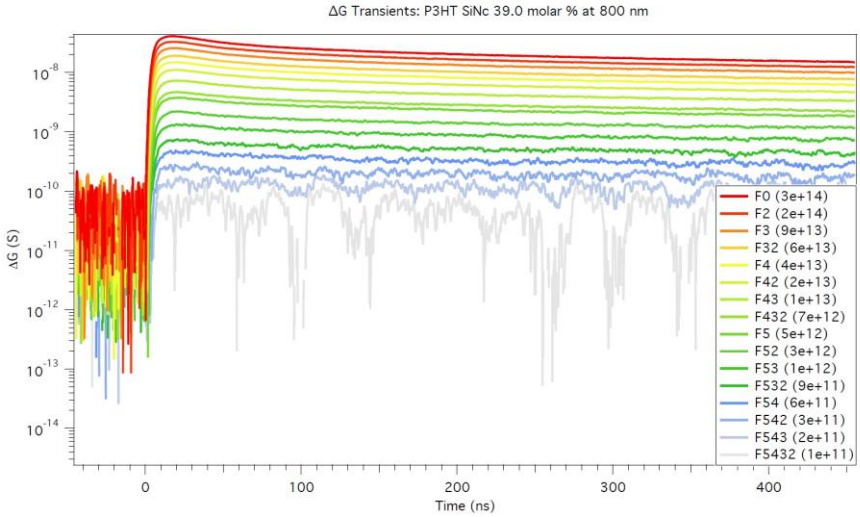

Figure C-20. Experimental photoconductance (ΔG) transients for a thin film sample of neat P3HT with SiNc (39.0 molar percent), spin-coated on quartz and excited at 800 nm.

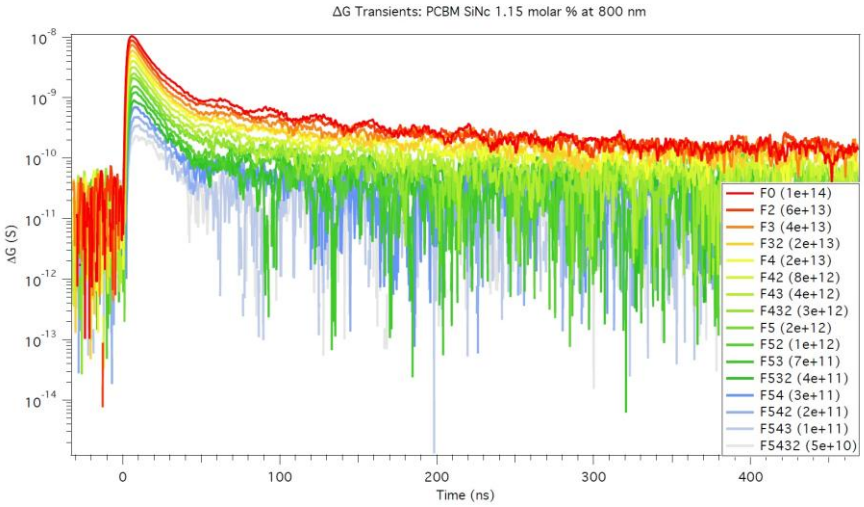

Figure C-21. Experimental photoconductance (ΔG) transients for a thin film sample of neat $PC_{60}BM$ with SiNc (1.15 molar percent), spin-coated on quartz and excited at 800 nm.

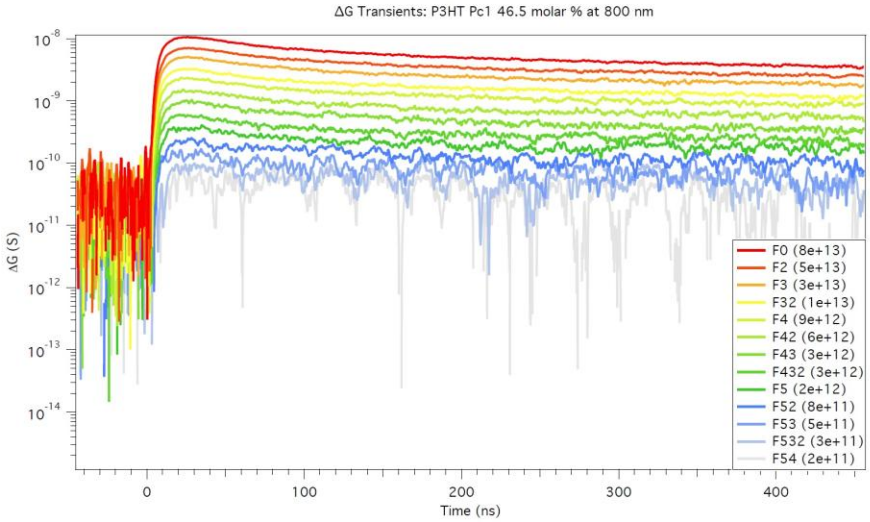

Figure C-22. Experimental photoconductance (ΔG) transients for a thin film sample of neat P3HT with Pc1 (46.5 molar percent), spin-coated on quartz and excited at 800 nm.

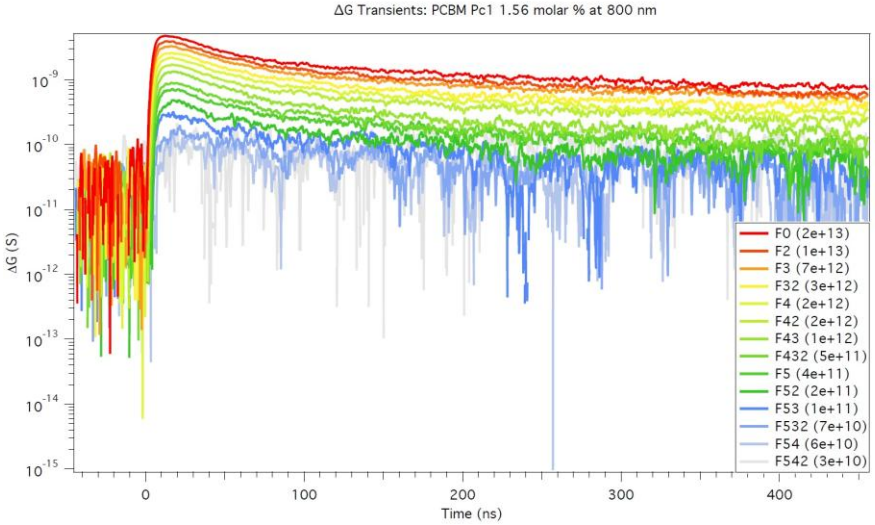

Figure C-23. Experimental photoconductance (ΔG) transients for a thin film sample of neat $PC_{60}BM$ with Pc1 (1.56 molar percent), spin-coated on quartz and excited at 800 nm.

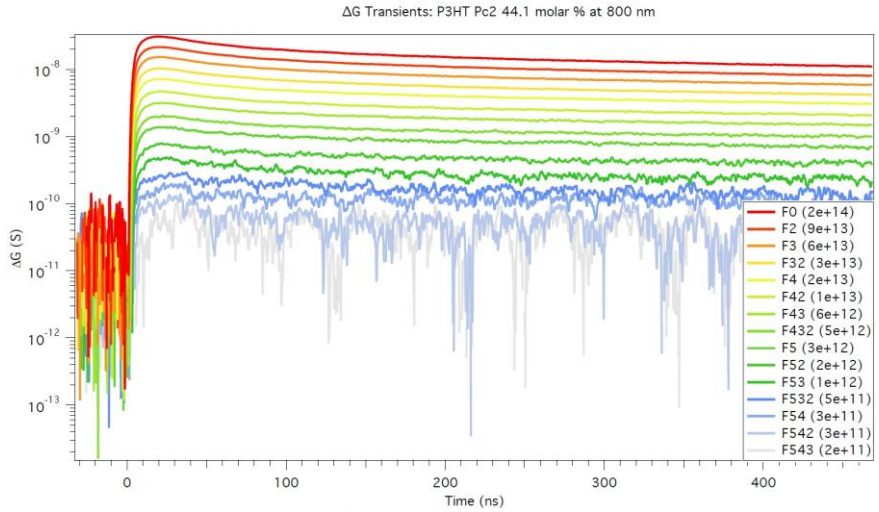

Figure C-24. Experimental photoconductance (ΔG) transients for a thin film sample of neat P3HT with Pc2 (44.1 molar percent), spin-coated on quartz and excited at 800 nm.

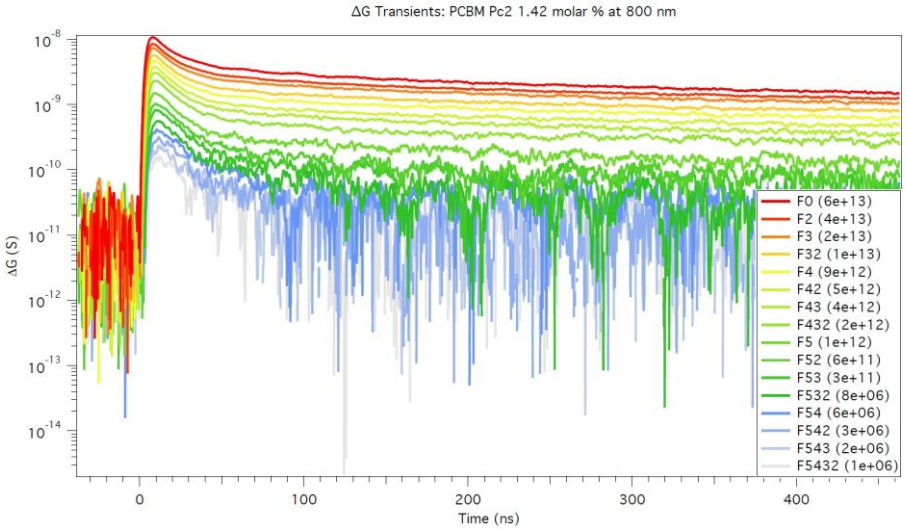

Figure C-25. Experimental photoconductance (ΔG) transients for a thin film sample of neat $PC_{60}BM$ with Pc2 (1.42 molar percent), spin-coated on quartz and excited at 800 nm.

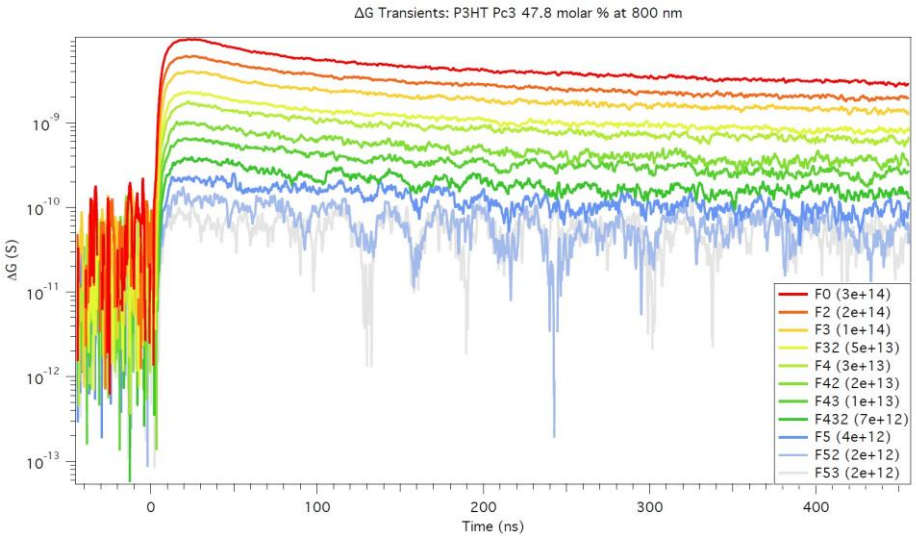

Figure C-26. Experimental photoconductance (ΔG) transients for a thin film sample of neat P3HT with Pc3 (47.8 molar percent), spin-coated on quartz and excited at 800 nm.

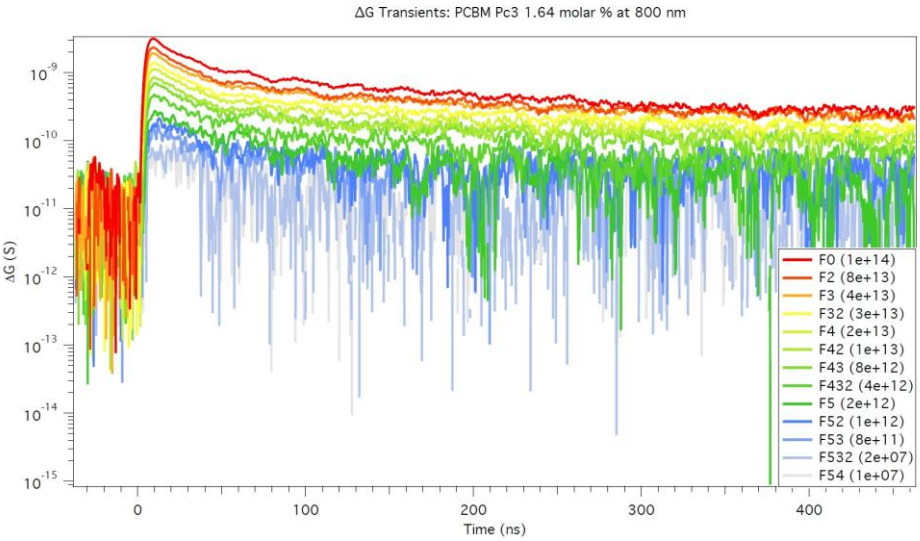

Figure C-27. Experimental photoconductance (ΔG) transients for a thin film sample of neat $PC_{60}BM$ with Pc3 (1.64 molar percent), spin-coated on quartz and excited at 800 nm.

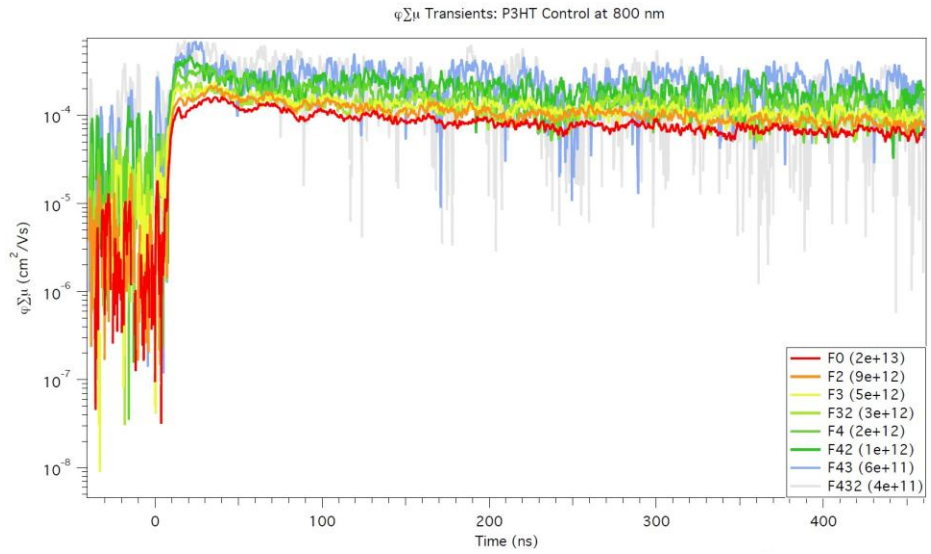

Figure C-28. Experimental yield mobility product (φΣμ) transients for a thin film sample of neat P3HT, spin-coated on quartz and excited at 800 nm.

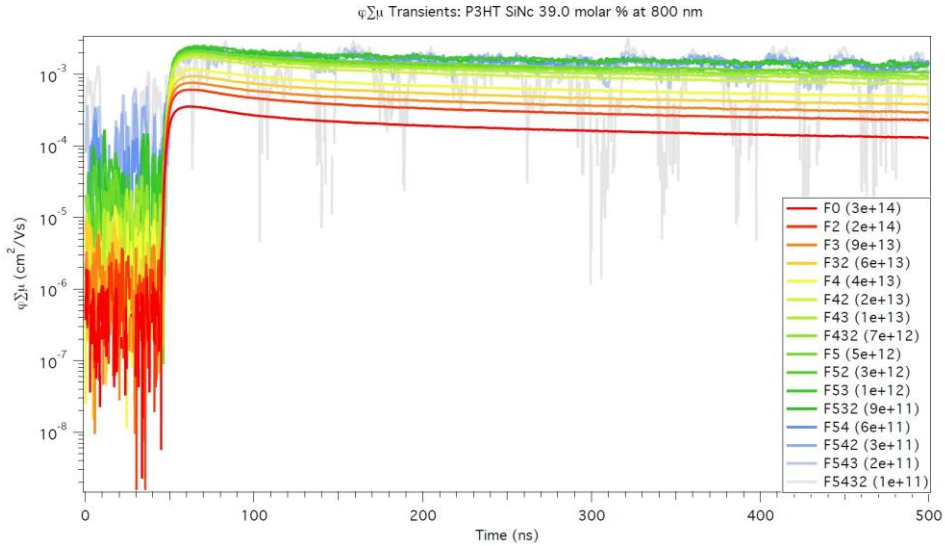

Figure C-29. Experimental yield mobility product (φΣμ) transients for a thin film sample of neat P3HT with SiNc (39.0 molar percent), spin-coated on quartz and excited at 800 nm.

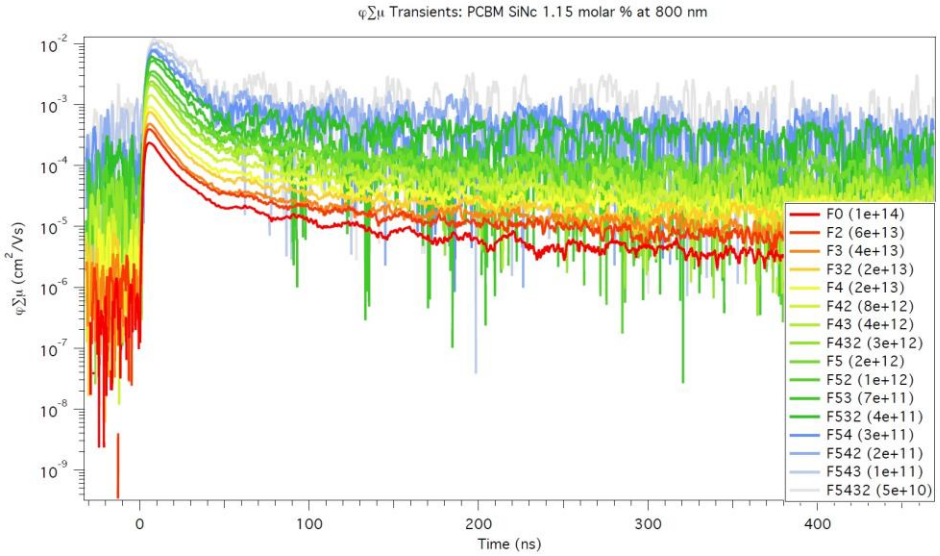

Figure C-30. Experimental yield mobility product (φΣμ) transients for a thin film sample of neat $PC_{60}BM$ with SiNc (1.15 molar percent), spin-coated on quartz and excited at 800 nm.

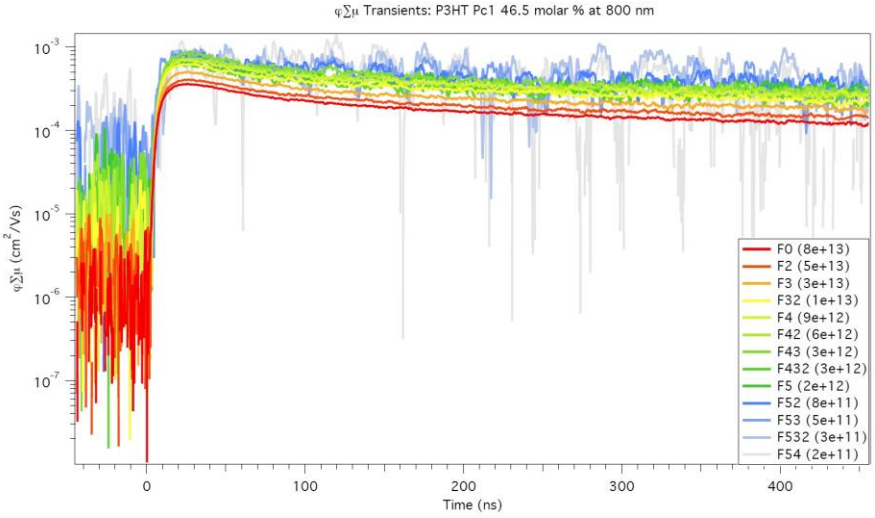

Figure C-31. Experimental yield mobility product (φΣμ) transients for a thin film sample of neat P3HT with Pc1 (46.5 molar percent), spin-coated on quartz and excited at 800 nm.

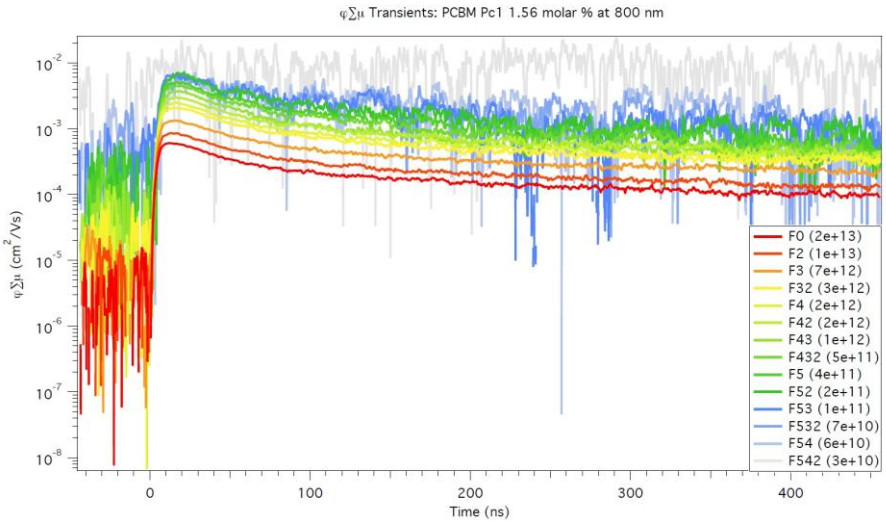

Figure C-32. Experimental yield mobility product (φΣμ) transients for a thin film sample of neat $PC_{60}BM$ with Pc1 (1.56 molar percent), spin-coated on quartz and excited at 800 nm.

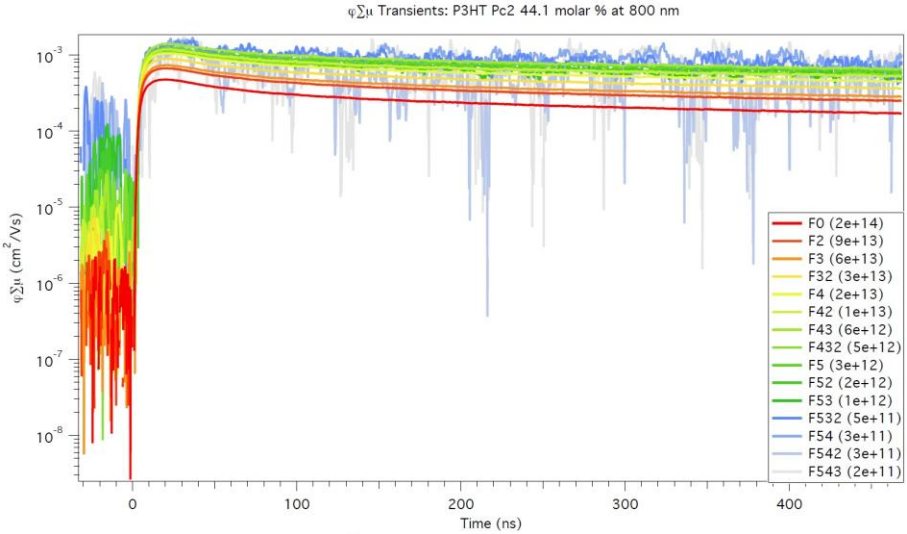

Figure C-33. Experimental yield mobility product (φΣμ) transients for a thin film sample of neat P3HT with Pc2 (44.1 molar percent), spin-coated on quartz and excited at 800 nm.

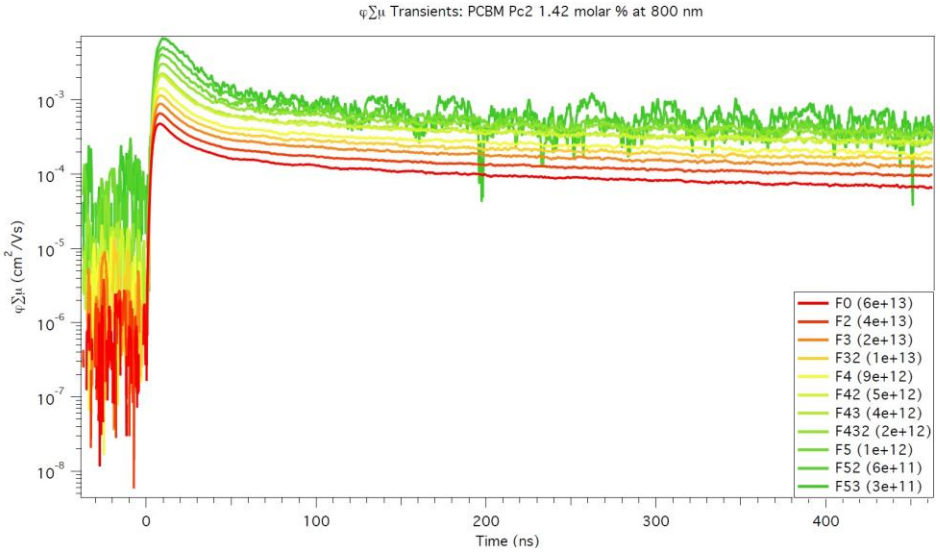

Figure C-34. Experimental yield mobility product (φΣμ) transients for a thin film sample of neat $PC_{60}BM$ with Pc2 (1.42 molar percent), spin-coated on quartz and excited at 800 nm.

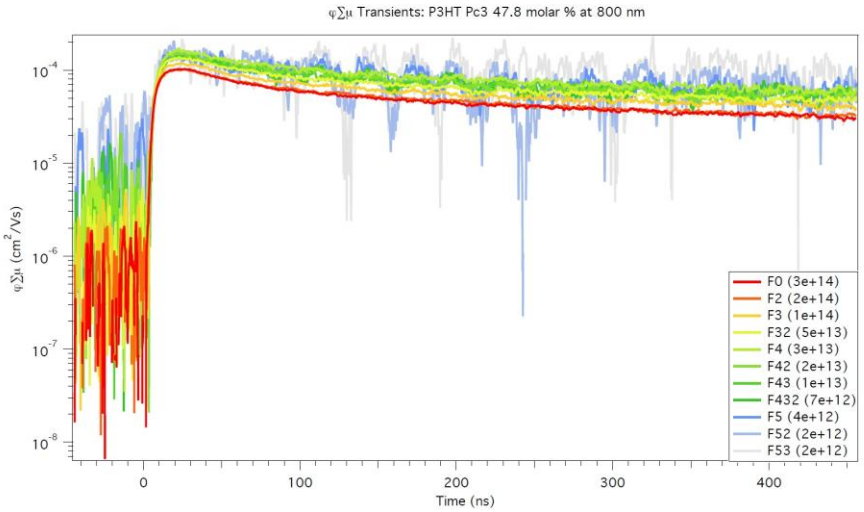

Figure C-35. Experimental yield mobility product (φΣμ) transients for a thin film sample of neat P3HT with Pc3 (47.8 molar percent), spin-coated on quartz and excited at 800 nm.

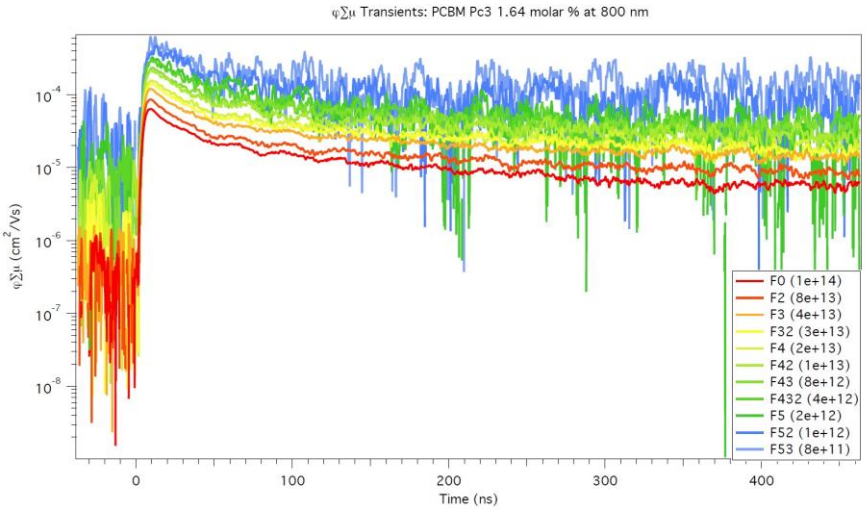

Figure C-36. Experimental yield mobility product (φΣμ) transients for a thin film sample of neat $PC_{60}BM$ with Pc3 (1.64 molar percent), spin-coated on quartz and excited at 800 nm.

Bibliography

1. Hankey, R. *U.S. Energy Information Administration* **2014**, 1-215.

2. Hoffert, M.; Caldeira, K.; Benford, G.; Criswell, D.; Green, C.; Herzog, H.; Jain, A.; Kheshgi, H.; Lackner, K.; Lewis, J.; Lightfoot, H.; Manheimer, W.; Mankins, J.; Mauel, M.; Perkins, L.; Schlesinger, M.; Volk, T.; Wigley, T. *Science.* **2002**, *298*, 981-987.

3. Sawin, J.; Sverrisson, F. *Ren21*. **2014**, 1-215.

4. Tilman, D.; Hill, J.; Lehman, C. *Science.* **2006**, *314*, 1598-1600.

5. Green, M.; Emery, K.; Hishikawa, Y.; Warta, W.; Dunlop, E. *Prog. Photovolt: Res. Appl.* **2012**, *20*, 12-20.

6. Neugebauer, H.; Brabec, C.; Hummelen, J.C.; Sariciftci, N.S. *Solar Energy Materials & Solar Cells*. **2000**, *61*, 35-42.

7. Bliznyuk, V.N.; Carter, S.A.; Scott, J.C.; Klarner, G.; Miller, R.D.; Miller, D.C. *Macromolecules*. **1999**, *32*, 361-369.

8. Noh, Y.; Kim, D.; Yoshida, Y.; Yase, K.; Jung, B.; Lim, E.; Shim, H. *Applied Physics Letters*. **2005**, *86*, 043501.

9. Jorgensen, M.; Norrman, K.; Krebs, F. *Solar Energy Materials & Solar Cells*. **2008**, *92*, 686-714.

10. Liu, M.; Johnston, M.; Snaith, H. *Nature.* **2013**, *501*, 395-398.

11. Ball, J.; Lee, M.; Hey, A.; Snaith, H. *Energy Environ. Sci.* **2013**, *6*, 1739-1743.

12. You, J.; Hong, Z.; Yang, Y.; Chen, Q.; Cai, M.; Song, T.; Chen, C.; Lu, S.; Liu, Y.; Zhou, H.; Yang, Y. *ACS Nano*. **2014**, *8*, 1674-1680.

13. Ameri, T.; Dennler, G.; Lungenschmied, C.; Brabec, C. *Energy Environ. Sci.* **2009**, *2*, 347-363.

14. You, J.; Dou, L.; Yoshimura, K.; Kato, T.; Ohya, K.; Moriarty, T.; Emery, K.; Chen, C.; Gao, J.; Li, G.; Yang, Y. *Nature Communications.* **2013**, 1-10.

15. Nozik, A. *Physica E.* **2002**, *14*, 115-120.

16. Kirmani, A.; Carey, G.; Abdelsamie, M.; Yan, B.; Cha, D.; Rollny, L.; Cui, X.; Sargent, E.; Amassian, A. *Adv. Mater.* **2014**, 1-7.

17. Chuang, C.; Brown, P.; Bulovic, V.; Bawendi, M. *Nature Materials.* **2014**, 1-6.

18. Olson, J.; Kurtz, S.; Kibbler, A.; Faine, P. *Applied Physics Letters*. **1990**, *56*, 623-625.

19. Gratzel, M. *Nature.* **2001**, *414*, 338-344.

20. Nelson, J. *Science.* **2001**, *293*, 1059-1060.

21. Shaeen, S.; Ginley, D.; Jabbour, G. *Mat. Res. Soc. Bull.* **2005**, *30*, 10-19.

22. Hoth, C.; Choulis, S.; Schilinsky, P.; Brabec, C. *Adv. Mater.* **2007**, *19*, 3973-3978.

23. Brabec, C.; Hauch, J.; Schilinsky, P.; Waldauf, C. *MRS Bulletin.* **2005**, *30*, 50-52.

24. Gregg, B. *J. Phys. Chem.* **2003**, *107*, 4688-4698.

25. Halls, J.; Pichler, K.; Friend, R.; Moratti, S.; Holmes, A. *Applied Physics Letters*. **1996**, *68*, 3120-3122.

26. Blom, P.; Mihailetchi, V.; Koster, L.; Markov, D. *Adv. Mater.* **2007**, *19*, 1551-1566.

27. Russell, D.; Arias, A.; Friend. R.; Silva, C.; Ego, C.; Grimsdale, A.; Mullen, K. *Applied Physics Letters*. **2002**, *80*, 2204-2206.

28. Haugeneder, A.; Neges, M.; Kallinger, C.; Spirkl, W.; Lemmer, U.; Feldmann, J. *Physical Review B.* **1999**, *59*, 15346-15351.

29. Savenije, T.; Warman, J.; Goossens, A. *Chemical Physics Letters.* **1998**, *287*, 148-153.

30. Barker, J.; Ramsdale, C.; Greenham, N. *Physical Review B.* **2003**, *67*, 075205-1 - 075205-9.

31. Halls, J.; Walsh, C.; Greenham, N.; Marsegila, E.; Friend, R.; Moratti, S.; Holmes, A. *Nature*. **1995**, *376*, 498-500.

32. Hoppe, H.; Sariciftci, N. *J. Mater. Res.* **2004**, *19*, 1924-1945.

33. Snaith, H.; Arias, A.; Morteani, A.; Silva, C.; Friend. R. *Nano Letters.* **2002**, *2*, 1353-1357.

34. Hoppe, A.; Sariciftci, N. *J. Mater. Chem.* **2006**, *16*, 45-61.

35. Collins, B.; Gann, E.; Guignard, L.; He, X.; McNeill, C.; Ade, H. *J. Phys. Chem. Lett.* **2010**, *1*, 3160-3166.

36. Collins, B.; Tumbleston, J.; Ade, H. *J. Phys. Chem. Lett.* **2011**, *2*, 3135-3145.

37. He, X.; Collins, B.; Watts, B.; Ade, H.; McNeill, C. *Small*. **2012**, *8*, 1920-1927.

38. Kim, Y.; Cook, S.; Tuladhar, S.; Choulis, S.; Nelson, J.; Durrant, J.; Bradley, D.; Giles, M.; McCulloch, I.; Ha, C.; Ree, M. *Nature Materials*. **2006**, *5*, 197-203.

39. Kozub, D.; Vakshouri, K.; Orme, L.; Wang, C.; Hexemer, A.; Gomez, E. *Macromolecules*. **2011**, *44*, 5722-5726.

40. Mihailetchi, V.; Xie, H.; de Boer, B.; Koster, L.; Blom, P. *Adv. Funct. Mater.* **2006**, *16*, 699-708.

41. Verploegen, E.; Mondal, R.; Bettinger, C.; Sok, S.; Toney, M.; Bao, Z. *Adv. Funct. Mater.* **2010**, *20*, 3519-3529.

42. Wu, W.; Jeng, U.; Su, C.; Wei, K.; Su, M.; Chiu, M.; Chen, C.; Su, W.; Su, C.; Su, A. *ACS Nano*. **2011**, *5*, 6233-6243.

43. Yin, W.; Dadmun, M. *ACS Nano*. **2011**, *5*, 4756-4768.

44. Chatten, A.; Tuladhar, S.; Choulis, S.; Bradley, D.; Nelson, J. *Journal of Materials Science*. **2005**, *40*, 1393-1398.

45. Kobashi, M.; Takeuchi, H. *Macromolecules*. **1998**, *31*, 7273-7278.

46. Jaiswal, M.; Menon, R.; *Polym. Int.* **2006**, *55*, 1371-1384.

47. Ehinger, K.; Roth, S. *Solid State Sciences Series*. **1985**, *63*.

48. Mihailetchi, V.; Xie, H.; de Boer, B.; Koster, L.; Blom, P. *Adv. Funct. Mater.* **2006**, *16*, 699-708.

49. Chua, L.; Zaumseil, J.; Chang, J.; Ou, E.; Ho, P.; Sirringhaus, H.; Friend, R. *Nature*. **2005**, *434*, 194-199.

50. Sirringhaus, H.; Brown, P.; Friend, R.; Nielsen, M.; Bechgaard, K.; Langeveld-Voss, B.; Spiering, A.; Janssen, R.; Meijer, E.; Herwig, P.; Leeuw, D. *Nature*. **1999**, *401*, 685-688.

51. Lim, B.; Bloking, J.; Ponec, A.; McGehee, M.; Sellinger, A. *ACS Appl. Mater. Interfaces.* **2014**, *6*, 6905-6913.

52. Bergkamp, J.; Sherman, B.; Marino-Ochoa, E.; Palacios, R.; Cosa, G.; Moore, T.; Gust, D.; Moore, A. *J. Porphyrins Phthalocyanines*. **2011**, *15*, 943-950.

53. Zhang, C.; Zhang, J.; Hao, Y.; Lin, Z.; Zhu, C. *Journal of Applied Physics.* **2011**, *110*, 064504-1 - 064504-7.

54. White, M.; Olson, D.; Shaheen, S.; Kopidakis, N.; Ginley, D. *Applied Physics Letters*. **2006**, *89*, 143517-1 - 143517-3.

55. Scharber, M.; Muhlbacher, D.; Koppe, M.; Denk, P.; Waldauf, C.; Heeger, A.; Brabec, C. *Adv. Mater.* **2006**, *18*, 789-794.

56. Ferguson, A.; Kopidakis, N.; Shaheen, S.; Rumbles, G. *J. Phys. Chem. C.* **2011**, *115*, 23134-23148.

57. Sun, S. *Solar Energy Materials & Solar Cell*. **2005**, *85*, 261-267.

58. Marcus, R. *Nobel Lecture*. **1992**, 1-24.

59. Meade, T.; Gray, H.; Winkler, J. *J. Am. Chem. Soc.* **1989**, *111*, 4353-4356.

60. Feldt, S.; Wang, G.; Boschloo, G.; Hagfeldt, A. *J. Phys. Chem. C.* **2011**, *115*, 21500-21507.

61. Coffey, D.; Larson, B.; Hains, A.; Whitaker, J.; Kopidakis, N.; Boltalina, O.; Strauss, S.; Rumbles, G. *J. Phys. Chem. C.* **2012**, *116*, 8916-8923.

62. Dicker, G.; de Haas, M.; Siebbeles, L.; Warman, J. *Physical Review B.* **2004**, *70*, 045203-1 - 045203-8.